LUND UNIVERSITY

Decoding the Sense of Touch. Neural Representation and Processing of Tactile Sensory Input in the Neocortex

Mogensen, Hannes

2018

Document Version:
Publisher's PDF, also known as Version of record

[Link to publication](#)

Citation for published version (APA):
Mogensen, H. (2018). *Decoding the Sense of Touch. Neural Representation and Processing of Tactile Sensory Input in the Neocortex*. [Doctoral Thesis (compilation), Neural Basis of Sensorimotor Control]. Lund University: Faculty of Medicine.

Total number of authors:
1

Decoding the Sense of Touch

Neural Representation and Processing of Tactile Sensory Input in the Neocortex

HANNES MOGENSEN
FACULTY OF MEDICINE | LUND UNIVERSITY
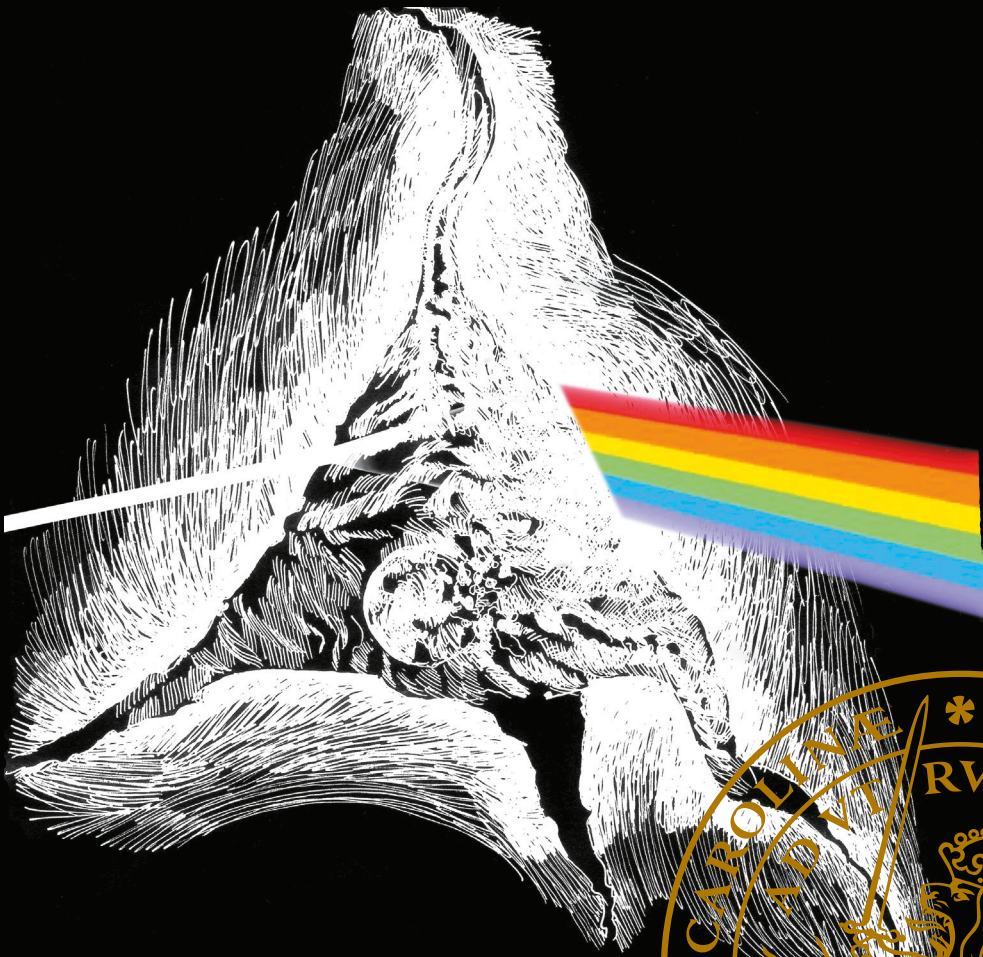
Decoding the Sense of Touch

Decoding the Sense of Touch

Neural Representation and Processing of Tactile Sensory Input in the Neocortex

Hannes Mogensen

LUND UNIVERSITY

Organization	Document name:
LUND UNIVERSITY	Doctoral Dissertation
Author	**Date of issue**
Hannes Mogensen	February 9th 2018
	Sponsoring organization
	Lund University

Title and subtitle

Decoding the Sense of Touch. Neural Representation and Processing of Tactile Sensory Input in the Neocortex

Abstract

This thesis presents studies on how tactile sensory input is represented and processed in the neocortex. We used an experimental setup with electrical activation of cutaneous receptors for innocuous touch in the second digit of the forepaw of anesthetized rats. The activation consisted of a set of eight reproducible spatiotemporal patterns. Using cell-attached and whole-cell patch clamp *in vivo*, we measured the response in neocortical neurons.

The studies provided support for a distributed model of cortical processing, where ensembles of neurons in the primary somatosensory cortex are significantly better than single neurons at decoding different types of tactile stimulations, but individual neurons are at the same time able to separate between single pulse stimulations of adjacent receptive fields.

We also showed that the intracellular response to identical cutaneous stimulation can be classified as one out of a finite set of typical responses for the neuron. Our data hence suggested that tactile sensory processing is dependent not only on the direct afferent input, but also on its internal state and projections from other parts of the nervous system. The cerebellum has connections to the neocortex and is therefore an important regulator of internal states. The cerebellar output cells are in part driven by tactile input from sensorimotor signals in spinocerebellar systems and as part of the dissertation we also studied the synaptic plasticity of those inputs. The study showed that the connection between the spinal cord and deep cerebellar nuclei neurons have a low or non-existent medium-term plasticity in the adult nervous system.

Our analysis suggests that neocortical sensory processing is mediated through parallel streams of overlapping network activity, each with its own local state variation over time. In order to increase the sensitivity of tactile processing, differentiation in neuronal activity is enforced, causing neurons to respond differently to the same afferent input.

Key words

Somatosensory system, neocortex, cerebellum, tactile processing, distributed coding

Classification system and/or index terms (if any)

Supplementary bibliographical information	Language
	English

ISSN and key title	**ISBN**
1652-8220	978-91-7619-579-6

Recipient's notes	**Number of pages** 38	**Price**
	Security classification	

I, the undersigned, being the copyright owner of the abstract of the above-mentioned dissertation, hereby grant to all reference sources permission to publish and disseminate the abstract of the above-mentioned dissertation.

Signature _Hannes Mogensen_ Date _2018-01-02_

Decoding the Sense of Touch

Neural Representation and Processing of Tactile Sensory Input in the Neocortex

Hannes Mogensen

LUND
UNIVERSITY

"The cerebral cortex is a very difficult theme, perhaps the most difficult study presented to any anatomist; the supreme dignity of the organ and the inextricable complexity of its function would demand a corresponding fabric of immense complexity, whose threads the most sagacious investigators will be able to disentangle only partially, and in which will become constantly entangled and lost, all those who imagine that nature is capable of developing multifarious and highly elevated functions by means of simple mechanisms and schematic formulae."

Santiago Ramón y Cajal
Nuevo concepto de la histologia de los centros nerviosos (1892)

"And everything under the sun is in tune but the sun is eclipsed by the moon"

Roger Waters
Eclipse (1973)

Table of Contents

Abstract

This thesis presents studies on how tactile sensory input is represented and processed in the neocortex. We used an experimental setup with electrical activation of cutaneous receptors for innocuous touch in the second digit of the forepaw of anesthetized rats. The activation consisted of a set of eight reproducible spatiotemporal patterns. Using cell-attached and whole-cell patch clamp *in vivo*, we measured the response in neocortical neurons.

The studies provided support for a distributed model of cortical processing, where ensembles of neurons in the primary somatosensory cortex (S1) are significantly better than single neurons at decoding different types of tactile stimulations, but individual neurons are at the same time able to separate between single pulse stimulations of adjacent receptive fields.

We also showed that the intracellular response to identical cutaneous stimulation can be classified as one out of a finite set of typical responses for the neuron. Our data hence suggested that tactile sensory processing is dependent not only on the direct afferent input, but also on its internal state and projections from other parts of the nervous system. The cerebellum has connections to the neocortex and is therefore an important regulator of internal states. The cerebellar output cells are in part driven by tactile input from sensorimotor signals in spinocerebellar systems and as part of the dissertation we also studied the synaptic plasticity of those inputs. The study showed that the connection between the spinal cord and deep cerebellar nuclei (DCN) neurons have a low or non-existent medium-term plasticity in the adult nervous system.

Our analysis suggests that neocortical sensory processing is mediated through parallel streams of overlapping network activity, each with its own local state variation over time. In order to increase the sensitivity of tactile processing, differentiation in neuronal activity is enforced, causing neurons to respond differently to the same afferent input.

List of original papers

I.   **Mogensen H.**, Bengtsson F., Jörntell H.: No Medium-Term Spinocerebellar Input Plasticity in Deep Cerebellar Nuclear Neurons In Vivo? *Cerebellum* 16(3):638-647 (2017)

II. Oddo, CM., Mazzoni A., Spanne A., Enander J.M.D., **Mogensen H.**, Bengtsson F., Camboni D., Micera S., Jörntell, H.: Artificial spatiotemporal touch inputs reveal complementary decoding in neocortical neurons. *Scientific Reports* 7:45898 (2017)

III. Norrlid J.*, **Mogensen H.***, Enander J.M.D., Jörntell H.: Evidence for multiple parallel processing streams in neocortical circuitry in vivo. *Preliminary manuscript*

IV. **Mogensen, H**., Norrlid, J., Enander, J.M.D., Wahlbom, A., Jörntell, H: Correlation patterns between pairs of adjacent neocortical neurons *in vivo*. *Preliminary manuscript*

* shared first authorship based on equal contribution

Abbreviations

AIN anterior interpositus nucleus

BC basket cell

CF climbing fiber

CNS central nervous system

DCN deep cerebellar nuclei

DN dentate nucleus

EPSP excitatory post synaptic potential

fMRI functional magnetic resonance imaging

IO inferior olive

GoC golgi cell

GrC granule cell

LTMR low-threshold mechanoreceptor

M2 secondary motor cortex

MF mossy fiber

MRI magnetic resonance imaging

PC purkinje cell

PET position emission tomography

PF parallel fiber

S1 primary somatosensory cortex

SC stellate cell

SpTKDE spike-triggered kernel density estimator

Introduction

The discovery of the neuron in the 19th century, followed by the ambitious depiction of different cellular morphologies by Ramón y Cajal, inspired the belief that specific functions or parameters of the nervous system could be pinpointed to specific neurons (Nicolelis 2011). Two hundred years later, it is still an ongoing dispute whether the function of the nervous system can best be understood as a distributed network phenomena, or if cerebral functions can be ascribed to individual neurons or distinct groups of neurons. The first section of this chapter summarizes some of the theories of cortical sensory processing, primarily from a historical perspective. The subsequent sections give a more specific context to paper I, II, III and IV.

Models of sensory processing in the neocortex

When the tip of your finger touches an object, during exploratory search or passive sensing, a multitude of cutaneous receptors are activated. Excluding the receptors for temperature and noxious stimulation, there are still more than two hundred low-threshold mechanoreceptors (LTMRs) for innocuous touch per square centimeter of the fingertip (Johansson and Vallbo 1979; Darian-Smith and Kenins 1980). The evoked receptor responses are propagated as action potentials to the neocortex, via relay stations in the dorsal column of the spinal cord, the cuneate nucleus and the thalamus[1] (Abraira and Ginty 2013). According to the labelled line hypothesis of sensory processing, the signals from different receptive fields of the skin are separated from each other as they travel along the posterior column-medial lemniscus pathway, resulting in a somatotopic map of the skin in the cerebral cortex (Mountcastle 1997; Guyton and Hall 2006; Pereira and Alves 2011; Kandel, Schwartz et al. 2013).

---

[1] There is a parallel pathway for innocuous sensory signals to the neocortex, primarily from hairy skin areas. This pathway transmits information via the lateral cervical nucleus and the thalamus, but it has been omitted from the summary above as it is vestigial in humans (Abraira and Ginty 2013).

Hubel and Wiesel (1961) used a retinotopic map in the visual cortex as a substrate to tentatively suggest that cortical sensory processing is a hierarchical process, where neurons receiving thalamocortical afferent signals from adjacent receptive fields will have a common postsynaptic neuron that integrates the information to form a more complex picture of the external source of stimulation. Felleman and van Essen (1991) build on this idea to create a detailed model of the somatosensory and visual sensory processing faculties of the cortex, including ten layers of the visual processing hierarchy and nine layers of the somatosensory processing hierarchy. The field of neuroscience has obviously undergone a few transformations since Felleman and van Essen published their article more than a quarter of a century ago, but the principle of hierarchical sensory processing is still widely assumed to be true (Kandel, Schwartz et al. 2013).

Barlow (1972) uses the principle of hierarchical sensory processing to conceptualize a grandmother neuron - a neuron that the sensory signals will converge to and activate when the subject perceives his or her older relative. One caveat with the grandmother neuron hypothesis is that it heavily constrains the realm of possible human perceptions, since there are a finite number of neurons assigned to the final stage of perception but at least theoretically an infinite number of conceivable perceptions. As a solution to this conundrum, Barlow suggests that the neuronal constituents of our real-world phenomena could be according to some abstract classification we are unaware of. Each constituent is then represented by a canonical neuron. To explain how the activity of several canonical neurons is combined to form a comprehensive perception, Barlow uses boolean arithmetic as an analogue.[2]

In other models of cortical processing, the single neuron as the smallest functional unit is replaced by cortical columns (Mountcastle 1997; Buxhoeveden and Casanova 2002). The columnar organization model emanates from studies on the embryological development of cerebral cortex (Buxhoeveden and Casanova 2002), and studies of the barrel cortex of mice and rat (Woolsey and Van der Loos 1970; Petersen 2007). Neocortical cells migrating from the ventral zone of the telencephalon have been observed to form radial columns in the developing neocortical laminae (Rakic 1995; Mountcastle 1997), and the barrel cortex of adult rats is believed to contain vertically aligned neurons, neatly organized in rows of columns in the transversal plane. Each barrel column receives synaptic input primarily from a single principal whisker. If the sensory stimulation from a whisker is suppressed during development, the corresponding connections

---

[2] Barlow extends the analogue of boolean arithmetic by acknowledging that the firing frequency of a neuron can be graded, so that the state of a neuron is not binary but can assume more than two distinct, functionally relevant values. Thus this part of Barlow's model could be described as something akin to fuzzy logic, however he does not use this term himself, possibly since the concept was still fairly novel at the time.

between principal whisker and corresponding barrel column will be compromised in the adult rat (Simons and Land 1987).

According to Buxhoeveden and Casanova (2002), a cortical minicolumn contains 80 - 100 neurons. Mountcastle (1997) describes how a macrocolumn in turn is made up of about 80 minicolumns. Nissl staining and 2-deoxy glucose metabolic labelling reveal vertical alignment of neurons in several cortical areas (Buxhoeveden and Casanova 2002), but there are several theories regarding which organizational unit that is the smallest functional entity (Swindale 1990).

Neocortex

The studies included in this dissertation show that while different cells are tuned to respond with individual specificity to tactile stimulation, the information content in an ensemble of neurons is far superior to that of an isolated neuron, even for the type of stimulations to which the individual neuron responds with high specificity (paper II). Since neurons from the same study have also been found able to differentiate between single pulses delivered to adjacent receptive fields, the findings imply that the brain utilizes a distributed strategy for cortical sensory processing of tactile information.

Types of neural coding

Spanne and Jörntell (2015) make the distinction between local coding, sparse coding and dense coding. While local coding allows for only one context per cell, the sparse and dense coding allow for overlapping spatiotemporal patterns between different contexts at the same time. The fact that there is no unambiguously defined boundary between the sparse and dense coding regimes is a potential source of misunderstandings to discussions on the subject. Qualitatively, the difference is that in the former case the neural signalling is as limited as possible, whereas the latter case is characterized by continuous activation of large parts of the network. The dense coding regime is more easily applicable to a system with a large percentage of inhibitory neurons, some of which may have a role in mitigating positive feedback loops that otherwise would increase synaptic efficacy out of optimal bounds for the system (Jörntell 2016b). Spanne and Jörntell (2015) conclude that the dense coding regime allow for more dynamic calibration of synaptic weights and more generalizations in spatiotemporal patterns between contexts. Furthermore, a more dense coding regime will reduce the impact of the inherent stochasticity in spike firing.

Redundancy in the somatosensory system

Studies on cortical and subcortical sensory systems have shown what appears to be a redundancy in the number of cells transmitting a signal (Strehler and Lestienne 1986; Swindale 1986; Bengtsson, Brasselet et al. 2013). Given the energy cost in maintaining a larger network the redundancy should serve a vital purpose, or it would have been removed by evolutionary pressure. There are at least three reasons to have a perceived redundancy in a system such as the mammalian nervous system. The first reason is that it increases robustness in information transmission, which can be used to mitigate the adverse effects of damage inflicted to single neurons or fibers. Given the relatively low risk of sustaining serious damage to the nervous system versus the energy cost of redundancy, increased robustness is likely not the main reason for the perceived redundancy. The second reason is that a network with more nodes or higher level of interconnectedness under some circumstances will have fewer constraints on what it can be configured to do. The third reason is that what is perceived to be redundant information does in fact contain meaningful deviations from the coarse signal that is yielded from averaging the activity of several cells.

The last hypothesis is supported by studies in this dissertation (paper II), as well as previous studies (Jörntell, Bengtsson et al. 2014). This finding does not rule out that the apparent redundancy also provides an increased robustness on a more coarse level of input processing. In paper II and III we show that neurons in S1 respond differently depending on the type of tactical stimulation of the skin.

Intracortical, corticocortical and thalamocortical networks

The majority of thalamocortical projections relaying afferent somatosensory signals terminate in layer IV (Bruno and Sakmann 2006). Sherman (2016) makes the distinction between driver neurons and modulatory neurons. The conceptual difference is that drivers transmit the main message while modulators assert influence over the affinity to driver inputs. More specifically, drivers are characterized by paired-pulse depression, all-or-none response profile, strong initial excitatory postsynaptic potentials (EPSPs) when there is a response, and an absence of a metabotropic glutamatergic receptor component. Modulators in turn are characterized by paired-pulse facilitation, graded response profile with small initial EPSPs, and the presence of a metabotropic glutamatergic receptor component.

One pervasive message that runs through the work of Sherman is that the thalamus is not merely a relay center, but is part of a dynamic recurrent thalamocortical network (Sherman 2007). For instance, it has been shown that layer V and layer

VI neurons exert modulatory and direct feedback to the thalamus, and that thalamic nucleus are also actively involved as relay stations for corticocortical networks, for instance between the motor and the somatosensory cortex. Studies in mice have shown that the secondary motor cortex (M2) evoke persistent firing in layer V neurons of S1, and that there are top-down regulating circuits between M2 and S1, exemplified by degeneration of sensory perception during optogenetic stimulation of M2 to S1 axons (Manita, Suzuki et al. 2015). The motor cortex also sends efference copies of motor commands via collaterals to the thalamus (Guillery and Sherman 2011).

There is a lack of consensus regarding the functional classification of neocortical neurons, as well as the nature of their cortical and subcortical connections (Jiang, Shen et al. 2015). The neocortical neurons can be more broadly classified as pyramidal tract neurons and intertelencephalic neurons (Gerfen, Paletzki et al. 2013; Harris and Shepherd 2015), based on the nature of their cortical and subcortical connections. Morphologically, neurons are often classified as spiny and non-spiny, based on the appearance of their dendritic branching. The most common neocortical cell is the spiny pyramidal cell (DeFelipe and Fariñas 1992).

Bruno and Sakmann (2006) estimate that 85 % of the neocortical connections in layer IV are intracortical, and only 15 % stem from the thalamus. They also note that although corticothalamic connections are more numerous than the thalamocortical connections, the efficacy of thalamocortical connections is stronger, in fact among the strongest that has been found in the central nervous system (CNS). They suggest that the strength of this connection is due to synchronization of thalamic cells rather than extraordinarily high synaptic strength of individual connections, since unitary EPSPs evoked by a single presynaptic thalamic neuron is relatively small, with an amplitude of order of magnitude of 1 mV or lower.

Cerebellum

In humans the cerebellum contains somewhere around 80 percent of the brain's neurons, but it comprises only ten percent of its size (Azevedo, Carvalho et al. 2009). In other words, the neurons of the cerebellum are densely packed. Importantly, they are packed according to a regular pattern that repeats itself throughout the brain structure (Dean, Porrill et al. 2009). The generic microcircuit that connects the cerebellar neurons is summarized in Figure 1. The microcircuit is arranged in a way that facilitates parallel processing of massive amounts of incoming synaptic information (Jörntell 2016a). It receives extracerebellar synaptic input from mossy fibers (MF) and climbing fibers (CF). The mossy fibers

connect to deep cerebellar nuclei (DCN) neurons and granule cells (GrC), There are up to four mossy fibers per granule cell, often conveying information from the same receptive field (Jörntell and Ekerot 2006). A majority of the GrC – PC connections are however so-called silent synapses, with close to zero synaptic efficacy (Isope and Barbour 2002).
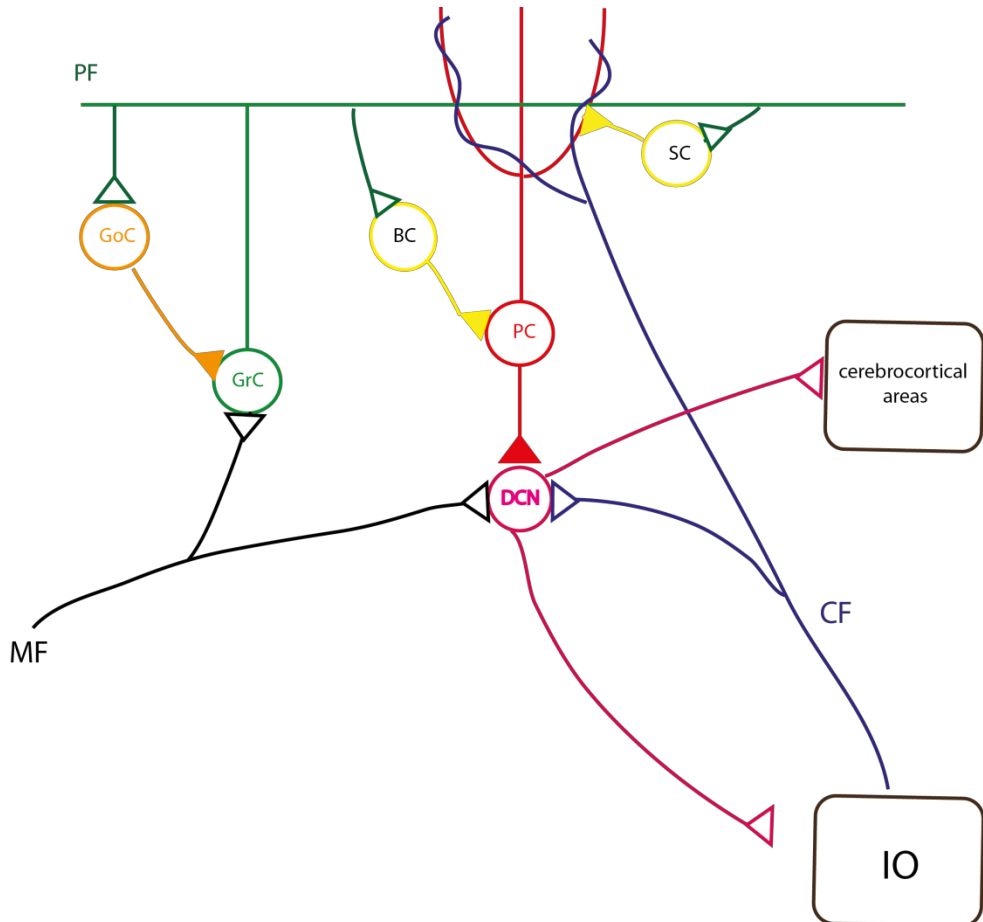
Figure 1. The cerebellar microcircuit.
MF mossy fibers; GrC granule cells, PF parellel fibers, GoC golgi cells, BC basket cells, SC stellar cells, PC purkinje cells, DCN deep cerebellar neurons, CF climbing fibers, IO inferior olive. Empty triangles represent excitatory input, filled triangles represent inhibitory input.

The climbing fibers originate in the inferior olive (Gibson, Horn et al. 2004), making synaptic connections on PCs in the cerebellar cortex and DCN neurons (Jörntell 2016b). Their activity is much lower than what can be observed in the mossy fibers, with a mean firing frequency below 1 Hz during behavior (Gibson, Horn et al. 2004), but the synaptic efficacy of individual CF - PC synapses is high (Jörntell 2016b). According to the Marr Albus theory of cerebellar plasticity, the

climbing fiber signal works as an error signal to the cerebellar microcircuit. The error signal is then used to calibrate the MF signals in order to increase or maintain coordination of CNS functionality (Marr 1969).

There are cerebrocortial connections from both the dentate nucleus (DN) (Dum and Strick 2003) and the anterior interpositus nucleus (AIN) (Jörntell and Ekerot 1999). DN receives afferent sensory information from the spinal neurons of the dorsal horn, while AIN receive proprioceptive information via the spinocerebellar tract. The latter input contains motor commands for the limb and hand movement, but the efferent signals are mixed with afferent signal conveying tactile input (Spanne and Jörntell 2013; Bengtsson and Jörntell 2014).

Since the cerebellum samples information from many cerebral and spinal systems, it is well suited to coordinate the activity of cortical and subcortical circuits according to what is to be achieved on a global level. Lesion studies support the notion that the cerebellum has a general coordinating role in functions performed by other parts of the CNS, since damages to the cerebellum will impair the ability to perform a broad spectrum of activities (Frank, Schoch et al. 2007). One way of performing such extracortical control of the sensory processing is to influence the internal state of intracortical circuits. This will be discussed more in detail in the discussion.

Results

In **paper I** we investigate the medium-term (< 60 minutes) plasticity in synaptic connections between mossy fibers and neurons of the deep cerebellar nuclei. We use three different plasticity inducing protocols in decerebrated adult cats, and measure the response to mossy fiber activation using cell-attached neuronal patch clamp recordings *in vivo*. We conclude that if there is any medium-term plasticity it is very weak, in particular in comparison to the plasticity that has previously been reported *in vitro* for juvenile mice (Pugh and Raman 2008) but also in comparison with the corresponding input to the Purkinje cells of the cerebellar cortex *in vivo* (Jörntell and Ekerot 2002). Figure 2 depicts the results for a protocol involving skin bursts and delayed stimulation of the inferior olive.
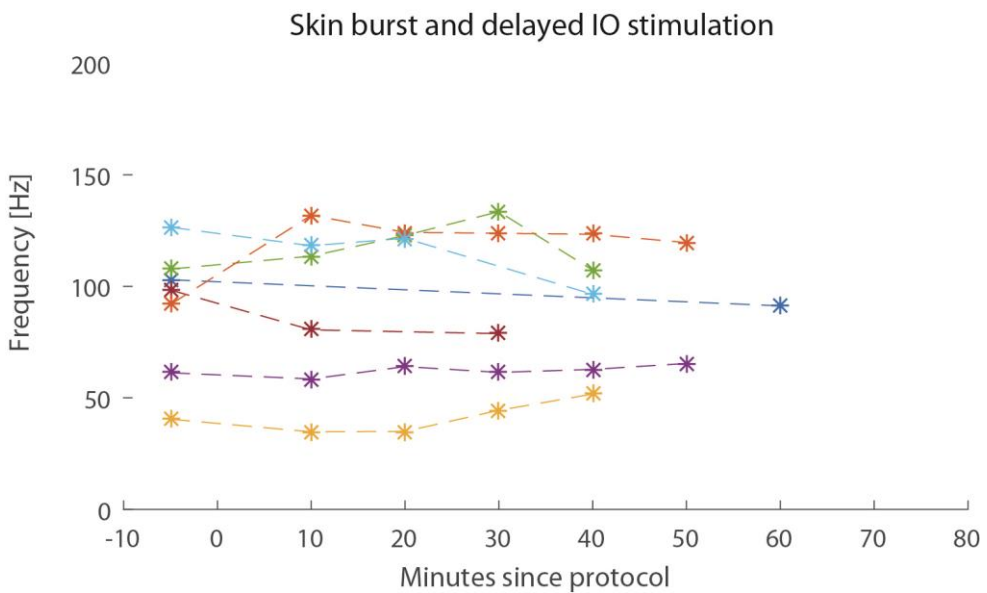
Figure 2. Result from plasticity inducing protocol in paper I.
Result for one of the three protocols that were used to induce plasticity in the synaptic connections between MF and DCN. The responses were measured at regular intervals after that the protocol had been applied. Each dashed line represent a single DCN cell from a separate experiment.

In **paper II** we use a novel stimulation protocol to generate eight different spatiotemporal patterns of activation in LTMR cutaneous afferents in the second

digit of the forepaw of anaesthetised rats. The spatiotemporal patterns mimic the touching of objects with different curvatures, but since it is delivered through electrical pulses it is repeatable with a significantly higher resolution than if a real physical object would have been used for the stimulation. The neocortical response to the stimulation patterns is recorded using *in vivo* whole-cell patch clamp. Using a mathematical classifier on the recorded spike data, we show that neuron assemblies are better than single neurons at decoding these spatiotemporal input patterns (Fig. 3). Figure 4 shows that while several neurons are better at decoding the input patterns, the activity from a single neuron can still be used to separate single stim pulses on different stimulation channels from each other, which is quite remarkable given the small differences in their spatial location on the ventral skin of the distal second digit. We also investigate the correlation between cortical depth and decoding ability, and conclude that the decoding ability is independent of cortical depth.
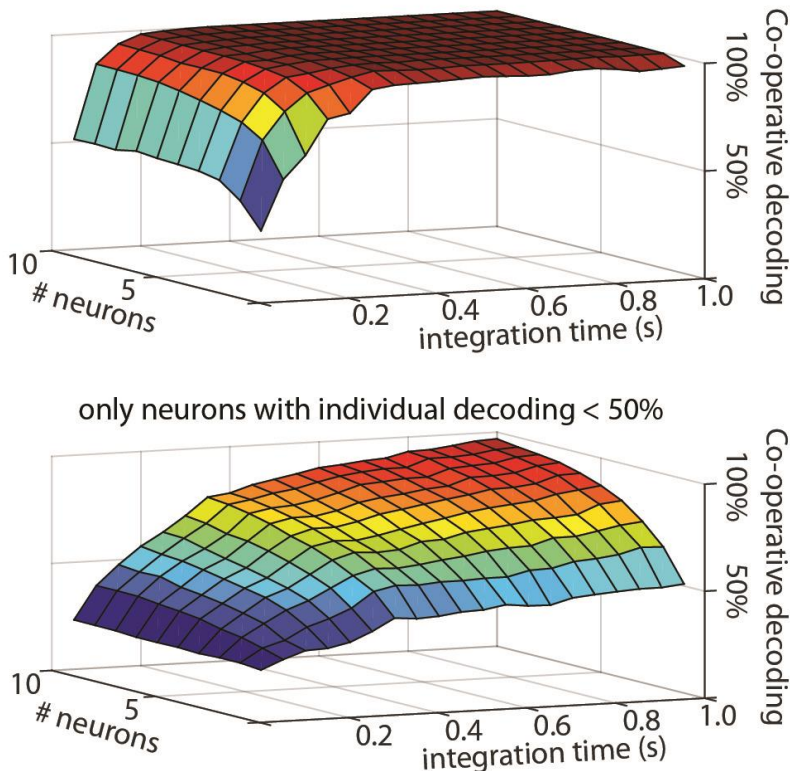
Figure 3. Distributed decoding properties for up to ten neurons (paper II).
Top: result for from 1 to 10 high-performing neurons, for up to one second after stimulation onset. Bottom: result for relatively low-performing neurons
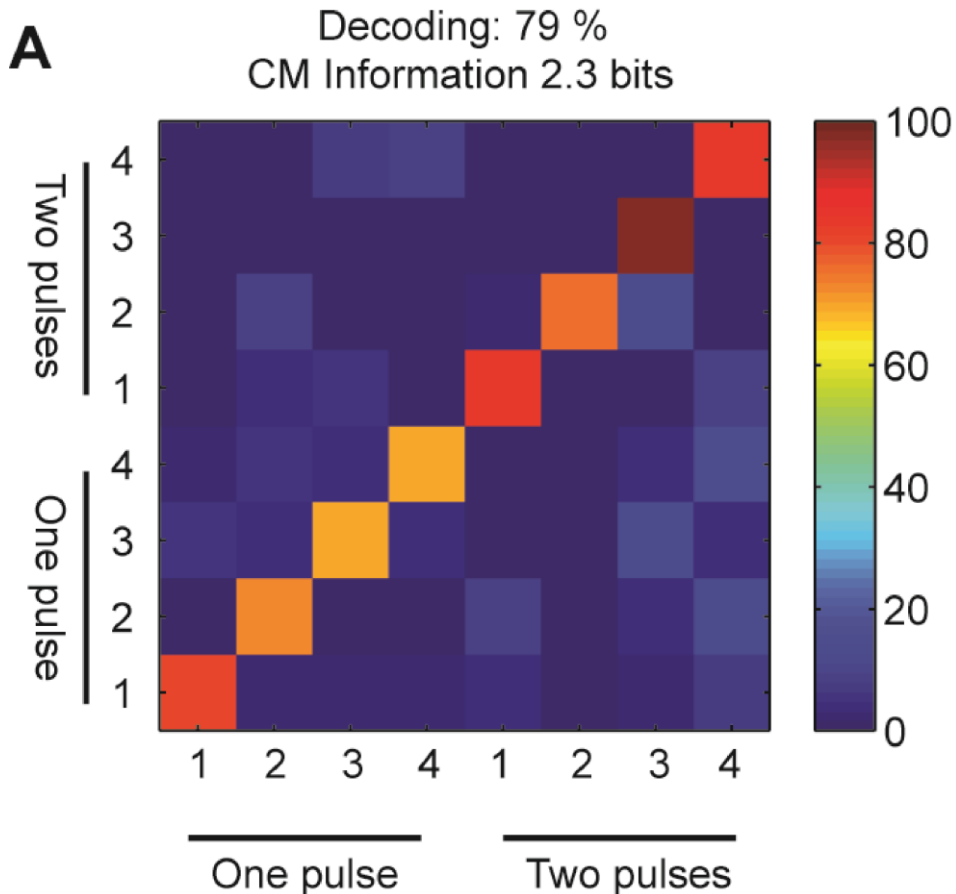
Figure 4. Single and double pulse decoding of a single high-performing neuron (supplementary material, paper II)
The diagonal depicts the decoding level for single and double pulses of each channel. Since there are eight patterns, the chance decoding rate is 12.5 %

In **paper III** we investigate the intracellular response to the stimulation patterns used in paper II. In paper II the focus was on spikes (that can be recorded both extracellularly and intracellularly), although some analysis was performed on the intracellular signals. In paper III we focus only on the intracellular signal, and show that the response to an individual stimulation pulse from a spatiotemporal stimulation pattern can vary depending on i) the temporal position of the pulse in the spatiotemporal pattern ('the timing'), ii) what pattern the pulse was part of ('the context'), and iii) the internal mode of the brain at the moment ('the state'). We make the analogy of a distributed artificial network with several processes running in parallel. The notion of separate states is of course somewhat an abstract construct, but Fig. 5 shows that the cell has a number of characteristic responses -

the amplitude and shape of the EPSP appear to fall in one out of a finite number of distinct response types.
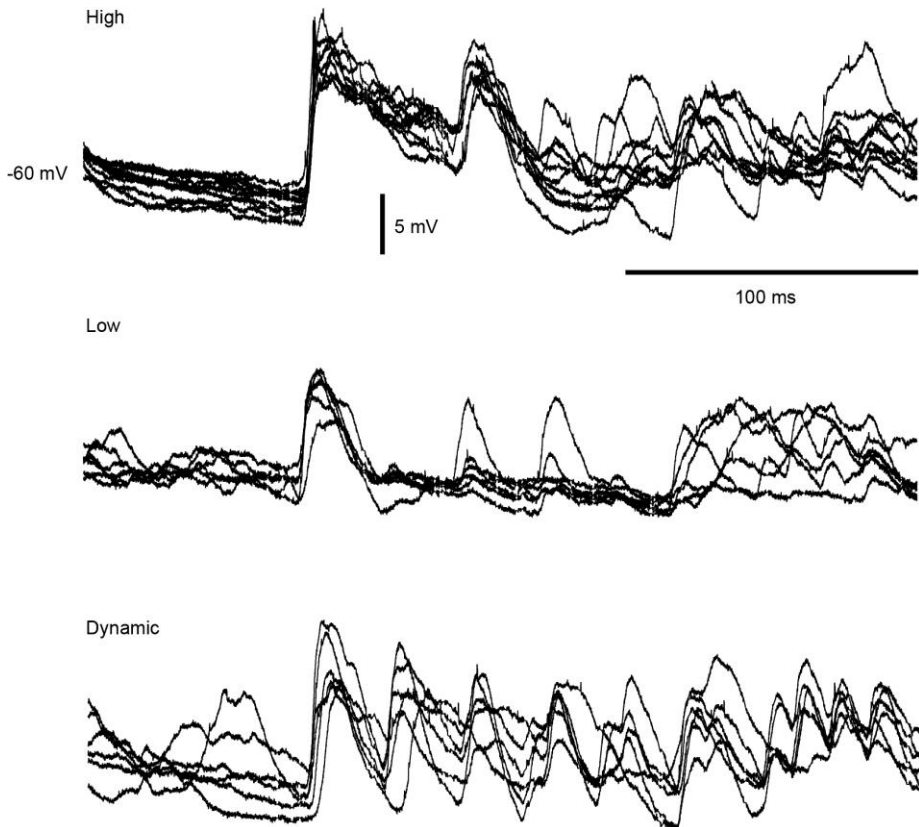
Figure 5. Intracellular response to the same cutaneous spatiotemporal pattern (paper III).
Three different intracellular responses to electrical stimulation of the skin in identical spatiotemporal patterns.

In **paper IV** we focus on pairs of adjacent S1 neurons that were measured simultaneously. We find that the nature of connections between adjacent neurons varies to a large extent, and that the variation is not directly correlated to the cortical depth (or cortical layer) of the neuron. For many neurons the correlograms show a correlation in spike firing, although not primarily stemming from direct synaptic connections. A few neurons however do appear to be monosynaptically connected. The conclusion is that the neocortical circuits have no simple generic formula that is applicable on the level of individual pairs of connected neurons.

16

Methods

Patch clamp

Patch clamp gives a high-resolution insight into the ion currents flowing in and out of an individual cell. The method was developed by Nobel laureates Neher and Sakmann (Hamill, Marty et al. 1981; Zhao, Inayat et al. 2009). To obtain a measurement of the cell activity, a glass pipette is carefully attached to the cell membrane of a neuron. In the whole-cell recording mode, the aim is to generate a hole in the membrane underneath the pipette, which has a diameter of one or a few micrometers. Inside the pipette there is a fluid with the same dominant solute composition that can be found inside the cell, in order to avoid a net migration of solutes in either direction. The pipette is connected to an electric amplifier system, so that the flow of electrical charges through the tip of the pipette, or the potential difference between the inside and the outside of the pipette, can be measured. There are two distinct ways of measuring the cell activity, current clamp and voltage clamp. When measuring in current clamp mode, the flow of electrical charges through the tip is minimized by continuously adjusting the voltage inside the pipette so that it equals the intracellular voltage. Then the membrane potential can be measured as the potential between the inside and the outside of the pipette. In voltage clamp mode, the voltage in the cell is kept constant by injecting currents. Then the flow of current can be used to continuously measure the cell membrane conductivity. In our studies, we have employed the current clamp method.

Bionic finger and generation of spatiotemporal patterns

Since we were interested in looking at the activity of individual cells, it was very important that the stimulation applied to the skin could be repeated in the same animal with a high reproducibility. Having a real object making contact with the research animal's skin will introduce noise and artefacts to the system. A slight change in position or inclination of the contact surface between the object and the skin will result in changes in receptor activation. Another factor to be taken into

account includes the inherent stochasticity in receptor activation. While the global, 'macroscopic' perception of touch could well be identical regardless of these disturbances, the variance introduced is a hindrance to repeatable measurements on the level of individual neurons.

Psychophysical studies have shown that the application of electrical pulses to the skin of a subject are able to evoke the sensation of touching a real object (Oddo, Raspopovic et al. 2016). With an accurate understanding of the activation patterns of the different mechanoreceptors of the skin, it is possible to create a model for how the cutaneous primary afferents will respond to mechanical indentation.

Oddo, Raspopovic et al. (2016) have implemented such a model in a prosthetic fingertip, with the primary afferents of a real finger replaced by piezoresistive sensors. The signals from the sensors are sampled by a microprocessor, where the raw data signals are processed and applied to a spiking neuron model (Fig. 6A). The neuronal model outputs a biomimicking spike pattern representing the signal generated by a population of sensory neurons (Oddo, Mazzoni et al. 2017).
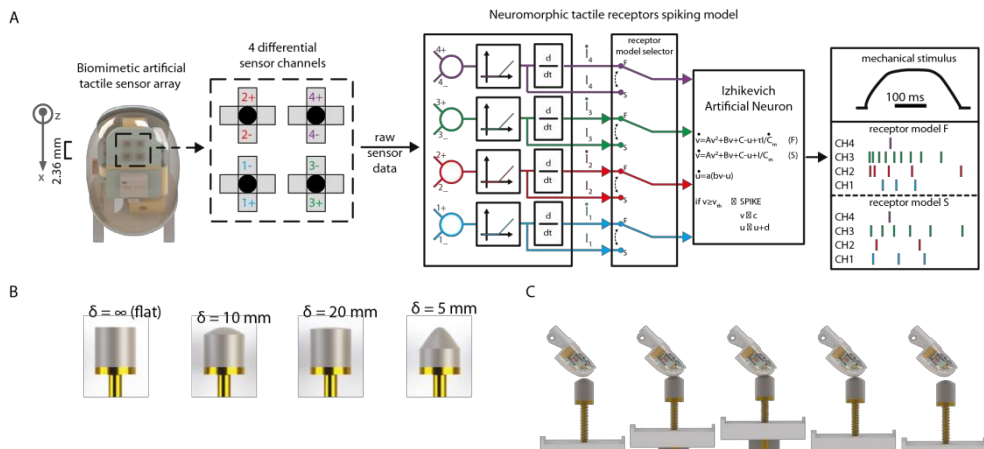
Figure 6. Bionic fingertip sensor (From paper II, including supplementary material)
A. Sensor orientation in artificial fingertip. Transfer function from sensor output to cutaneous receptor activation patterns. B. Curvature of knob that is touched. C. Scotch-yoke mechanism for generation of spatiotemporal patterns.

Using a scotch-yoke mechanism, the bionic finger was set to touch knobs of four different curvatures (Fig. 6B, C). The signal from each piezoresistive sensor was sampled at 380 Hz. The difference in output signal between two adjacent sensors were used as input to a neuron spiking model (Izhikevich 2013). Two different types of receptors were mimicked (see Fig. 7A) In the first case, the measured signal was used directly as input, in the second case the time derivative of the signal was used. Using the derivative as input mimics the behavior of fast adapting neurons (i.e. neurons that primarily respond to change in indentation). With four

different curvatures of the knob, we had a total of eight different spatiotemporal input patterns.
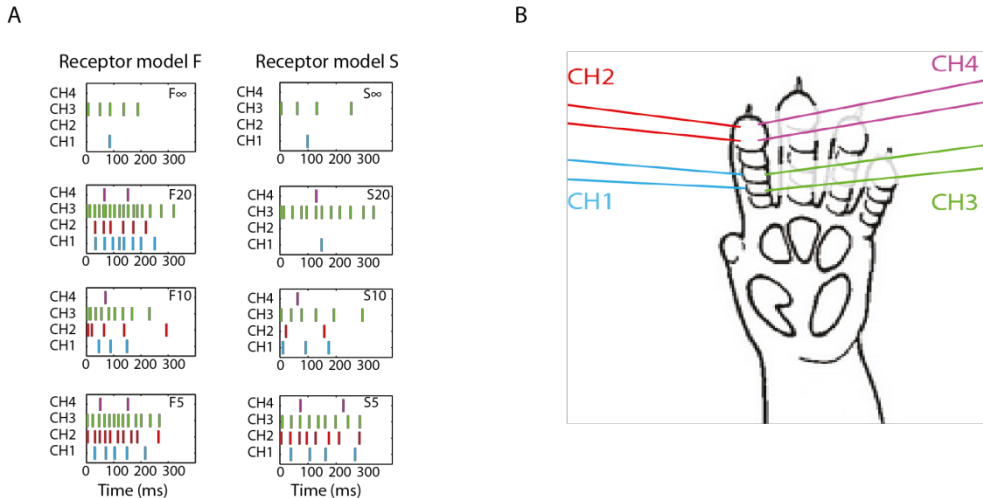
Figure 7. Experimental setup (from paper II)
A. Spatiotemporal patterns for fast adapting and slow adapting neurons. B. Electrode placement in rat digit.

The output from a single cycle of the scotch-yoke mechanism will only yield a sample of the underlying stochastic distribution. Therefore, the process was repeated 100 times for each input pattern, and a representative sample was used as the input in all subsequent experiments. Refer to supplementary material in paper II for a more detailed description of how the spatiotemporal input patterns were generated.

The eight patterns are delivered in a pseudo-randomized order, with electrodes placed as schematically depicted in Fig. 7 B. If the touch stimulation was authentic, there would be some disturbances from noise and stochastic variations in receptor activation. Adding this disturbance would however ruin the purpose of our experimental setup, as we want to create repeatable stimulations, down to a level of the timing of activation of individual primary afferents.

Anesthesia

The rats are initially anesthetized using isoflurane, followed by ketamine and xylazine. The level of anesthesia is continually monitored using an EEG electrode, and by checking for withdrawal reflexes of the limb when the paw is being pinched. The anesthesia was maintained so that the EEG showed sleep spindles and the pinch test did not induce withdrawal reflexes.

Post processing of recorded data

Sampling and filtering

Nearly all postprocessing was performed in Matlab (Mathworks, 2013 – 2017). Some of the template detection and sampling of data for paper I was performed in a previous system that was developed in assembler code.

The sampled patch pipette signal is smoothed using a moving average filter, with a width of 5 samples (50 μs). The stimulation pulses induce transient artefacts to the measured signal. By collecting all post stimulatory transients for each individual electrode, the shape of the transient can be estimated and subtracted from the raw data signal if necessary. We have used the median height for each post-stimulatory sample time point. Normally the transient, if there was one, had disappeared within less than 50 μs.

Spike removal

For some of the studies of intracellular signals (paper II, III), it was necessary to remove intracellular or extracellular spikes. Each spike shape (corresponding to a unique cell) was detected using template matching, and then the generic shape of the spike was estimated. Since the detection time from the template matching can wiggle a couple of sample points around the onset of the action potential, a recursive fitting algorithm was used. At first, the median spike shape was estimated as for the artefacts above. Then the spike time was shifted an integer set of sample time steps for each single spike to minimize the residual. To refine the fit further, the generic spike shape was approximated with a smoothing spline interpolation (Matlab function *spaps*), and then a least square optimization algorithm was applied recursively to find the optimal spike time with a precision that exceeded the constraint given using discrete sampling times. It was rare that intracellular or extracellular spikes interfered with the analysis of the intracellular analysis, but using the recursive filtering approach we were able to determine the height and latency of EPSPs also when they were superimposed by spikes.

Template matching of spikes

The cellular spikes and EPSPs were detected from templates that were defined using a tailor-made click-and-drag interface, available at https://github.com/Neural-basis-of-sensorimotor-control/matlab-analysis

Parametric versus nonparametric tests

If there is an option between parametric and nonparametric tests, the former is obviously better. When data was sparse or not normally distributed we were however confined to perform nonparametric tests, such as Wilcoxon sign rank or rank sum. The main test in paper I, for instance, is a nonparametric test.

The Monte Carlo simulation in paper III is based on the null hypothesis that a single stimulation pulse to the skin has the same probability to evoke an EPSP response in a neocortical neuron, regardless of time and context of the pulse in a spatiotemporal pattern, and the state of the intracortical circuits of the neocortex. The P values in Fig. 6 and 7 of paper III, on the other hand, have been determined with Wilcoxon rank sum test.

Discussion

Cerebellar plasticity

Despite using three different plasticity protocols, we could not detect a potentiation of cerebellar MF – DCN synaptic connections. A negative finding requires bigger sample sizes to prove than a positive finding, but in comparison with previous studies of plasticity in the cerebellar microcircuit it is evident that if there is a synaptic medium-term potentiation, it is significantly smaller than what has been observed in slice studies of juvenile mice (Pugh and Raman 2008).

The extensive branching of the PC dendritic tree allows for the integration of a large number of inputs. This makes it a likely candidate for being the primary mediator of adaptive learning in the adult cerebellum, since the numerous synaptic inputs will increase its chances of finding the most appropriate associations. The high level of plasticity in MF – DCN synapses in cerebellar slices from juvenile mice, reported by Pugh and Raman (2008), can be interpreted from the perspective that the juvenile nervous system first establishes some coarse principles for cerebellar control. In the adult individual, the short and medium term calibration of the cerebellar microcircuit is then primarily carried out by adjustment of synaptic PF - PC weights.

The MF - GrC connections are limited in that there are at most four mossy fibers terminating on each granule cell (Jörntell 2016b). If this was the principal site of plasticity, the selection of mossy fiber inputs that could be associated with other inputs would be heavily constrained compared to if the principal site of plasticity was the PF - PC synapses. The inhibitory Go - GrC connections are more likely to work as regulators that stop the synaptic efficacy to go out of bounds. When the GrC activity goes too high, the inhibitory interneurons will dampen the firing rate. Besides regulating the momentary firing rate, inhibitory interneurons also set a limit to the induced facilitation of synapses of the network (Jörntell 2016b).

Anesthesia

Patch clamp measurements are not stable enough to perform long lasting neuronal recordings (> 30 minutes) in awake animals, but such recordings can be made under anesthesia. It is therefore important to elucidate how neocortical neurons in the neocortex are affected by the anaesthesia. Luczak, Barthó et al. (2009) have shown that the recruitment order for a population of neurons that respond to auditory or somatosensory stimulation is similar to the recruitment order for the same population of neurons during initiation of spontaneous upstates. The recruitment order is also preserved - with some stimuli-specific adjustments - between auditory stimulations of different frequencies. This correlation applies both under anaesthesia and during quiet wakefulness. I have not found a similar study where recruitment order is being compared for the same cortical population during anesthesia and during awakeness, but Constantinople and Bruno (2011) have shown that the average membrane potential during spontaneous upstates is preserved.

Neocortical organization

There is no lack of studies of the visual, auditory and somatosensory system where the cortex - implicitly or explicitly - is divided into distinct areas according to the neuron doctrine or the principle of columnar organization(Swindale 1990; Mountcastle 1997; Doetsch 2000; Buxhoeveden and Casanova 2002; Nicolelis 2011). I will here argue for a more distributed model of cortical processing, by providing alternative interpretations to the studies supporting the labelled line or functional isolationist view presented in the introductory chapters.

The neuron doctrine and the labeled line model

As mentioned in the introduction, the concept of barrel columns in the rat and mice somatosensory cortex has spawned a model of cortical organization that is frequently being applied to sensory processing in general. Although it is an important finding that increased activity in a small area of the barrel cortex can be linked to stimulation of a principal whisker, Brecht and Sakmann (2002) have shown that deflection of a single whisker activates neurons in several barrels of the rat somatosensory cortex. The fact that migrating neurons aggregate in columns as the cortex is being developed (Rakic 1995), as well as that staining protocols in the mature cortex reveal vertical columnar organization in parts of the cortex

(Mountcastle 1997) is also not sufficient to draw conclusion about cortical columns being functionally isolated units. Mountcastle (1997) has pioneered the functional mapping of cortical columns, by stimulating a small receptive field and then measuring the spike response in different parts of the somatosensory cortex. By gradually moving the measurement electrode, the size and location of several cortical columns is estimated. The measured responses are however tainted with other activity going on in the neocortex, both spontaneous activity of neocortical neurons and activity originating in other external or internal processes. The estimated size of a functional column will therefore depend on experimenter's threshold value for what counts as activation. Neurons whose response activity falls under the threshold will drown in the background activity, even when their activity is functionally relevant.

In the introduction I traced the birth of the functional isolationist view of the brain to the ambitious work by Cajal in mapping the morphology of different neurons. Another reason for the persistency of the isolationist view throughout the centuries could be that methodological limitations have resulted in skewed empirical data. The easiest way to create reproducible input to the somatosensory system is to stimulate an isolated receptor or a small group of receptors with electrical single pulses, and then measure the response in the cerebral cortex. However, since this minimalistic input is very different from the authentic tactile stimulation the brain has evolved to process, the measured response will not necessarily answer relevant questions about the authentic sensory processing of the brain. As discussed in paper II, our setup with electrical pulse stimulation with constant voltage amplitude on four channels is also lacking in authenticity when comparing to the afferent signals that would be generated by a physical object indenting the skin. The latter experimental setup lack however in reproducibility between single repetitions of the same stimulation. In order words, there is a trade-off to be made between authenticity and reproducibility of the stimulations.

The emergence of non-invasive imaging methods such as MRI and PET may also have caused a bias towards functional isolationist models. While such methods will provide information of the aggregated activity of neuronal populations, they do not give enough spatial or temporal resolution to monitor the activity of individual neurons. (Logothetis 2008) If, contrary to the labelled line hypothesis, the cortical and subcortical sensory processing is indeed a distributed network phenomena, its underlying principles cannot be elucidated at the level of neuronal populations alone. The use of magnetic resonance imaging techniques to understand the function of the brain has - arguably unduly - been compared to

using a thermometer to reverse-engineer a computer, by measuring the temperature at different locations in its processor (Klingberg 2009). [3]

The hierarchical model of sensory processing is linked to the functional isolationist view of the cortex, but deserves a discussion of its own. From a theoretical perspective, a hierarchical system for sensory processing will not have the same ability to self-assemble or change adaptively as a distributed system. Since the neurons at a lower stage of cortical processing will not receive continuous information about the activity of neurons at higher processing stages, the establishment of synaptic connections from the lowest to the highest level of cortical processing requires the existence of a detailed map with à priori information about which connections to be made in order to arrive at a functional connectome at the end. A more distributed system can change synaptic weights incrementally through a bootstrapping process. There has of course to be a coarse connectional map for the bootstrapping process to be viable, but once in place a distributed system allows for more flexibility from a perspective of an individual both most likely also from an evolutionary perspective. It also provides an explanation as to how we are able to recover from damages to the nervous system or acquire new skills throughout life.

Distributed coding and internal states

The plethora of functional classifications of neocortical neurons on the basis of dendritic morphology, stimuli specificity or other biophysical properties (Doetsch 2000) is clear evidence that no single theory of neocortical connectivity and function has yet been proven convincingly enough to establish consensus in the scientific community. The differentiation in neuronal responses (paper II and III) and in firing correlograms of adjacent neurons (paper IV) show that cortical circuitry is likely heterogeneous and does not follow a simple generic formula. Our comparisons also failed to show a correlation between cortical depth and connectional properties.

Our recordings show that individual neurons have the information from several adjacent receptive fields at hand, but it does not explicitly prove that this is how

---

[3] This critique of MRI and fMRI was briefly mentioned in the book 'Den översvämmade hjärnan' av Torkel Klingberg (Klingberg 2009). Klingberg himself has a prominent career in fMRI research, so the quote is likely not representative of his own opinion. Since he was gratuitous enough to include this counterargument in a work of his, I can reciprocate by quoting neuroanatomist Valentino Braitenberg. Upon being asked how much the spatial and temporal resolution of MRI would have to increase before it could be used as a tool to understand brain function, Braitenberg allegedly replied that 'it makes no sense to read a newspaper using a microscope' (Logothetis 2008).

the information is being used. Luczak's finding about a preserved recruitment order (Luczak, Barthó et al. 2009; Luczak and Barthó 2012) can however be used as a model to interpret our results. The stimuli-specific responses appear to be variations around a consistent pattern of activation. The fact that the majority of connections to cortical neurons are intracortical or corticocortical rather than thalamocortical (Bruno and Sakmann 2006) indicates that the recruitment order is the result of robust internal circuitry. Since single neurons are at the same time able to decode single pulse stimulations from different receptive fields (Fig. 4), the preserved recruitment order is not merely caused by hierarchical architecture of sensory processing networks. Another indication that the neocortical neurons are not only part of feed-forward networks is that the decoding ability increases with time. The shortest time for a single pulse to reach the cortex is on the order of a few ms for rats, yet the decoding efficiency increases several hundred ms after the last stimulation pulse in a pattern (paper II). Some of the delay can be attributed to subcortical processing, but the fact that the first synaptic signals reach the cell at an early stage is a strong indication that intracortical network dynamics play an important role in sensory processing.

The spike-triggered kernel density estimators (SpTKDE) from paired neuron measurements (paper IV) show that adjacent neurons often fire in synchrony, but with the same internal order since there is a sharp peak either before or after t = 0 ms. The number of spikes used to construct the correlograms is large (several hundred or thousands of spikes per neuron), so if the recruitment order was not consistent for the neuron pairs the SpTKDE would have been bloated out around 0 ms. The fact that the SpTKDEs look similar independent of whether there are ongoing stimulation or not is also in line with the findings of Luczak, Barthó et al. (2009).

The intracellular traces depicted in Fig. 5 gives an indication that the response can change between a finite set of states. On a neuronal level, the transition between states can be interpreted as that there are some pathways that are shut off, and others that are opened for transmitting signals (Fig. 8). Given that the amplitude of a unitary EPSP in cortical neurons is of the order of magnitude of 1 mV or less (Bruno and Sakmann 2006; Schoonover, Tapia et al. 2014), the EPSPs in Fig. 5 appears to be generated by tens or hundreds of presynaptic neurons providing simultaneous input. The exact mechanisms mediating the change between states are a question for future investigations, but cerebellar projections to the cortex is a good candidate, as mentioned in the section about the cerebellum above. In a preceding chapter I mentioned that the cerebellum works as associative memory, with a massive storage capacity provided by the Purkinje cell dendritic trees. Since the cerebellum samples information from a large set of spinal, cortical and subcortical systems, it is well equipped to coordinate the states of cortical circuits in order to increase the global performance of the CNS.
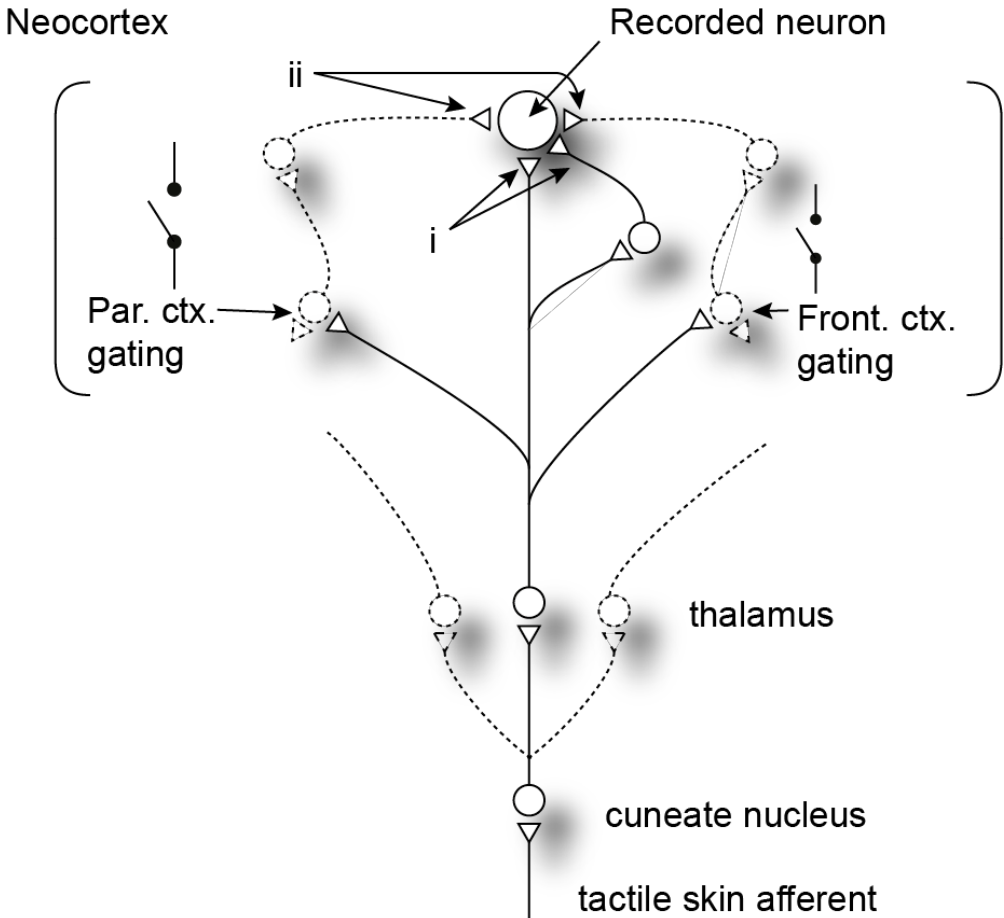
Figure 8. Schematic network model for tactical processing.
The network will allow for different pathways to be activated, depending on the internal state of the circuit. There is also room for parallel processing streams to activate the network simultaneously.

Self-assembly

When discussing how millions of neocortical neurons can self-organize to form a functional model of distributed sensory processing, it helps to bear in mind that the biomechanical properties of joints, muscles and tendons will create natural constraints for which neurons that fire together. It is likely that an important part of the self-assembly process is to strengthen synaptic connections that naturally fire together during everyday behavior. Jörntell (2016a) has outlined a model where afferent sensory information is used to continuously coordinate the motor system, primarily via cerebellar activity. The sensory processing is then not only a

distributed phenomenon in itself, but it is also inseparably intertwined with the efferent signals of the motor system.

Returning to the discussion of neural coding in a previous chapter, it is worth pointing out that a dense coding regime is much more compatible with the boot-strapped distributed model of sensory processing than a sparsely or locally coded regime. The more sparse the coding is, the less information each neuron will have at hand to steer the self-assembly process during development, neural repair or acquisition of new skills. The discussion about redundancy in sensory signalling is also relevant in this context. As mentioned in a previous section, studies on the cuneate nucleus (Jörntell, Bengtsson et al. 2014), shows that the redundancy in neural signalling that exists at a coarse level disappears when more refined experimental methodologies are employed. From a developmental perspective, it makes sense if the signalling is first established at a coarse level, and then the information content can be gradually increased by adjusting the synaptic weights of individual neurons, without losing the information in the coarse signal. Renart, de la Rocha et al. (2010) have presented a theoretical model where neurons sharing synaptic input end up having negatively correlated synaptic currents, through a feedback process involving the activity excitatory and inhibitory neurons in conjunction. In paper IV we conclude that although the firing pattern of adjacent cortical neurons is synchronized it is not simultaneous. Since adjacent neurons can be assumed to have similar synaptic input at least to some degree, our study supports the model of enforced differentiation in neuronal activity. Another benefit of the enforced differentiation is that it allows for the information in the coarse (averaged) signal to be kept intact, since the increase and decrease in individual response patterns can be synchronized so that they cancel each other out at the coarse level.

Animal research – ethical questions

If research on animals had not been necessary for the advancement of biomedical research, it would have been abolished a long time ago. The costs and methodological challenges associated with animal research compared to using theoretical models such as computer simulations, or other less invasive research methods is vast. In order to study the integrative physiology of the nervous system or other bodily functions, laboratory animals cannot be dispensed of.

Animals bred and raised for research purposes generally get a better treatment than animals raised for being consumed as meat, or even some of the animals kept as pets. The reason is not only legislature and the private moral considerations of the people in the research industry, but also that a stressed, malnourished or diseased animal will yield less trustworthy results than an animal that is in a good condition physically and mentally. During the experimental procedure the animals are anesthetized following rigorously articulated regulations, and it is critical for the outcome of the experiment that the animals do not come out of the anesthesia or in other ways percept pain or discomfort. At the end of the experiment the animal is sacrificed with an injection. In the case of decerebrate preparations (paper I), the animal is initially anaesthetized, and then the connections between the cerebrum and the brainstem is removed. From a clinical perspective, and our current understanding of consciousness and cognition, this is a state in which the cognitive functions have ceased to exist.

The discussion of whether animals at all can be used as means for human ends is beyond the scope of this text, refer to Singer (1993) or Scruton (2000) for a more comprehensive discussion on the topic.

Populärvetenskaplig sammanfattning på svenska

Den här avhandlingen handlar om hur hjärnan behandlar sinnesintryck. Vi har valt att titta på hudstimuleringar, men de processer vi studerar rör allmängiltiga frågor om hur hjärnan fungerar.

När vi vidrör något med vårt pekfinger aktiveras hudreceptorer i fingret, som skickar en signal till hjärnbarken (den yttersta, skrynkliga delen av hjärnan). Signalen går inte direkt till hjärnbarken utan den omkopplas via celler i ryggraden, hjärnstammen och talamus. Hjärnstammen sitter som en utväxt på ryggraden, och talamus är en rund struktur mitt i hjärnan som tar emot och skickar information mellan olika delar av hjärnan. Det finns olika teorier för hur bearbetningen går till, både innan signalen når hjärnbarken och efter att den har nått hjärnbarken. En förklaringsmodell för hur signalen fortplantas innan den når hjärnbarken som förekommer i många textböcker och artiklar kallas för *labelled line*-hypotesen. Enligt labelled line-hypotesen hålls informationen från varje mikroskopiskt hudområde separerad från informationen från andra hudområden tills den når hjärnbarken. Enligt denna hypotes går det att peka på ett enskilt område i hjärnbarken och säga exakt vilket mikroskopiskt hudområde det tar emot information från.

En populär teori för hur informationsbearbetningen går när signalerna nått hjärnbarken kallas för *grandma neuron hypothesis*. Den säger att det finns en enskild hjärncell som aktiveras när man ser, hör eller läser om sin mormor. På samma sätt finns det en annan hjärncell som aktiveras när man ser, hör eller läser om Jennifer Aniston, Halle Barry, Eiffeltornet, operahuset i Sydney etcetera[4]. För att all information som rör ens mormor skall kunna konvergera till en enskild hjärncell så måste informationsbearbetningen i hjärnbarken vara hierarkiskt organiserad. Mormorsneuronet är givetvis bara ett hypotetiskt exempel för att förklara denna mer generella princip. I många fall har hypotesen modifierats genom att man ersätter enskilda neuron med grupper av neuron (så kallade

---

[4] Exemplen är tagna från Quiroga, R., L. Reddy, et al. (2005). "Invariant visual representation by single neurons in the human brain." <u>Nature</u> **435**: 1102-1107.

kortikala kolumner) som minsta funktionella enhet. Principen med hierarkisk informationsbearbetning är dock kvar.

Vi har stimulerat huden i pekfingret med elektriska signaler i ett mönster som skall efterlikna beröring. En anledning att vi använder oss av elektriska signaler istället för riktig beröring är att man då kan upprepa samma 'beröring' flera gånger utan att det blir för stora skillnader mellan varje gång. Sedan har vi mätt aktiviteten i hjärnceller i hjärnbarken. Vi har använt oss av matematiska metoder för att avgöra hur mycket information från det stimulerade hudområdet som varje enskild hjärncell har tillgång till. Vi har dragit slutsatsen att hjärnceller som arbetar tillsammans är mycket bättre på att avgöra skillnaden mellan olika typer av beröring än enskilda hjärnceller, samtidigt som enskilda hjärnceller har information från flera olika hudreceptorer. Att flera hjärnceller som arbetar tillsammans är bättre på att avgöra vilken typ av beröring huden utsätts för talar för att informationsbearbetningen är distribuerad snarare än hierarkiskt organiserad. Att enskilda hjärnceller har tillgång till information från flera olika hudreceptorer tyder på att signalerna *inte* är separerade från varandra på vägen till hjärnbarken, utan att de blandas och att en del av informationsbearbetningen sker redan i ryggraden, hjärnstammen och / eller talamus. Sammanfattningsvis innebär det att våra resultat strider mot vad som förutsägs av både labelled line-hypotesen och grandma neuron hypothesis.

En annan struktur som är inblandad i behandlingen av sinnesintryck är lillhjärnan. Lillhjärnan har kopplingar till många olika delar av nervsystemet, och påverkar bland annat koordinationen mellan känselsinnet och rörelseapparaten. Känselsinnet är inte bara en passiv funktion i hjärnan, tänk exempelvis på hur omöjligt det vore att knäppa en knapp eller knyta sina skor med slutna ögon om man inte kunde vägledas av sitt känselsinne. Eftersom man både under uppväxten och som vuxen ständigt lär sig nya saker (som att knäppa knappar, spela piano eller skriva för hand) är inlärning ett viktigt koncept även när man talar om känselsinnet. Studier på människor och andra djur har bekräftat att lillhjärnan har en central roll vid inlärning. Den är uppbyggd av enhetliga mikrostrukturer, som upprepas i hela den globala strukturen (se figur 1, sidan 10). Den första artikeln i denna avhandling handlar om *var* i lillhjärnans mikrostruktur inlärningen sker. Vi kommer fram till att den del av mikrostrukturen vi tittar på (MF - DCN i figur 1) är relativt statisk i vuxna individer. Tidigare studier har dock visat att denna koppling är mer plastisk vid inlärning i växande än färdigvuxna individer. Det talar för att mekanismen för att uppdatera nervsystemet när man lär sig nya färdigheter ser olika ut i växande jämfört med vuxna individer.

Acknowledgements

When I graduated from Lund University with a degree in Engineering in combination with some electives in cell biology, starting a PhD in neuroscience seemed to be the most logical thing to do. However, after reviewing the different opportunities at hand, I chose to work with software engineering and algorithm development for a number of years, and ended up in Stockholm for a while. I was still keeping half an eye open for positions in neuroscience, just in case I was moving back to Skåne at some point. The call to action came when I got in contact with **Henrik Jörntell** in late spring 2012. About a year after our first contact I started as a PhD student under his supervision.

I am very grateful to have had Henrik as a supervisor, and that is no joke. The door to his room has always been open whenever I needed to discuss some aspects of my work. In the course of completing my PhD I have been blessed with two children (Frans and Finn) and strived to maintain my alternative career as an engineer. This would not have been possible without Henrik allowing me to work at odd times sometimes. I have been given ample doses of both freedom and responsibility in how take things on.

The second thing I am grateful about is the group. Everyone seems to have at least two or three different projects running in parallel, inside and outside of academia, but still I have always had help with whatever question I always wanted to discuss. I especially want to thank the following people: **Kersti Larsson**, for your surgical skills and patience with my initial lack thereof. **Pontus Geborek**: for teaching me about the practicalities of patch clamp recording and getting me started on the data analysis. **Johanna Norrlid**, for contributing both with experimental data and analysis on the papers we have done together. **Anton Spanne**: for providing advice on everything from mathematical statistics to gardening. **Anders Wahlbom**, for all the invaluable experimental data you have provided. **Fredrik Bengtsson:** for getting me started in the lab and being a good co-supervisor. **Jonas Enander**, for letting me tap into some of your knowledge about Python programming. And thanks to **Helén Axelberg** for taking over after Kersti, although I resigned from lab work before you started here. **Astrid**, **Samuel**, **Tina**, **Erik**, **Erik**, - thanks for contributing with analysis during your respective thesis work, and for being beta testers of my software tools for spike detection and analysis.

The Calogero Oddo group - thanks for excellent collaboration. There have been so many Italian students and researchers here that I dare not name them all, for fear of omitting someone, but a special thanks to **Udaya**, **Clara** and **Calogero**.

The **Germund Hesslow** group - thanks for being inspirational and good company. Hopefully our groups will keep being neighbors for a long time to come.

To go further back in time, the initial seed that developed into the idea of venturing into this scientific field full of rabbit holes and contradictory views was born at a lecture by Professor **John Barton Furness** more than ten years ago. The idea took a more concrete form when I attended a conference talk by **Rune Berg**, from Copenhagen University, in 2009.

There are many people outside the university that have been important in the context of writing this thesis. The help of my parents **Karin** and **Peter**, as well as Edith's parents **Kathrin** and **Paul** in taking on the children has been absolutely essential, and that is also no joke. Looking back at my old upbringing, I realize that they will be as important to my children as my grandparents - **Lill** and **Sten**, **Lena** and **Bengt** - have been to me, which is a very comforting thought.

I cannot stress enough the help of my better half **Edith**, who has always had my thesis in mind when planning her work, holidays and other aspects of our life. Without Edith there would not have been a dissertation at all, and if there hypothetically would have been one, it would not have been as fun to complete. And **Frans** and **Finn**, you are the sunshines of our lives.

References

Abraira and Ginty (2013). "The Sensory Neurons of Touch." Neuron **79**(4).

Azevedo, F. A. C., L. R. B. Carvalho, et al. (2009). "Equal numbers of neuronal and nonneuronal cells make the human brain an isometrically scaled-up primate brain." J. Comp. Neurol **513**: 532-541.

Barlow, H. B. (1972). "Single units and sensation: a neuron doctrine for perceptual psychology?" Perception **1**(4): 371-394.

Bengtsson, F., R. Brasselet, et al. (2013). "Integration of Sensory Quanta in Cuneate Nucleus Neurons *In Vivo*." PLoS ONE **8**(2).

Bengtsson, F. and H. Jörntell (2014). "Specific Relationship between Excitatory Inputs and Climbing Fiber Receptive Fields in Deep Cerebellar Nuclear Neurons " PLOS ONE **9**(1).

Brecht, M. and B. Sakmann (2002). "Dynamic representation of whisker deflection by synaptic potentials in spiny stellate and pyramidal cells in the barrels and septa of layer 4 rat somatosensory cortex." Journal of Physiology **543**(1): 49-70.

Bruno, R. and B. Sakmann (2006). "Cortex is driven by weak but synchronously active thalamocortical synapses." Science **16**(312(5780)): 1622-1627.

Buxhoeveden, D. and M. Casanova (2002). "The minicolumn hypothesis in neuroscience." 125 **2**: 935-951.

Constantinople, C. M. and R. M. Bruno (2011). "Effects and Mechanisms of Wakefulness on Local Cortical Networks." Neuron **69**(6): 1061–1068.

Darian-Smith and Kenins (1980). "Innervation density of mechanoreceptive fibres supplying glabrous skin of the monkey's index finger." The Journal of Physiology **309**: 147-155.

Dean, P., J. Porrill, et al. (2009). "The cerebellar microcircuit as an adaptive filter: experimental and computational evidence." Nature Reviews Neuroscience **11**: 30.

DeFelipe, J. and I. Fariñas (1992). "The Pyramidal Neuron of the Cerebral Cortex: Morphological and Chemical Characteristics of the Synaptic Inputs." Prog Neurobiol. **39**(6): 563-607.

Doetsch, G. (2000). "Patterns in the brain. Neuronal population coding in the somatosensory system." Physiol Behav. **69**(1-2): 187-201.

Dum, R. P. and P. L. Strick (2003). "An Unfolded Map of the Cerebellar Dentate Nucleus and its Projections to the Cerebral Cortex." J Neurophysiol **89**: 634-639.

Felleman, D. and D. van Essen (1991). "Distributed hierarchical processing in the primate cerebral cortex." Cereb Cortex. **1**(1): 1-47.

Frank, B., B. Schoch, et al. (2007). "Cerebellar Lesion Studies of Cognitive Function in Children and Adolescents - Limitations and Negative Findings." Cerebellum **6**(3): 242–253.

Gerfen, C. R., R. Paletzki, et al. (2013). "GENSAT BAC cre-recombinase driver lines to study the functional organization of cerebral cortical and basal ganglia circuits." Neuron **80**(6): 1368-1383.

Gibson, A., K. Horn, et al. (2004). "Activation of Climbing Fibers." Cerebellum **3**(4): 212-221.

Guillery, R. and S. Sherman (2011). "Branched thalamic afferents: what are the messages that they relay to the cortex?" Brain Res Rev. **66**(1-2): 205-219.

Guyton and Hall (2006). Textbook of Medical Physiology, Elsevier.

Hamill, O., A. Marty, et al. (1981). "Improved patch-clamp techniques for high-resolution current recording from cells and cell-free membrane patches." Pflugers Arch. **391**(2): 85-100.

Harris, K. and G. Shepherd (2015). "The neocortical circuit: themes and variations." Nat Neurosci. **18**(2): 170-181.

Hubel, D. and T. Wiesel (1961). "Receptive fields, binocular interaction and functional architecture in the cat's visual cortex." The Journal of Physiology **160**(1): 105-154.

Isope, P. and B. Barbour (2002). "Properties of unitary granule cell --> Purkinje cell synapses in adult rat cerebellar slices." J Neurosci. **22**(22): 9668-9678.

Izhikevich, E. (2013). "Simple model of spiking neurons." IEEE Transactions on Neural Networks **14**(6): 1569 - 1572.

Jiang, X., S. Shen, et al. (2015). "Principles of connectivity among morphologically defined cell types in adult neocortex." Science **350**(6264).

Johansson and Vallbo (1979). "Tactile sensibility in the human hand: relative and absolute densities of four types of mechanoreceptive units in glabrous skin." The Journal of Physiology **286**: 283-300.

36

Jörntell, Bengtsson, et al. (2014). "Segregation of tactile input features in neurons of the cuneate nucleus." Neuron **83**(6): 1444-1452.

Jörntell, H. (2016a). "Cerebellar physiology: links between microcircuitry properties and sensorimotor functions." J Physiol. **595**(1): 11-27.

Jörntell, H. (2016b). "Cerebellar Synaptic Plasticity and the Credit Assignment Problem." Cerebellum **15**(2): 104-111.

Jörntell, H. and C. Ekerot (1999). "Topographical organization of projections to cat motor cortex from nucleus interpositus anterior and forelimb skin." J Physiol. **514**(2): 551-566.

Jörntell, H. and C. Ekerot (2006). "Properties of somatosensory synaptic integration in cerebellar granule cells in vivo." J Neurosci. **26**(45): 11786-11797.

Kandel, Schwartz, et al. (2013). Principles of Neural Science, The McGraw-Hill Companies, Inc.

Klingberg, T. (2009). Den översvämmade hjärnan, Natur & Kultur.

Logothetis (2008). "What we can do and what we cannot do with fMRI." Nature **453**: 869–878.

Luczak, A. and P. Barthó (2012). "Consistent sequential activity across diverse forms of UP states under ketamine anesthesia." Eur J Neurosci. **36**(6): 2830-2838.

Luczak, A., P. Barthó, et al. (2009). "Spontaneous events outline the realm of possible sensory responses in neocortical populations." Neuron **62**(3): 413-425.

Manita, S., T. Suzuki, et al. (2015). "A Top-Down Cortical Circuit for Accurate Sensory Perception." Neuron **86**(5): 1304-1316.

Marr, D. (1969). "A theory of cerebellar cortex." J Physiol. **202**(2): 437-470.

Mountcastle, V. B. (1997). "The columnar organization of the neocortex." Brain Res Rev. **120**(4): 701-722.

Nicolelis, M. (2011). Beyond boundaries: the new neuroscience of connecting brains with machines - and how it will change our lives.

Oddo, C. M., A. Mazzoni, et al. (2017). "Artificial spatiotemporal touch inputs reveal complementary decoding in neocortical neurons." Sci Rep **8**: 45898.

Oddo, C. M., S. Raspopovic, et al. (2016). "Intraneural stimulation elicits discrimination of textural features by artificial fingertip in intact and amputee humans." eLife **5**(09148).

Pereira, J. J. and R. Alves (2011). "The labelled-line principle of the somatosensory physiology might explain the phantom limb phenomenon." Med Hypotheses. **77**(5): 853-856.

Petersen (2007). "The Functional Organization of the Barrel Cortex." Neuron **56**(2): 339-355.

Pugh, J. and I. Raman (2008). "Mechanisms of potentiation of mossy fiber EPSCs in the cerebellar nuclei by coincident synaptic excitation and inhibition." J Neurosci. **28**(42): 10549-10560.

Quiroga, R., L. Reddy, et al. (2005). "Invariant visual representation by single neurons in the human brain." Nature **435**: 1102-1107.

Rakic, P. (1995). "Radial versus tangential migration of neuronal clones in the developing cerebral cortex." Proc. Natl Acad Sci **92**: 11323–11327.

Renart, A., J. de la Rocha, et al. (2010). "The Asynchronous State in Cortical Circuits." Science **327**(5965): 587-590.

Schoonover, C. E., J.-C. Tapia, et al. (2014). "Comparative Strength and Dendritic Organization of Thalamocortical and Corticocortical Synapses onto Excitatory Layer 4 Neurons." The Journal of Neuroscience **34**(20): 6746 – 6758.

Scruton, R. (2000). Animal Rights and Wrongs, Metro Books, in association with Demos.

Sherman, S. M. (2007). "The thalamus is more than a relay." Current opinion in neurobiology **17**(4): 417-422.

Sherman, S. M. (2016). "Thalamus plays a central role in ongoing cortical functioning." Nat Neurosci. **19**(4): 533-541.

Simons, D. and P. Land (1987). "Early experience of tactile stimulation influences organization of somatic sensory cortex." Nature **326**(6114): 694-697.

Singer, P. (1993). Practical Ethics, Cambridge University Press.

Spanne, A. and H. Jörntell (2013). "Processing of Multi-dimensional Sensorimotor Information in the Spinal and Cerebellar Neuronal Circuitry: A New Hypothesis " PLOS Computational Biology **9**(3).

Spanne, A. and H. Jörntell (2015). "Questioning the role of sparse coding in the brain." Trends Neurosci. **38**(7): 417-427.

Strehler, B. L. and R. Lestienne (1986). "Evidence on precise time-coded symbols and memory of patterns in monkey cortical neuronal spike trains." Proc Natl Acad Sci USA. **83**(24): 9812-9816.

Swindale, N. V. (1986). "Neurophysiology. Parallel channels and redundant mechanisms in visual cortex." Nature **322**(6082): 775-776.

Swindale, N. V. (1990). "Is the cerebral cortex modular?" TINS **13**(12): 487-492.

Woolsey, T. A. and H. Van der Loos (1970). "The structural organisation of layer IV in the somatosensory region (SI) of the mouse cerebral cortex: the description of a cortical field composed of discrete cytoarchitectonic units." Brain Res. **17**: 205-242.

Zhao, Y., S. Inayat, et al. (2009). "Patch clamp technique: Review of the current state of the art and potential contributions from nanoengineering." Proceedings of the Institution of Mechanical Engineers Part N Journal of Nanoengineering and Nanosystems **222**(1): 1-11.

Paper I

CrossMark

No Medium-Term Spinocerebellar Input Plasticity in Deep Cerebellar Nuclear Neurons In Vivo?

Hannes Mogensen[1] · Fredrik Bengtsson[1] · Henrik Jörntell[1]

Abstract The existence of input plasticity in the deep cerebellar nuclear (DCN) cells of the adult cerebellum could have profound implications for our understanding of cerebellar function. Whereas the existence of plastic changes in mossy fiber (mf) synaptic responses in DCN neurons has been demonstrated in juvenile slices, there has so far been no direct demonstration of this form of plasticity in the adult cerebellum in vivo. In the present paper, we recorded from neurons in the anterior interposed nucleus (AIN) and stimulated the spinocerebellar tracts (SCT) directly or via the skin to obtain mf activation and the inferior olive to activate climbing fibers (cfs) in the nonanesthetized, adult, decerebrated cat. We used three different types of protocols that theoretically could be expected to induce plasticity, each of which involved episodically intense afferent activation lasting for 10 min. These were conjunctive mf-cf activation, which effectively induces plasticity in cortical neurons; mf and cf activation in a pattern resembling the protocol for inducing classical conditioning; and conjunctive activation of two excitatory mf inputs. None of these protocols had any statistically significant effect on the evoked responses in the AIN neurons. We conclude that the input plasticity for excitatory mfs in the AIN cells of the adult cerebellum in vivo is likely to be less effective than that of parallel fiber synaptic inputs in cerebellar cortical cells, at least in the timespan of 1 h.

Keywords Plasticity · Deep cerebellar nuclear neurons · Mossy fibers · Climbing fibers

✉ Henrik Jörntell
  henrik.jorntell@med.lu.se

[1] Neural Basis of Sensorimotor Control, Department of Experimental Medical Science, Lund University, BMC F10, Tornavägen 10, 221 84 Lund, Sweden

Introduction

Plasticity in the neurons of the deep cerebellar nuclei as a substrate for behavioral learning has been debated for a long time, and theoretical predictions and circumstantial evidence have been used to argue that it may be required in some situations of presumed cerebellar-dependent adaptation [7, 24, 25, 29, 34]. Plasticity of deep cerebellar nuclear (DCN) neuron intrinsic excitability [1] and mossy fiber (mf) inputs [26, 27] have been demonstrated in vitro, but in these cases, only for slice preparations of the juvenile cerebellum. Whereas major changes in the circuitry structure and physiology may be expected to occur during development, cerebellar adaptation works also in adult life and it is important for our understanding of the functioning of the cerebellum to know whether these changes can occur and consequently contribute to adaptation and learning also during adult life. A recent indication that this may be the case was a study where sprouting of mf axons in the DCN was observed after a period of intense training over several days, but this is typically one order of magnitude slower than the timescale on which the cerebellar adaption is believed to work [5]. In any case, it remains to be shown that the effective input to the DCN neurons increases under these conditions.

From a limb control point of view, an important source of information to the neurons of the interpositus nuclei comes from the spinocerebellar and spinoreticulocerebellar systems (SCTs). These are among the few mf systems that have been shown to directly innervate DCN neurons through collaterals of their axons that pass by the nuclei before they form mf synapses in the cortex [3, 19–23, 33]. These mf systems sample information about ongoing activity in spinal sensorimotor circuits, which may be crucial for our capacity to achieve limb intersegment coordination [31]. Hence, synaptic plasticity in the mf-DCN connections of these systems could theoretically

🖄 Springer

alter the conditions for limb coordination control. A consistent relationship between the location of the cutaneous climbing fiber (cf) receptive field and the distribution of skin areas from which excitatory inputs were evoked in anterior interposed nucleus (AIN) neurons was recently described [3]. This relationship suggests the presence of a cf-dependent plasticity mechanism for regulating the excitatory mf inputs to DCN neurons. Alternatively, the location of the cf receptive field reflects the motor control function of the DCN cell [6, 13], and the synapses of the spinocerebellar tract (SCT) mfs most frequently associated with that specific motor control function could be strengthened through activity-dependent mechanisms, possibly NMDA-receptor dependent [27], triggered by the degree of correlated pre- and postsynaptic activity.

In the present study, we addressed the issue of mf-DCN neuron plasticity using direct electrical activation of the SCTs or skin stimulation to activate the cutaneously activated components of the SCTs. These inputs were combined with each other to address the possible induction mechanism described above. To also explore protocols known to be effective at the cortical level, we combined the SCT input with conjunctive cf input [14] or, alternatively, let the train of SCT stimulation be followed by cf activation, i.e., a similar temporal relationship as in classical conditioning protocols [11] (Fig. 1). The inputs were repeated at high intensity for 10 min, and the effects on the mf-AIN input were tracked for about 1 h. We find that neither of the three protocols produces any statistically significant change in the AIN cell responses to inputs from the mf pathways. The contrast with the previously described dramatic input plasticity effects in the neurons of the cerebellar cortex, using similar protocols, is discussed.

Materials and Methods

Ethics Statement

The experimental procedures were approved in advance by the Malmö/Lund Animal Research Ethics Committee (permit number and approval-ID: M32-09 and M05-12). Initial surgery was performed under propofol anesthesia, and all efforts were made to minimize suffering. Our EEG recordings were characterized by a background of periodic 1–4 Hz oscillatory activity, periodically interrupted by large-amplitude 7–14 Hz spindle oscillations lasting for 0.5 s or more. These forms of EEG activities are normally associated with deep stages of sleep. The pattern of EEG activity and the blood pressure remained stable and did not change with noxious stimulation throughout experiments.

Preparation

Adult cats ($N = 14$) were prepared as previously described. Briefly, following an initial anesthesia with propofol (Diprivan® Zeneca Ltd., Macclesfield Cheshire, UK), the animals were decerebrated at the intercollicular level and the anesthesia was discontinued. The animals were artificially ventilated and the end-expiratory CO_2, blood pressure, and rectal temperature were continuously monitored and maintained within physiological limits. Mounting in a stereotaxic frame, drainage of cerebrospinal fluid, pneumothorax, and clamping the spinal processes of a few cervical and lumbar vertebral bodies served to increase the mechanical stability of the preparation. The dorsal part of the pars intermedia of the left cerebellum was exposed to allow microelectrode access to the AIN. An additional exposure was made of the brainstem/ spinal cord junction between the base of the skull and the first cervical vertebra. All exposed areas were covered in paraffin oil to prevent tissue drying.

Recordings and Stimulation

Patch clamp pipettes or metal microelectrodes (tungsten-in-glass microelectrodes, exposed tip 10–20 μm) were advanced to target the AIN as previously described [3, 4]. All neurons included in this study were putative glutamatergic projections neurons, based on the preponderance of short (<25 ms) interspike intervals and intermediate spike-widths [4]. We recorded neurons from both forelimb and hindlimb regions of this nucleus, as identified using the location of the cf receptive field of the afferent Purkinje cells (Fig. 1). This location can be mapped out using electrical stimulation of the skin (0.1 ms pulses of 1.0 mA applied through percutaneous needle electrodes [16])—if the cfs of the locally afferent Purkinje cells are activated by the stimulation, characteristic local field potentials [6, 8] and postinhibitory rebound responses of the DCN neurons can be recorded [4]. In this way, the location of the cf receptive field can be identified.

In order to stimulate the spinocerebellar and spinoreticulocerebellar tracts, which provide direct mf synaptic inputs to the interpositus nuclei, we placed a tungsten-in-glass microelectrode (exposed tip 50–150 μm) for stimulation laterally at the border between the spinal cord and brainstem. Using this stimulation microelectrode, mf field potentials recorded inside the AIN were routinely evoked at threshold intensities of <20 μA (single stimulus pulse of 0.1 ms duration), suggesting an effective recruitment of directly and synaptically activated (via the lateral reticular nucleus) mf synapses. In addition, we used electrical skin stimulation (pair of percutaneous needle electrodes with 5–10 mm spacing, stimulated at 1 mA shocks with 0.1 ms duration) to recruit another putative pool of spinocerebellar mfs. Cutaneous input is known to activate parts of the spinocerebellar neuron population, and since the other pathway mediating cutaneously activated mf input, the main cuneate nucleus does not terminate in the AIN [9]; potent excitatory responses evoked from the skin [3] are
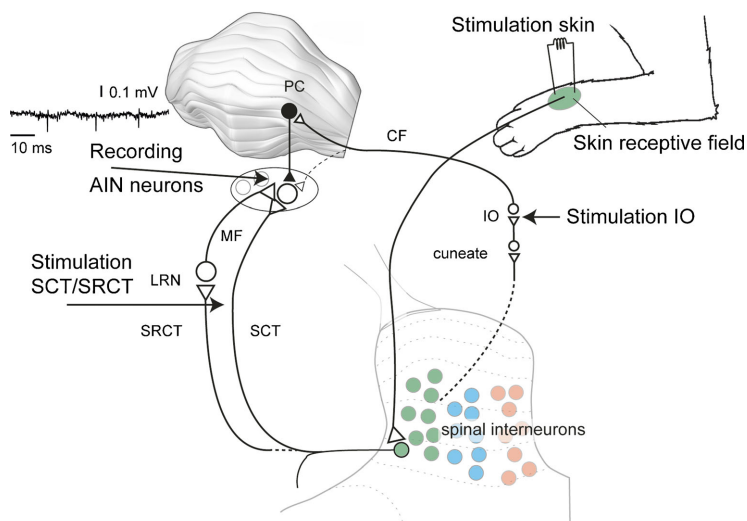
Fig. 1 Targeted circuitry structures. Recordings were made from neurons of the anterior interposed nucleus (*AIN*). Direct electrical activation at the level of the lateral reticular nucleus (*LRN*) in the brainstem presumably activated both fibers of passage of the spinocerebellar tracts (*SCTs*) and the spinoreticulocerebellar tract or pathway (*SRCT*), where the latter represents spinal interneuron information that is forwarded to the cerebellum after a synapse in the LRN. SCT and SRCT pathways, which make mossy fiber (*MF*) synapses with the AIN neurons, were also activated using electrical stimulation of the skin. Importantly, the electrical skin stimulation was made from specific receptive fields that did not overlap the climbing fiber (*CF*) receptive field of the Purkinje cells (*PCs*) that were afferent to the AIN neuron recorded from [4, 6]. Climbing fiber activation was achieved by direct electrical stimulation in the inferior olive (*IO*).

likely due to spinocerebellar mfs which should be at least partly non-overlapping with the population of mfs activated from the brain stem. The skin stimulation used was verified to not activate the afferent cfs and evoked a monophasic excitatory response [3].

In order to activate cfs, a second stimulation electrode was placed in the inferior olive, where low-threshold cf responses (evoked at <10 μA) could be evoked in the pars intermedia of the cerebellar cortex and in the AIN [4, 15].

Protocols

Using the SCT or skin stimulation as test stimulation, we applied three different stimulation protocols to investigate whether plasticity in the input to the AIN neurons could be recorded. In most cases, more than one protocol was applied in the same experiment. When this was the case, the recording electrode was moved to a different location in the AIN, where neurons had substantially different location of their cf receptive fields (i.e., hindlimb versus forelimb, or proximal versus distal parts of the limb). We also moved the SCT stimulation electrode to recruit a different set of mfs, and also the skin stimulation used to evoke mf inputs was moved to a distinctly different location. The three different protocols that we used were as follows:

1. The combined SCT and skin burst stimulation protocol. The SCT electrode was stimulated with 15 pulses at 200 Hz, and the skin was stimulated 10 times at 333 Hz. With this configuration, the two inputs evoked largely overlapping time windows of excitation. The SCT stimulation intensity was typically 30–70 μA, in a couple of cases 100 μA.
2. The skin burst and simultaneous, single inferior olive (IO) stimulation protocol. The IO was stimulated once, and a skin burst stimulation of 50 pulses at 333 Hz was started 10 ms in advance in order for the first mf input to arrive at the same time as the cf input (the mf input evoked from the periphery needs at in the order of 10 ms to reach the cerebellar nuclei [3]).
3. The skin burst and delayed single IO stimulation protocol. A skin burst stimulation of 50 pulses at 333 Hz and at the time point of the last stimulation pulse, a single-pulse IO stimulation was applied.

For all three protocols, the bursts were repeated at 0.33 Hz for 10 min, i.e., for a total of 200 repetitions.

Analysis

We quantified the responses obtained from a single-pulse stimulation, either to the SCT or to the skin, before and after

a burst stimulation protocol. For the protocols involving skin bursts and the simultaneous or delayed IO stimulation, respectively, the responses were quantified using peristimulus histograms of raw spike time data (5 ms bin width). For the display and analysis of the combined skin burst and SCT stimulation protocol, we used a kernel density estimation (KDE) plot, i.e., each spike was replaced by a Gaussian distribution with standard deviation of 0.5 ms. The averaged sum of all Gaussian distributions transforms a discrete spiking pattern into a continuous function describing the spiking probability on a continuous time scale. The standard deviation of the kernels was set so that the total spiking probability function was smooth across neurons. This was done as the responses to the SCT stimulation were brief, which reduced the total number of spikes and made the responses more sensitive to chance distributions of single spikes. The KDE helped in reducing this problem. See Hoebeek et al. [10] for a more comprehensive discussion on KDE.

In all cases, the response was quantified as the mean firing frequency during the time window of the response, with the firing frequencies being obtained either from the KDE plots or the peristimulus histograms. To smooth the signal used in the analysis, the peristimulus histograms were filtered with a moving average of width 15 ms. The response onset was counted from the first occurrence of at least two consecutive bins with an activity that exceeded the baseline activity by at least two standard deviations. The end of the response was defined as the bin where the activity decreased to the threshold. For each cell, the time window for the response was initially calculated individually for every peristimulus histogram (i.e., control and all the post-protocol time points). Then the median start and end points of the responses were used to

define the response time window for the cell, in which the response was quantified. The response was quantified as the mean net activity during the defined time window. For responses evoked by SCT, the responses obtained were typically evoked between 1.5 to 4.0 ms after the onset of the stimulation. The KDE in itself did not allow a rigorous setting of the time limits, but histograms of the raw data provided a support for the chosen time limits in a similar fashion as above. For responses evoked by the skin, the quantified data was typically evoked within a response latency time window of 10–30 ms after the onset of the skin stimulation.

Subsequently, the relative response for each set of single-pulse stimulations was compared to the relative response before onset of the burst protocol and the change in response from each cell was analyzed in separate consecutive time spans of 10 min (time points). The null hypothesis that there was no net change in the response was tested using Wilcoxon signed-rank test. The signed-rank test was computed for each time point by comparing the total number of cells with the number of cells with a positive response. The probability for the outcome is calculated, assuming there is a 50% probability for each cell having a positive change in response.

Results

DCN neurons were recorded (Fig. 2a) in the left AIN (Fig. 1). A primary source of mf input to the AIN neurons is the spinocerebellar and spinoreticulocerebellar tracts (SCTs) (Fig. 1). Therefore, we located a stimulation electrode laterally at the level of caudal brainstem/rostral spinal cord which could

Fig. 2 Sample AIN neuron recording and response to single shock spinocerebellar tract (*SCT*) stimulation. **a** Long raw trace of loose-patch cell-attached AIN cell recording. **b** Ten superimposed traces to illustrate the spike responses to a single shock SCT stimulation. The stimulus shock artifact was blanked for clarity. **c** Peristimulus histogram (bin width 1 ms) of responses evoked by SCT stimulation (*N* = 50 repetitions). **d** Same responses as in **c** but in this case, a kernel density estimation (KDE) curve. KDE was used to evaluate the responses for the first set of experiments as the SCT stimulation evoked fast and brief responses, for which KDE provided a better reflection
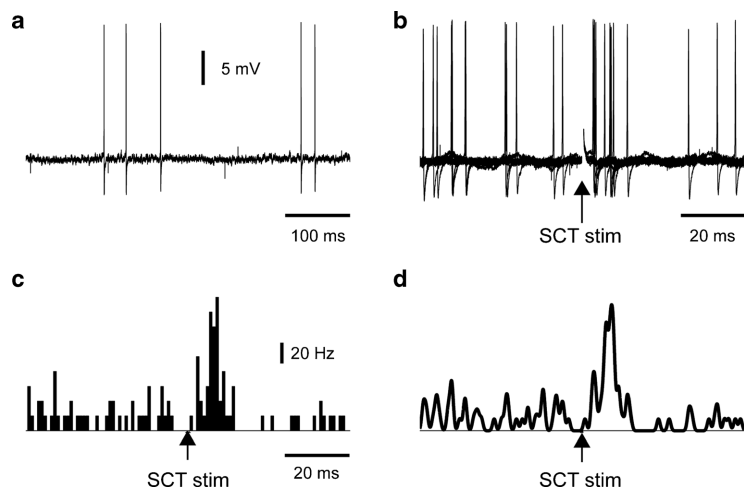
stimulate the ascending SCTs on the left side (similar mediolateral location as in Bengtsson and Jorntell [3] but with a more caudal location). AIN neurons had relatively robust responses to single shock SCT stimulation (Fig. 2b), as illustrated in peristimulus histograms obtained on repeated stimulation (Fig. 2c). Figure 2d shows the relation between a peristimulus histogram and a KDE plot, which was used for the analysis of the responses evoked by SCT stimulation.

Effects of Combined SCT Burst and Skin Burst Stimulation Protocol

Activation of SCTs can also be obtained using skin stimulation, as a proportion of the spinal neurons that projects through the SCTs are activated by skin afferents and the AIN neurons can be prominently excited by input from the skin [3] (Fig. 1). The dorsal column nuclei, which is the other source of cutaneous

mf input to the intermediate cerebellum, does not provide synapses to the AIN [9] or at least provides such synapses much more rarely than spinocerebellar axons [28]. For the first type of protocol, we wanted to combine the SCT input with another input that could serve to depolarize the AIN neuron and in this way increase the activation of NMDA receptors [2]. We found that electrical stimulation of skin afferents in bursts provided a maintained excitation of these neurons for the duration of the burst. This type of burst input was combined with simultaneous burst activation of the SCT and the combination generated highly intense spike responses in the AIN neurons (Fig. 3).

After the termination of the burst protocol (Fig. 4a), the responses evoked by a single shock SCT stimulation was monitored for up to 80 min and compared to the response to the same input recorded before the onset of the protocol (Fig. 4b). The first component of the response evoked by the SCT, which occurred before the onset of the first wave of

Fig. 3 Stimulation protocol of combined direct SCT burst stimulation and skin burst stimulation. **a** Five raw traces to illustrate the intensity of the response. **b** For the same neuron, KDE plot of the full set of responses (*N* = 200 stimulations) in this type of protocol
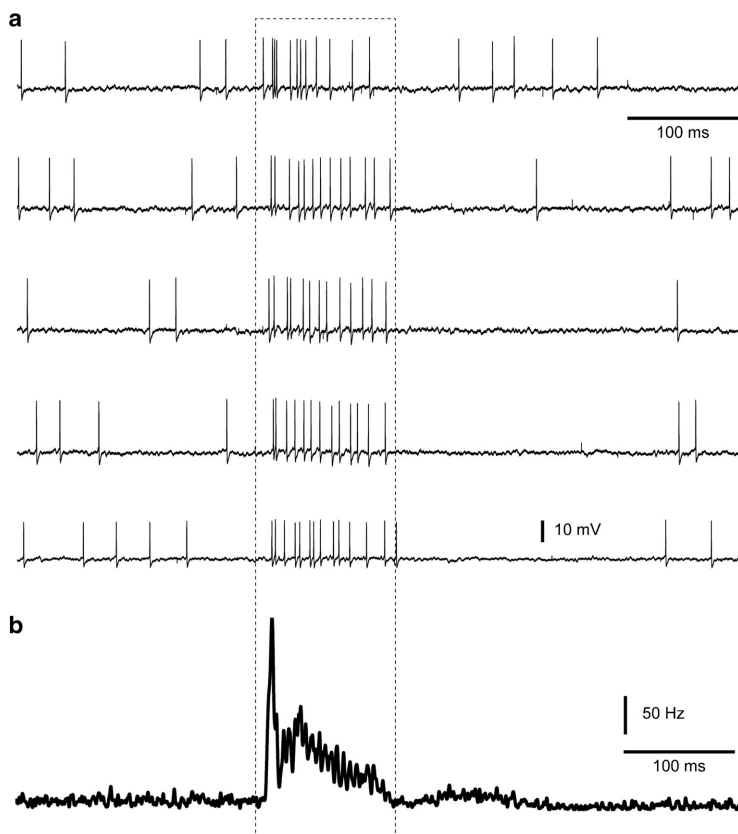
Fig. 4 Responses evoked by single shock SCT stimulation before and after the stimulation protocol. **a** Stimulation protocol of combined direct SCT burst stimulation and skin burst stimulation. The intention of the protocol is to induce a plastic change in the response amplitude to single shock SCT stimulation in the recorded AIN neuron. **b** *Top*, KDE plots for the responses ($N = 200$) evoked at three selected time points. *Arrows* indicate the time point of stimulation. The *dashed lines* indicate the time period in which the response was quantified. *Bottom*, superimposed raw traces of the spikes ($N = 10$ per panel) recorded from at different time points. Note that the small drop in spiking activity in the KDE plot around the stimulation time point is due to that some spikes occurring in conjunction with the stimulus artifact was hard to identify. This had no effect on the analysis of the change in the response, as this was measured relative to a long prestimulus time window of activity. **c** Individual spiking frequencies during the response time window for all neurons
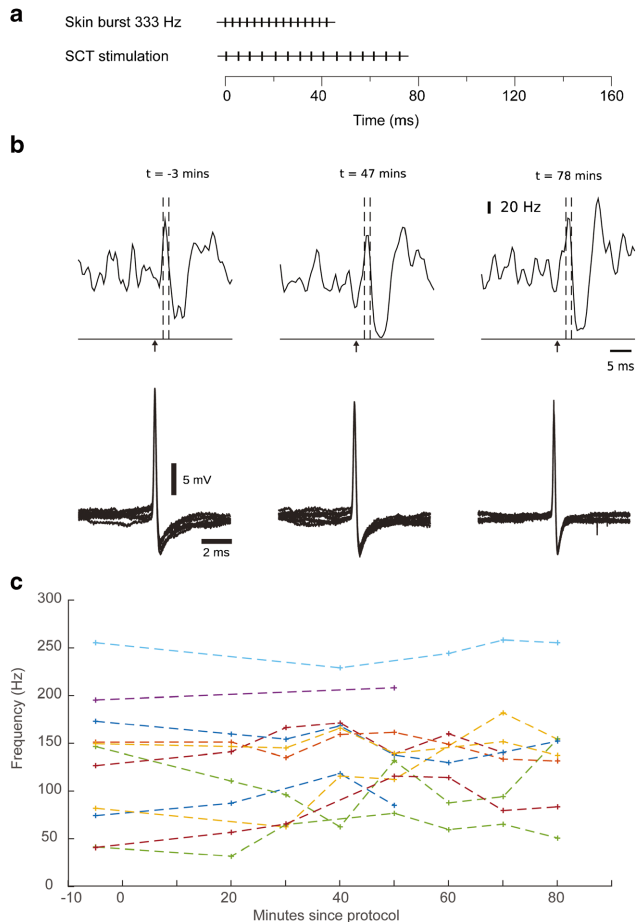
inhibition (cf. [3]), was quantified typically for a time window of 1.5–4.0 ms after the onset of the SCT stimulation. SCT evoked responses in all $N = 11$ cells. For each time point (10, 20, 30, 40, 50, 60, 70, 80, and 90 min after stimulation), there was experimental data from seven to ten out of $N = 11$ neurons. As can be seen in Fig. 4c, the inter-cell variance in firing activity is relatively large, which is the rationale for using the Wilcoxon signed-rank test as instead of calculating a mean for all cells in each time bin. The result of the statistical analysis can be found in Table 1; the raw data is provided in Fig. 4a to make it possible for the reader to judge the probability that there were any substantial and reliable changes induced by the protocol across the population of neurons recorded.

Effect of the Skin Burst and Simultaneous, Single IO Stimulation Protocol

In the cerebellar cortex, simultaneous burst stimulation of the excitatory parallel fiber (PF) synapses and a single shock stimulation of the cfs by a stimulation electrode in the IO are highly effective to induce long-term potentiation of PF inputs in Purkinje cells and their afferent interneurons [14]. We applied a similar protocol to AIN neurons, but replaced the PF stimulation with cutaneous input using localized electrical skin stimulation to a skin site that provided effective at least some excitation but was located outside the cf receptive field of the cell and therefore produced submaximal excitatory input to the cell [3] (Fig. 5a). As previously described [4], we

Table 1 Number of cells with positive changes in response amplitude versus the total number of cells shown, respectively, for each stimulation protocol and each time point. If there is no systematic potentiation or depression, on average, there should be as many cells with positive as with negative changes in response amplitude

Time (min)	Number of cells with positive response change	Total number of cells	Wilcoxon signed-rank test
Combined SCT and skin burst protocol			
15–25	4	8	1
25–35	3	8	1
35–45	5	8	0.54
45–55	7	10	0.28
55–65	3	7	1
65–75	6	9	0.65
75–85	4	8	0.84
85–95	6	7	0.05
Skin burst and simultaneous single IO stimulation protocol			
5–15	2	6	0.84
15–25	3	5	0.63
25–35	3	5	0.43
35–45	3	5	0.63
Skin burst and delayed single IO stimulation protocol			
5–15	1	5	0.31
15–25	2	5	0.31
25–35	3	4	0.25

Wilcoxon signed-rank test gives the P value (*rightmost column*) for the null hypothesis that there is no potentiation. Note that in pure chance data, 1 out of the 20 P values is expected to fall within the 5% range, which is also the case here (1 out of the 15 comparisons made)

carefully limited our data set to those AIN neurons in which the IO stimulation at low stimulation intensities ($\leq$50 µA) evoked a characteristic and distinct response sequence including early excitation-inhibition, representing the direct cf excitation of the DCN neuron followed by cf-driven, powerful, Purkinje cell inhibition and an ensuing postinhibitory rebound response (Fig. 5b, often also followed by inhibition after the rebound). Simultaneous IO stimulation and skin burst stimulation evoked substantial responses in the AIN neuron (Fig. 5c). However, the response to the single skin stimulation pulse, which was the test input, appeared to hardly change at all, neither in magnitude nor in temporal topography, after the protocol (Fig. 5d). These findings were repeated for up to six neurons and four time points (Fig. 5e), and in none of the cases could the null hypothesis that there was no post-protocol potentiation of the response be rejected (Table 1).

**Effect of the Skin Burst and Delayed Single IO Stimulation Protocol**

Since some of the theoretical arguments for plasticity in the mf-DCN synapse come from the field of classical conditioning of the eyeblink reflex [32], we also tested a protocol which resembles that used for inducing classically conditioned responses. This protocol was similar to the preceding protocol in that it used a skin burst stimulation to obtain intense excitation of the AIN neuron, but the single-pulse IO stimulation was applied

after the termination of the burst rather than at the time of its onset (delay conditioning protocol) (Fig. 6a, b). As described above, the AIN neurons were confirmed to have a prominent and characteristic response to the IO stimulation (Fig. 6c). As above, the responses obtained before and after the protocol were compared and were again found to be remarkably similar, both with respect to response magnitude and temporal topography (Fig. 6d). The summarized data, obtained from $N = 5$ AIN neurons (Fig. 5e), confirmed that no significant changes in response magnitude occurred (Table 1).

Discussion

In the present study, we tested whether the efficacy of mf input to DCN neurons could be altered using any out of the three different types of stimulation protocols in the adult cerebellum in vivo. Essentially, no effects were obtained over the first 10–90 min following the termination of any of the stimulation protocols. This is in contrast to the dramatic effects obtained in the neurons of the cerebellar cortex over a similar time span using related stimulation protocols [11, 12, 14, 16]. We conclude that at least in terms of efficacy and speed of induction, plasticity in the mf-DCN neuron synapse appears to be much less effective than in the parallel fiber synapses in the cortex. The potential consequences for our understanding of the function of the cerebellum in learning and adaptation are discussed.

Fig. 5 The effects of the simultaneous IO and skin burst activation protocol for a sample AIN neuron. **a** Stimulation protocol of simultaneous IO and skin burst activation. The intention of the protocol is to induce plastic changes in the response amplitudes to single-pulse electrical skin stimulation. **b** Net peristimulus histogram of responses evoked by IO stimulation (*N* = 200 responses, bin width 5 ms). **c** Net peristimulus histogram of responses evoked during the protocol (*N* = 200 repetitions), which consisted of a single IO stimulation and a burst stimulation to the skin applied at the same time point. **d** Development over time of the net response to single shock stimulation to the skin. Times are given relative to the start point of the stimulation protocol (for the control) and relative to the end point of the stimulation protocol (for all other histograms), respectively. Each histogram was obtained from 100–200 repetitions of the stimulation. **e** Spiking frequencies for each individual cell during the response time window
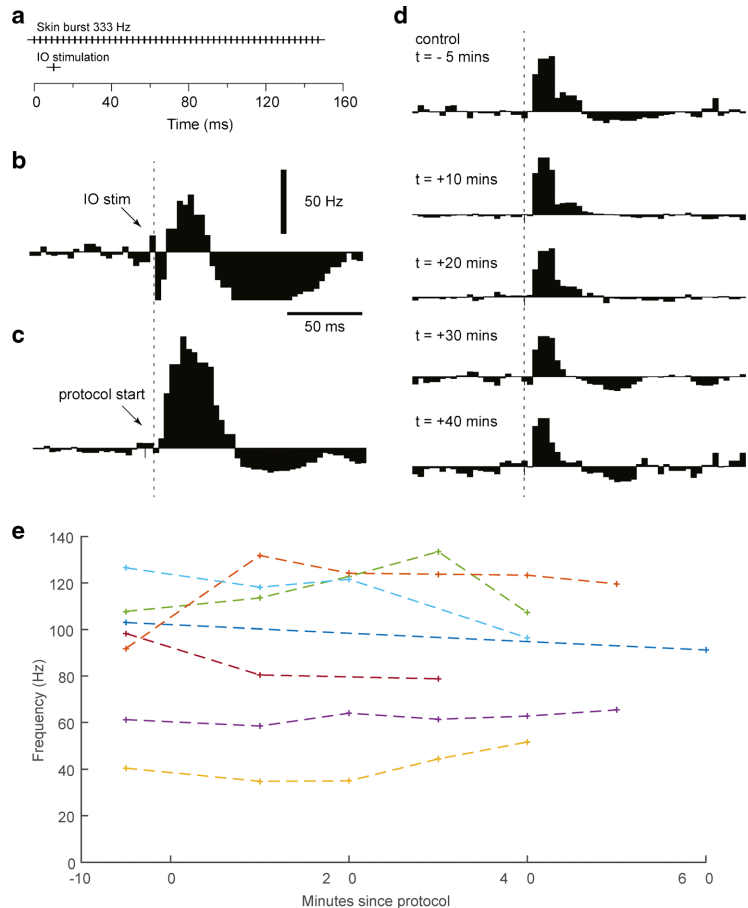
It could of course be argued that the data set was limited and that other results would have been obtained with more data. While this is always true for any data, visual inspection of the time course of net changes in post-protocol response amplitude in all cells revealed no trend in the data in either direction, again in contrast to data from the cerebellar cortex (see above). On basis of the absence of any trend, we could hence not defend extending the data acquisition in these very time consuming and difficult experiments. At the same time, the scientific community has repeatedly realized that it is important that also negative findings are published [17, 18], even though it can be argued that they are less conclusive.

First, it is important to point out that these findings do not imply that mf-interpositus plasticity does not exist in the adult cerebellum. It is of course possible that other protocols that we did not try would have been more effective. Perhaps a more likely possibility is that more long-term protocols and longer duration AIN cell recordings could have provided a different answer. In experiments of classically conditioned eyeblink responses, for example, effects in the Purkinje cell responses start to emerge at the same time scale as we were looking at here but they evolve substantially for hours after [11]. It should also be noted that we used much shorter intertrial intervals than in the latter paper, so comparisons cannot be made directly. The structural changes observed in mf collaterals to the DCN after repeated training protocols [5] was obtained only after several days of training, but it was not possible for us to follow single neurons for a comparable amount of time. In comparison with mf synaptic plasticity in juvenile slices
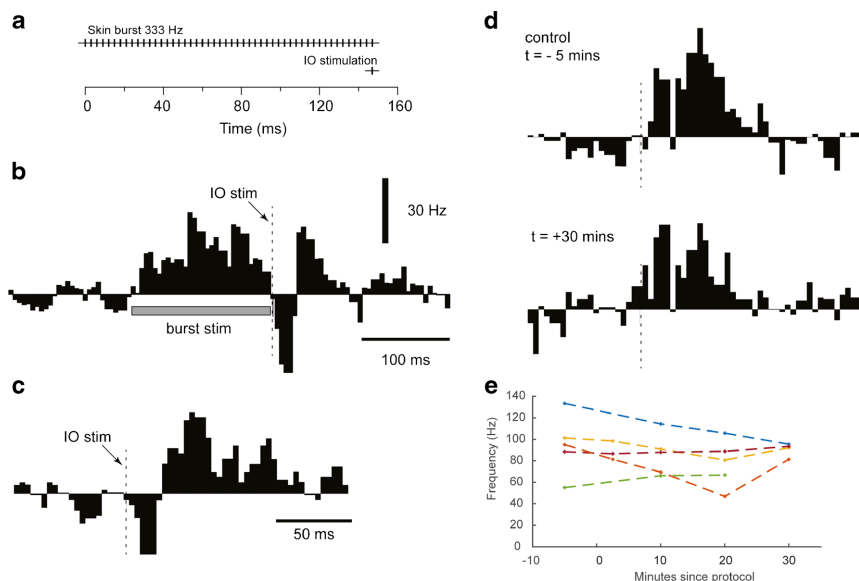
Fig. 6 The effects of the skin burst and delayed single IO stimulation protocol for a sample AIN neuron. **a** Stimulation protocol of skin burst and delayed IO stimulation. The intention of the protocol is to induce plastic changes in the response amplitudes to single-pulse electrical skin stimulation. **b** Net peristimulus histogram of the spike responses to the protocol ($N = 200$ repetitions, bin width 5 ms). **c** Net peristimulus histogram of the spike responses to IO stimulation alone ($N = 50$ repetitions). Note the more expanded time base compared to **a**. **d** Net peristimulus histograms of the spike responses evoked to single-shock skin stimulation before and after the protocol ($N = 100$–200 repetitions). **e** Spiking frequencies for each individual cell during the response time window

[26, 27], however, the time scales were comparable but the results were very different. Notably, apart from age differences there was also a striking difference between the protocols: an important component in the slice work was the presence of a 20–25-mV hyperpolarization of the DCN neuron during the stimulation of the mf synapses, which lasted for at least 150 ms in order to initiate a postinhibitory rebound [26]. In the in vivo setting, such a hyperpolarization would appear to translate to a simultaneous activation of all of the afferent Purkinje cells to firing rates of 200–300 Hz for the duration of the period of inhibition [4], which appears to be a completely unlikely scenario in the adult cerebellum. This does not necessarily exclude that the fundamental plasticity mechanism described in the slice [26, 27] applies in vivo, but may suggest that the mechanism could operate on a much slower time course in the adult cerebellum in vivo, where these extreme cases of concerted Purkinje cell activity may not appear.

An interesting aspect is the contrast to the effects observed in cerebellar cortical neurons using similar protocols and, in at least one case, comparable recording times [14, 16]. This suggests that there is likely to be a difference between the interpositus cells and the cortical neurons at least in their propensity for plasticity of excitatory inputs. From a functional point of view, this may make sense. The limb areas of the

AIN are an integral part of a motor command loop, which via direct connections to rubrospinal and thalamocortical neurons innervating the motor cortex can strongly influence the activity of spinal premotor interneurons [3]. These interneurons are probably very important for the synergy selection, i.e., which muscles are to be activated at what time during the execution of a complex, well-trained movement [30]. Since some of these interneurons provide feedback to the cerebellum, directly or via the lateral reticular nucleus, and since this feedback is the information that is provided by the spinocerebellar mf-DCN synapses, this synaptic linkage can be important for associating and linking specific synergy patterns into compound movements. As they are one of the fundaments of the core motor command loop, it may be important to let them become stabilized after development when basic movement patterns/synergy patterns have been acquired. Fine-tuning of the drive of these synergy patterns during specific phases/contexts of a movement can be achieved via the cerebellar cortex and its inhibitory control of the AIN neurons. This fine-tuning can be minor adaptations required by changes in muscle strength over time or context-dependent factors, for example, which do not require a change in the fundamental movement patterns. Such adaptations must be allowed to occur more rapidly and could be primarily brought about by alterations in the cortical network—this

would be an explanation for the different propensities for input plasticity in the cortex as compared to the AIN neurons.

Compliance with Ethical Standards

Conflict of Interest The authors declare that they have no conflict of interest.

References

1. Aizenman CD, Linden DJ. Rapid, synaptically driven increases in the intrinsic excitability of cerebellar deep nuclear neurons. Nat Neurosci. 2000;3:109–11.
2. Anchisi D, Scelfo B, Tempia F. Postsynaptic currents in deep cerebellar nuclei. J Neurophysiol. 2001;85:323–31.
3. Bengtsson F, Jorntell H. Specific relationship between excitatory inputs and climbing fiber receptive fields in deep cerebellar nuclear neurons. PLoS One. 2014;9:e84616.
4. Bengtsson F, Ekerot CF, Jorntell H. In vivo analysis of inhibitory synaptic inputs and rebounds in deep cerebellar nuclear neurons. PLoS One. 2011;6:e18822.
5. Boele HJ, Koekkoek SK, de Zeeuw CL, Ruigrok TJ. Axonal sprouting and formation of terminals in the adult cerebellum during associative motor learning. J Neurosci. 2013;33:17897–907.
6. Ekerot CF, Jorntell H, Garwicz M. Functional relation between corticonuclear input and movements evoked on microstimulation in cerebellar nucleus interpositus anterior in the cat. Exp Brain Res. 1995;106:365–76.
7. Freeman JH, Steinmetz AB. Neural circuitry and plasticity mechanisms underlying delay eyeblink conditioning. Learn Mem. 2011;18:666–77.
8. Garwicz M, Ekerot CF. Topographical organization of the cerebellar cortical projection to nucleus interpositus anterior in the cat. J Physiol. 1994;474:245–60.
9. Gerrits NM, Voogd J, Nas WS. Cerebellar and olivary projections of the external and rostral internal cuneate nuclei in the cat. Exp Brain Res. 1985;57:239–55.
10. Hoebeek FE, Witter L, Ruigrok TJ, de Zeeuw CI. Differential olivocerebellar cortical control of rebound activity in the cerebellar nuclei. Proc Natl Acad Sci U S A. 2010;107:8410–5.
11. Jirenhed DA, Bengtsson F, Hesslow G. Acquisition, extinction, and reacquisition of a cerebellar cortical memory trace. J Neurosci. 2007;27:2493–502.
12. Jirenhed DA, Bengtsson F, Jorntell H. Parallel fiber and climbing fiber responses in rat cerebellar cortical neurons in vivo. Front Syst Neurosci. 2013;7:16.
13. Jorntell H, Ekerot CF. Topographical organization of projections to cat motor cortex from nucleus interpositus anterior and forelimb skin. J Physiol. 1999;514(pt 2):551–66.
14. Jorntell H, Ekerot CF. Reciprocal bidirectional plasticity of parallel fiber receptive fields in cerebellar purkinje cells and their afferent interneurons. Neuron. 2002;34:797–806.
15. Jorntell H, Ekerot CF. Receptive field plasticity profoundly alters the cutaneous parallel fiber synaptic input to cerebellar interneurons in vivo. J Neurosci. 2003;9:9620–31.
16. Jomtell H, Ekerot CF. Receptive field remodeling induced by skin stimulation in cerebellar neurons in vivo. Front Neural Circuits. 2011;5:3.
17. Knight J. Negative results: null and void. Nature. 2003;422:554–5.
18. Matosin N, Frank E, Engel M, Lum JS, Newell KA. Negativity towards negative results: a discussion of the disconnect between scientific worth and scientific culture. Dis Model Mech. 2014;7:171–3.
19. Matsushita M. Projections from the lowest lumbar and sacral-caudal segments to the cerebellar nuclei in the rat, studied by anterograde axonal tracing. J Comp Neurol. 1999a;404:21–32.
20. Matsushita M. Projections from the upper lumbar cord to the cerebellar nuclei in the rat, studied by anterograde axonal tracing. J Comp Neurol. 1999b;412:633–48.
21. Matsushita M, Gao X. Projections from the thoracic cord to the cerebellar nuclei in the rat, studied by anterograde axonal tracing. J Comp Neurol. 1997;386:409–21.
22. Matsushita M, Xiong G. Projections from the cervical enlargement to the cerebellar nuclei in the rat, studied by anterograde axonal tracing. J Comp Neurol. 1997;377:251–61.
23. Matsushita M, Yaginuma H. Projections from the central cervical nucleus to the cerebellar nuclei in the rat, studied by anterograde axonal tracing. J Comp Neurol. 1995;353:234–46.
24. Ohyama T, Nores WL, Medina JF, Riusech FA, Mauk MD. Learning-induced plasticity in deep cerebellar nucleus. J Neurosci. 2006;26:12656–63.
25. Porrill J, Dean P. Cerebellar motor learning: when is cortical plasticity not enough? PLoS Comput Biol. 2007;3:1935–50.
26. Pugh JR, Raman IM. Potentiation of mossy fiber EPSCs in the cerebellar nuclei by NMDA receptor activation followed by postinhibitory rebound current. Neuron. 2006;51:113–23.
27. Pugh JR, Raman IM. Mechanisms of potentiation of mossy fiber EPSCs in the cerebellar nuclei by coincident synaptic excitation and inhibition. J Neurosci. 2008;28:10549–60.
28. Quy PN, Fujita H, Sakamoto Y, Na J, Sugihara I. Projection patterns of single mossy fiber axons originating from the dorsal column nuclei mapped on the aldolase c compartments in the rat cerebellar cortex. J Comp Neurol. 2011;519:874–99.
29. Raymond JL, Lisberger SG. Neural learning rules for the vestibulo-ocular reflex. J Neurosci. 1998;18:9112–29.
30. Santello M, Baud-bovy G, Jorntell H. Neural bases of hand synergies. Front Comput Neurosci. 2013;7:23.
31. Spanne A, Jorntell H. Processing of multi-dimensional sensorimotor information in the spinal and cerebellar neuronal circuitry: a new hypothesis. PLoS Comput Biol. 2013;9:e1002979.
32. Weeks AC, Connor S, Hinchcliff R, Leboutillier JC, Thompson RF, Petit TL. Eye-blink conditioning is associated with changes in synaptic ultrastructure in the rabbit interpositus nuclei. Learn Mem. 2007;14:385–9.
33. Wu HS, Sugihara I, Shinoda Y. Projection patterns of single mossy fibers originating from the lateral reticular nucleus in the rat cerebellar cortex and nuclei. J Comp Neurol. 1999;411:97–118.
34. Wulff P, Schonewille M, Renzi M, Viltono L, Sassoe-pognetto M, Badura A, Gao Z, Hoebeek FE, van Dorp S, Wisden W, Farrant M, de Zeeuw CI. Synaptic inhibition of Purkinje cells mediates consolidation of vestibulo-cerebellar motor learning. Nat Neurosci. 2009;12:1042–9.

Paper II

SCIENTIFIC REP⚙RTS

Artificial spatiotemporal touch inputs reveal complementary decoding in neocortical neurons

Calogero M. Oddo[1], Alberto Mazzoni[1], Anton Spanne[2], Jonas M. D. Enander[2], Hannes Mogensen[2], Fredrik Bengtsson[2], Domenico Camboni[1], Silvestro Micera[1,3] & Henrik Jörntell[2]

Investigations of the mechanisms of touch perception and decoding has been hampered by difficulties in achieving invariant patterns of skin sensor activation. To obtain reproducible spatiotemporal patterns of activation of sensory afferents, we used an artificial fingertip equipped with an array of neuromorphic sensors. The artificial fingertip was used to transduce real-world haptic stimuli into spatiotemporal patterns of spikes. These spike patterns were delivered to the skin afferents of the second digit of rats via an array of stimulation electrodes. Combined with low-noise intra- and extracellular recordings from neocortical neurons *in vivo*, this approach provided a previously inaccessible high resolution analysis of the representation of tactile information in the neocortical neuronal circuitry. The results indicate high information content in individual neurons and reveal multiple novel neuronal tactile coding features such as heterogeneous and complementary spatiotemporal input selectivity also between neighboring neurons. Such neuronal heterogeneity and complementariness can potentially support a very high decoding capacity in a limited population of neurons. Our results also indicate a potential neuroprosthetic approach to communicate with the brain at a very high resolution and provide a potential novel solution for evaluating the degree or state of neurological disease in animal models.

Haptic skin-object interactions necessary for touch perception generate spatiotemporal patterns of activation across multiple tactile skin sensors. When different kinds of objects interact with the same part of the skin, they can be expected to generate different such spatiotemporal patterns[1,2], which form part of the brain's perception of the skin-object interaction. Even though the interpretation of the 'what' such inputs represent is distributed across a large number of neocortical neurons, the information must to some extent be expressed also at the level of individual neurons. In other words, at least the bits and pieces of the population-level information should be represented in the single neuron. It has commonly been observed that skin-object interactions with different kinds of objects and shapes generate different neural responses[3–5], but the precision by which neocortical neurons can distinguish specific spatiotemporal patterns of tactile afferent input (i.e. identifying the 'what' of the input) from the same part of the skin has to our knowledge not previously been estimated.

Analysis and quantification of the specific decoding of tactile information in a cortical neuron requires the repeated presentation of reproducible spatiotemporal patterns of skin sensor afferent activation. But the mechanical activation of the skin[6], the mechanotransduction into an electrical receptor potential and the spike generation from that receptor potential in the tactile afferent axon[7] are potential sources of noise that could result in variability in the spatiotemporal pattern from one trial to another[2,8,9]. In addition, even small shifts in the position of a mechanical stimulus would result in that the spatiotemporal pattern of skin sensor activation shifts across the recruited population of sensors, which at the level of the decoding in the neuronal circuitry corresponds to a different task, even though the perception may be essentially the same. To overcome these difficulties, our aim was to by-pass the potentially variable steps that come with the mechanical skin sensor activation, so that the decoding capacity of central neurons could be estimated in relative isolation. Using direct electrical interfacing with the distal nerve fibers innervating the skin sensors, it becomes possible to investigate the neuronal decoding

[1]The BioRobotics Institute, Scuola Superiore Sant'Anna, Pisa, Italy. [2]Neural Basis of Sensorimotor Control, Department of Experimental Medical Science, Lund University, Lund, Sweden. [3]Bertarelli Foundation Chair in Translational NeuroEngineering, Center for Neuroprosthetics and Institute of Bioengineering, School of Engineering, École Polytechnique Federale de Lausanne, Lausanne, Switzerland. Correspondence and requests for materials should be addressed to H.J. (email: henrik.jorntell@med.lu.se)

of a 'frozen state' of sensor activation, isolated from the uncertainty in the mechanotransduction step. With this approach it becomes possible to repeat multiple spatiotemporal patterns a high number of times in a random order even within the lifetime of an intracellular neuronal recording. The findings obtained using direct neural stimulation also have potential translational importance for limb neuroprosthetics. The method was first introduced in human studies, using percutaneous electrical microstimulation of tactile afferents using a single channel electrode[10,11]. Using long-term peripheral nerve implants with temporally patterned direct electrical activation of different portions of a nerve trunk, diversified and meaningful perceptions of touch can be achieved[12–16], which indicates that the brain can actively engage in the processing of electrically induced tactile afferent input.

In auditory and visual cortical systems, 'natural scenes' of sensory input have been shown to evoke very different cortical responses compared to those evoked by simplified inputs[17,18]. This may indicate that the circuitry structure is adapted to some general features in the spatiotemporal patterns of sensor activation that may occur during natural behavior, and that this circuitry structure constrains the way the individual neurons in the network are activated. Following these considerations, we wanted as far as possible to achieve naturalistic, rather than arbitrarily designed, patterns of electrical skin sensor activation. For this purpose, we employed a biomimetic artificial fingertip equipped with an array of neuromorphic tactile sensors that generated spatiotemporal patterns of skin sensor output in response to mechanical touch or indentation with probes characterized by different curvature. The spatiotemporal patterns of spike output generated from this system during dynamic touch were delivered as electrical stimuli to the distal tactile afferents from the volar side of the second digit of the rat forepaw. With this approach, we hoped to mimic at least the general envelope of the overall temporal modulation of activation in the local population of skin sensors as it may occur in a conceivable natural touch. In this way, the spatiotemporal pattern of skin sensor activation that we delivered may be better tuned to the space of possible patterns of input that the circuitry of the adult animal may have been adapted to. In order to allow well-controlled, repeatable stimulus delivery and long-term *in vivo* whole cell patch clamp recordings from neocortical neurons in the absence of top-down modulations[19] we used anesthetized rats. We find that the decoding performance of individual neurons can be much higher than previously described and that there is a complementarity in their response profiles that provides for a very high decoding capacity even in small groups of neurons.

Results

Our aim was to study the decoding capacity of central neurons in isolation, separated from noise arising from mechanical interfacing with the skin and from intrinsic skin sensor noise (even highly controlled repeated activation of a single mechanical stimulus yields a range of variability in the spiking of the primary sensor afferents of 2 ms on average, with up to 8 ms jitter observed in the spike trains and even missing one or two spikes in each repeated run of a given touch condition[9]). For this purpose we used electrical stimulation of four skin sites (channels) of the volar side of digit 2 of the rat (a skin surface that through the lifetime of the animal would have been activated by a vast array of inputs via touch, locomotion and other motor activities). Using a low stimulation intensity of about 2.5 times threshold for primary afferent activation (Methods), such stimulation activates a limited number of tactile afferents (and no nociceptive afferents whose recruitment starts at 4 times threshold[20]) with a high temporal precision and reliability[21]. In order to generate spatiotemporal patterns of skin sensor activation with overall similarities with patterns that could be evoked under natural conditions such as active touch, we used an artificial fingertip equipped with an array of four separate neuromorphic sensors (Fig. 1A and Supplementary Fig. S1). These neuromorphic sensor have activation properties that are similar to biological tactile sensors for the type of stimuli we used here (Supplementary Fig. S2) as well as other types of stimuli[12]. The spatiotemporal patterns of electrical skin site stimulation to be used with the animal were first obtained from the artificial fingertip by moving it against probes of different shapes (Fig. 1A,B and Supplementary Fig. S1). Out of the many spatiotemporal spike output patterns recorded from the neuromorphic sensors, we selected two patterns for each of the four indentation probes used, to obtain a total of eight richly resolvable spatiotemporal patterns (Supplementary Fig. S1). The comparably high resolvability of the eight patterns used was an important component in our subsequent evaluation of the decoding performance of the neocortical neurons. These eight spatiotemporal patterns of multi-channel electrical skin site activation were used throughout the experimental series (Fig. 1E).

The responses of neocortical neurons to the repeated applications of these spatiotemporal patterns of electrical skin site stimulation were recorded in the paw region of the primary somatosensory cortex (Fig. 1C) using the whole cell patch clamp (N = 14 neurons) or loose-patch, cell-attached (N = 82 neurons) recording techniques. We morphologically recovered 11 neurons recorded in the whole cell mode (Fig. 1D), of which all were pyramidal neurons at layers II–V. Of the 82 cell-attached recordings, 12 neurons had a narrower spike width than the others and could be classified as putative interneurons according to Luczak, *et al.*[17], but these neurons did not stand out from the other neurons in terms of the response patterns described below and are hence not indicated separately.

Analysis of intracellular responses. With the whole cell patch clamp method, we recorded the intracellular membrane potential responses resulting from the synaptic inputs evoked by the spatiotemporal skin stimulation patterns (Fig. 1E,F). For each neuron, we first made pairwise comparisons of the responses evoked by two different stimulation patterns (Fig. 1F,G). The average intracellular membrane potential responses were typically unique for each stimulus pattern (Fig. 1H), so for each neuron we made such pairwise comparisons across all pairs of stimulation patterns available (N = 27). For the example cell illustrated in Fig. 1F–H the fraction of comparisons yielding statistically significant differences (KS-test) between pre- and poststimulus times was 93%, which indicates that the synaptic inputs to the cell could be used to separate almost all of the stimulation patterns. Across the population of neurons recorded in the whole cell mode (N = 14), 68+/−20% of the patterns could be separated in these pairwise comparisons, with 4 neurons separating the inputs in more than 90% of the comparisons. Hence, the evoked intracellular responses were relatively specific to the precise stimulation pattern
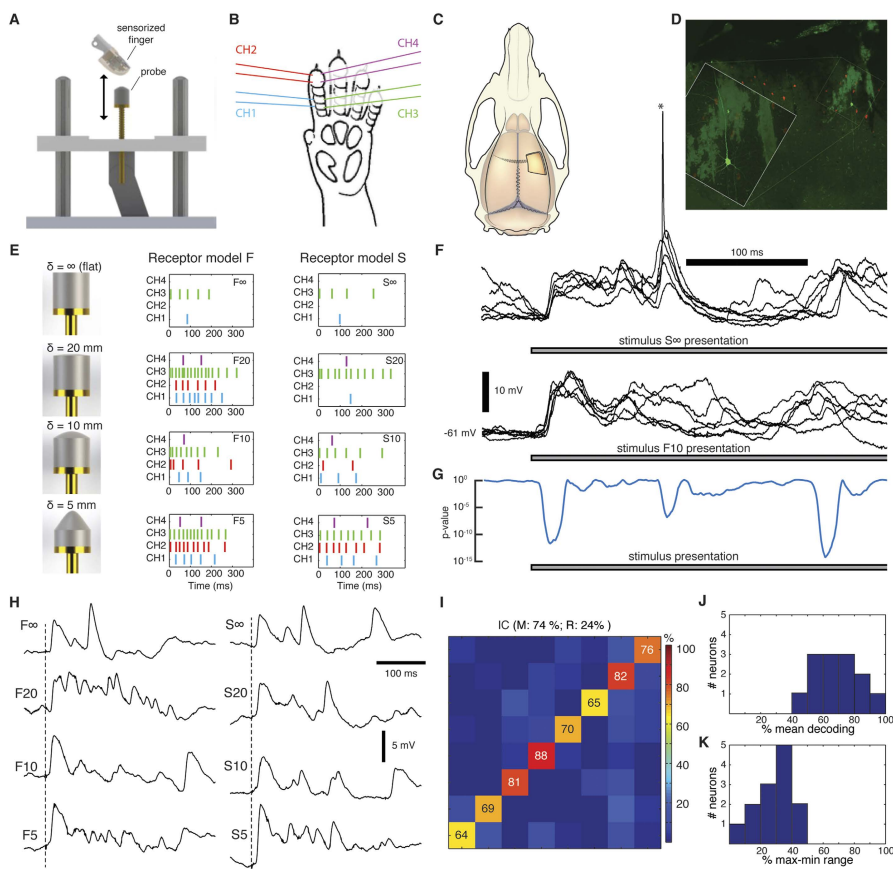
Figure 1. Synthesis of tactile patterns and intracellular responses *in vivo*. (A) Shapes with different curvatures were moved against an artificial fingertip using a cyclic motion. The artificial fingertip was equipped with an array of four neuromorphic sensors that generated spatiotemporal spike output patterns that were electrically delivered to the skin of the rat paw (Supplementary Fig. S1). **(B)** The location of the pairs of intracutaneous needle electrodes (channels) delivering the generated spike output patterns. **(C)** Illustration of approximate recording location (in the S1 digit region). **(D)** Sample morphology of a recorded neuron, identified as a layer III pyramid based on morphology and depth. Red staining is parvalbumin immunopositive neurons. **(E)** From left to right: the four types of probe shapes (Supplementary Fig. S1) used; the corresponding plots of the spike output patterns, equalling the spatiotemporal patterns of elementary current pulses delivered to the skin of the rat, obtained with the receptor model F; corresponding plots of the spike output patterns obtained with the receptor model S. **(F)** Superimposed raw intracellular responses evoked by two different stimulation patterns. One neuronal spike (asterisk) is included for display. **(G)** The Welch student's t-test dissimilarity measure displayed as p-values, comparing the responses evoked by the two stimulation patterns illustrated in (**F**). **(H)** Average intracellular responses of the neuron in (**D**) for each stimulation pattern in (**E**). **(I)** Confusion matrix of the PCA results of the decoding of the different spatiotemporal stimulation patterns for the illustrated neuron. 'M' indicates the mean decoding, and 'R' the range of decoding (max-min). **(J,K)** Mean and range of decoding for all intracellular recordings.

used. In addition to these pairwise comparisons, we also performed a principal component analysis (PCA) of the intracellular responses, where the decoding accuracy for each stimulation pattern could be analysed in relation to the decoding accuracy for all the other patterns. The mean decoding for the sample neuron, according to the PCA, was 74% across all of the eight patterns whereas the decoding of the individual stimulation patterns varied
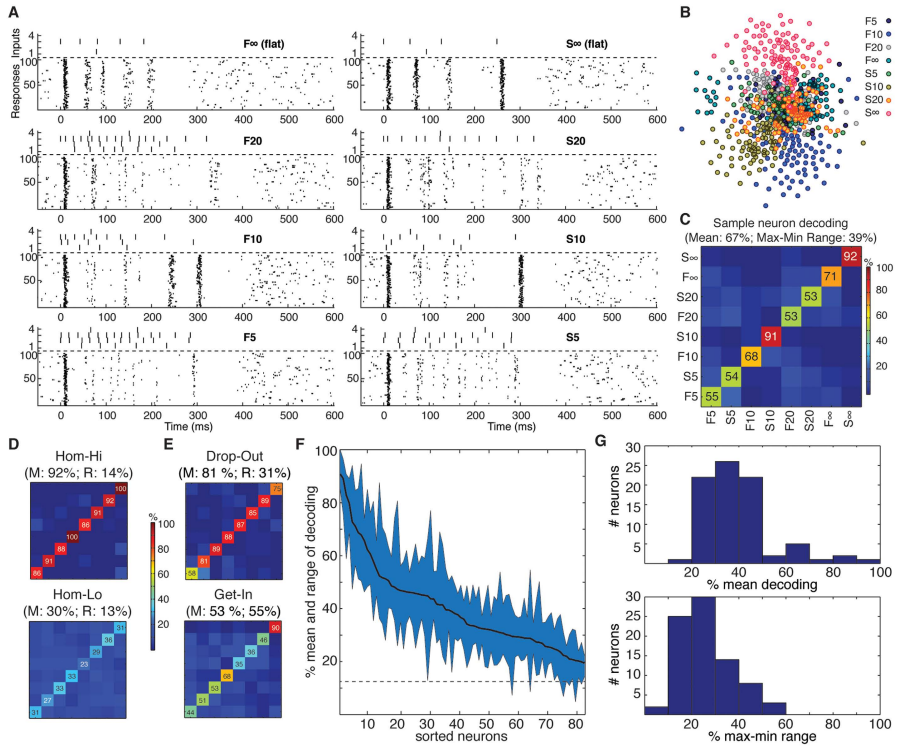
Figure 2. Single neuron decoding for spike output. (**A**) Raster plots of spike responses of a sample neuron to the stimulation patterns as indicated. (**B**) Cluster analysis of the same spike responses. The response to each stimulus presentation is shown color-coded. (**C**) Confusion matrix of the decoding performance for the neuron illustrated in (**A**,**B**) (see Supplementary Fig. S3 for illustration of this method). The title indicates the mean and the range of the decoding across the eight stimulation patterns. Numbers inside the matrix indicate the decoding rates for the individual stimulation patterns. (**D**) Example confusion matrices for two neurons with homogeneous decoding, one with high mean decoding and one with low mean decoding. (**E**) Example confusion matrices for two neurons with heterogeneous decoding. Top, example confusion matrix with 'drop-out' decoding. Bottom, confusion matrix for a 'get-in' neuron with selective decoding. (**F**) Mean and range of decoding across the population of neurons. The horizontal dashed line indicates chance level. (**G**) Distribution, over the population of neurons, of the mean decoding (top) and of the range of decoding (bottom).

within a relatively narrow range as indicated in the confusion matrix in Fig. 1I. For the population of neurons, the average mean decoding according to the PCA was 69+/−18% (Fig. 1J) with a variable range of decoding across the different stimulation patterns (Fig. 1K).

Analysis of spike responses in individual neurons. Although the intracellular analysis reveals the input information to the neuron, for the network of the brain the more relevant signal is the resulting neuronal spike output, which is the signal that is being processed by the neuronal network. As there seems to be no simple, direct relationship between the intracellular signal and the resulting pattern of spike output in central neurons[22,23], the spike output needed to be analyzed as well. To analyse the spike output, we used cell-attached recordings. In these recordings, spike responses were in many neurons reliable, precise and input-specific (Fig. 2A) and even the responses to single stimulus presentations could at least for some stimulation patterns form relatively reliable clusters (Fig. 2B). As for the intracellular signals (Fig. 1I–K), the spike responses of individual neurons (N = 82) were also processed via PCA and kNN decoding (Supplementary Fig. S3) to evaluate the precision by which the responses to repeated stimulus presentations could be used to decode the identity of the stimulation pattern applied (Fig. 2C). In the illustrated example (Fig. 2A–C), the neuron was able to segregate the eight stimulation
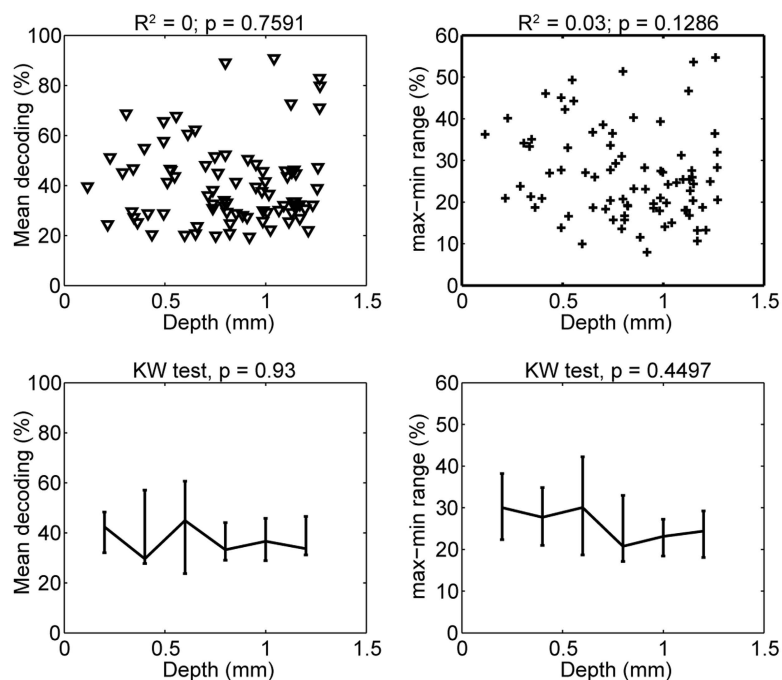
Figure 3. Relationship between neuronal depth and decoding. Lack of relationship between recording depth and decoding (left) and between recording depth and decoding heterogeneity (right). Bottom, corresponding box plots (median and interquartile range) with recording depths pooled in steps of 200 μm. Even though precise laminar information and neuronal type identity was not a focus of our study, the absence of relationship between decoding and recording depth strongly suggested (Pearson linear correlation test and Kruskal Walis test, see text) that there was no relationship between decoding performance and laminar location.

patterns with a mean accuracy of 68%. For one of the stimulation patterns, the decoding performance was as high as 92% (pattern S∞ in Fig. 2C).

Overall, the top performing neurons had a decoding performance as high as 80–90% (Fig. 2D, top), while most neurons had a mean decoding performance of 20–50% (Fig. 2D, bottom). But the PCA analysis also indicated that in the population of neurons, there was heterogeneity with respect to the decoding performance across the stimulation patterns. Some neurons showed specificity in the sense that the identification rate of at least one stimulation pattern was at least 20% units lower than the mean decoding performance ('drop-out', $N = 12$, Fig. 2E top). There were also neurons with highly specific decoding in the sense that the top decoded stimulation pattern had identification rate at least 20% units higher than the mean decoding performance ('get-in', $N = 9$, Fig. 2E bottom). The mean and range of decoding of the spike output varied across the population (Fig. 2F) (Supplementary Fig. S4 reports the corresponding information content for all the neurons). The distributions of the mean (Fig. 2G, top) and the range (Fig. 2G, bottom) of the decoding performance were compatible with a lognormal fitting ($p = 0.46$ and $p = 0.95$, respectively, one-sample KS test)[24]. Neither the mean nor the range of the decoding depended significantly on the depth at which the neuron was recorded (Pearson linear correlation test: $p > 0.1$ both variables; Kruskal Wallis test, $p > 0.1$) (Fig. 3). Notably, the mean decoding (Fig. 2G, top) was substantially lower than for the intracellular signals (Fig. 1I).

The decoding performance of the neurons depended on the interval over which the spike response was integrated, with some neurons allowing very high decoding with short integration windows (Fig. 4). Remarkably, for many other neurons the decoding level slightly increased even up to 1000 ms after the onset of the stimulation (Fig. 4B). As the longest duration of any of the spatiotemporal input patterns was 340 ms, the stimulation patterns hence produced organized activity in the neuronal networks long after the stimulation had ceased.

Responses evoked by stimulation of single channels. As complementary information to the results above using complex patterns of input, we also analysed responses evoked by simpler stimuli, specifically stimulation of the separate skin input channels with one or two pulses. Notably, although all of our neurons responded to
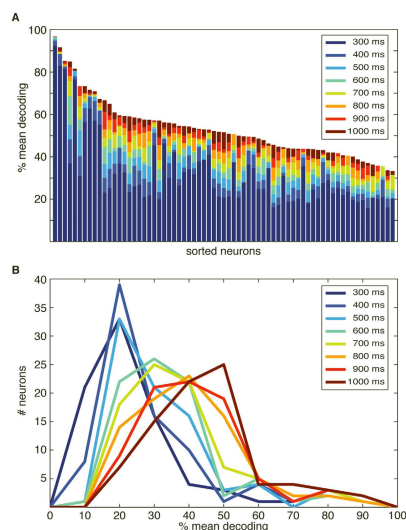
Figure 4. Information content in late response components. (**A**) Dependence of the mean decoding performance (accuracy) on the extent of the time window included in the analysis. Note that none of the stimulation patterns lasted for more than 340 ms, yet in almost all neurons the information increased all the way up to 1000 ms poststimulus time window. Interestingly, neurons also differed widely with respect to the increase in decoding accuracy obtained when the time window was expanded. Only neurons with a decoding above 30% at 1000 ms (N = 69) are included in the display. (**B**) Distribution of the mean decoding performance across the neurons as a function of the time integration window.

the complex patterns, only 57 out of our 82 neurons had a measurable response to single pulse for every channel. In this group of 57 neurons, we first asked if the neurons could decode whether the input was a single pulse or a double pulse, where the second pulse occurred 300 ms after the first (analysis time window limited to 450 ms in this case). Across each of the 4 stimulation channels (228 comparisons) the decoding was 79.3%, where 7 neurons with strong responses to single pulse stimulation could separate single from double pulse stimulation for at least one channel with 100% precision. In the next step, we asked whether the neurons could tell which of the 4 channels that were stimulated, and whether that channel was stimulated once or twice. Most of the neurons performed well on this task, with a mean decoding across the population of 43% and information content of 1.66 bits (out of 3 bits maximum) (Supplementary Fig. S5).

Complementary neuronal response patterns allow for co-operative decoding. Whereas the analysis above was limited to the decoding provided by individual neurons, we often noted a mismatch in the temporal response patterns of different neurons to the same stimulation pattern. Together with the tendency of some neurons to preferentially decode certain patterns better than others (Fig. 2E), this hinted at the possibility of complementary decoding between neurons. Such complementariness could allow for co-operative decoding within a small population of neurons, which together might provide a much higher capacity to segregate spatiotemporal patterns of tactile afferent input. To examine the potential for co-operative effects, we first focussed on a subset of our recordings, in which the spikes of two different neurons were recorded at the same time with the same patch pipette[25] (Fig. 5A, N = 5 pairs) or using two separate adjacent patch pipettes (N = 2 pairs). The temporal spike response patterns could be widely different between two adjacent neurons (Fig. 5B), a phenomenon previously also observed in awake monkeys[26,27]. Moreover, the mean decoding and the specific input selectivity (Fig. 5C) could differ substantially between the two neurons in such paired recordings (the range of the differences in the mean decoding was 2–38% units for N = 7 pairs).

A cross-neuron—cross-stimulation analysis of some of the top decoding neurons (Fig. 6A) confirmed that the temporal response patterns to the same stimulation pattern could be unique for each neuron. There was also a lack of 'cross-talk' between neurons in terms of their individual temporal response patterns to different spatiotemporal stimulation patterns (Fig. 6A). Therefore, we next analysed the potential cooperativity across the entire population of recorded neurons. Cluster analysis indicated that the decoding performance increased with the number of neurons (Fig. 6B), consistent with that each neuron in a population contributes unique information[27]. To further quantify the potential cooperativity effects, we performed a population level PCA (Fig. 6C). We first estimated the optimal population decoding among the entire ensemble of neurons in our dataset as a function of
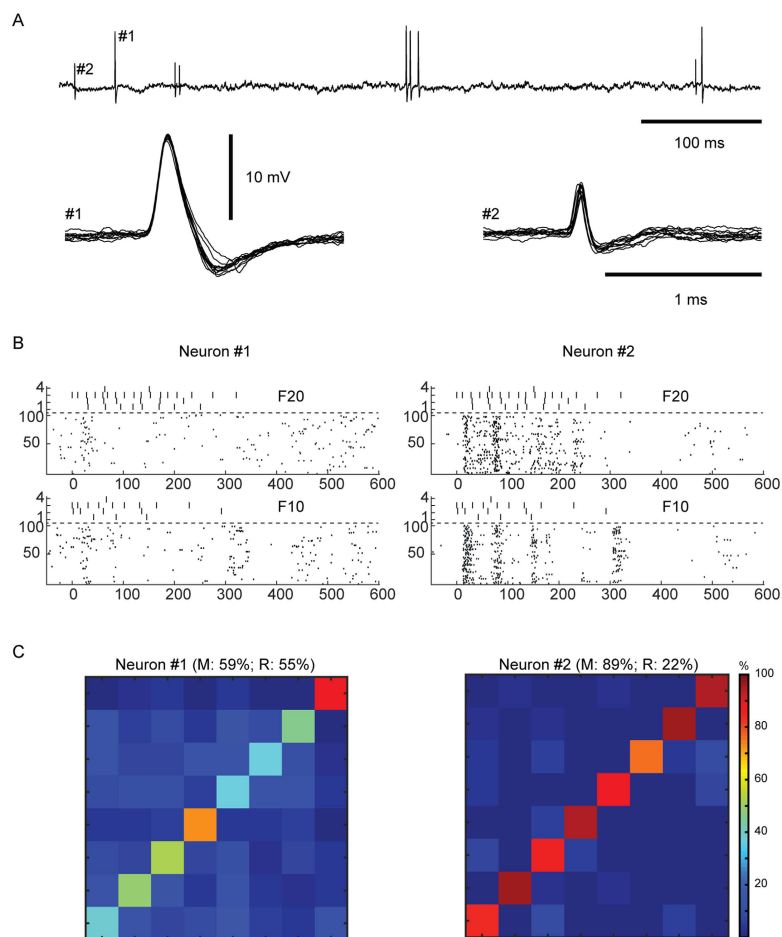
Figure 5. Adjacent neurons could display responses with contrasting temporal patterns. (**A**) Raw trace illustrating the spikes of two neurons recorded in parallel, at two different points in time. Below are shown 10 superimposed spikes from each neuron. Note the much faster spike of neuron #2, suggesting that it may belong to a smaller neuron or interneuron[17]. The amplitudes of the two spikes increased and decreased independently of each other during slight manipulation of the position of the recording electrode (0.3–20 μm of travel with the micromanipulator, not shown), indicating that they were recorded from two separate neurons (see also ref. 25). (**B**) Raster plots for the two neurons for two sample stimulation patterns. Note the large differences in the responses to the same patterns, despite that the neurons most likely were located within a few μm from each other. (**C**) Confusion matrices of the decoding across the stimulation patterns (as in Fig. 2C) for the two neurons.

integrated time and number of neurons included. In this case, the analysis of the potential for neuronal cooperativity indicated that saturation up to perfect decoding (>99%) within 350 ms was obtainable with just a few (3) neurons (Fig. 6C). The rapid attainment of a perfect segregation of the input patterns was not surprising given the outstanding performance of each of these neurons individually. However, in this type of analysis, even neurons with poorer performance in terms of mean individual decoding could together reach a near perfect segregation within a short period of time (Fig. 6D). While considering only neurons with individual decoding below 4 times chance level (i.e. mean decoding below 50%, cf. Fig. 2F,G), a very high population level decoding could be obtained within 800 ms provided that there were many (10) neurons contributing to the decoding (Fig. 6D).
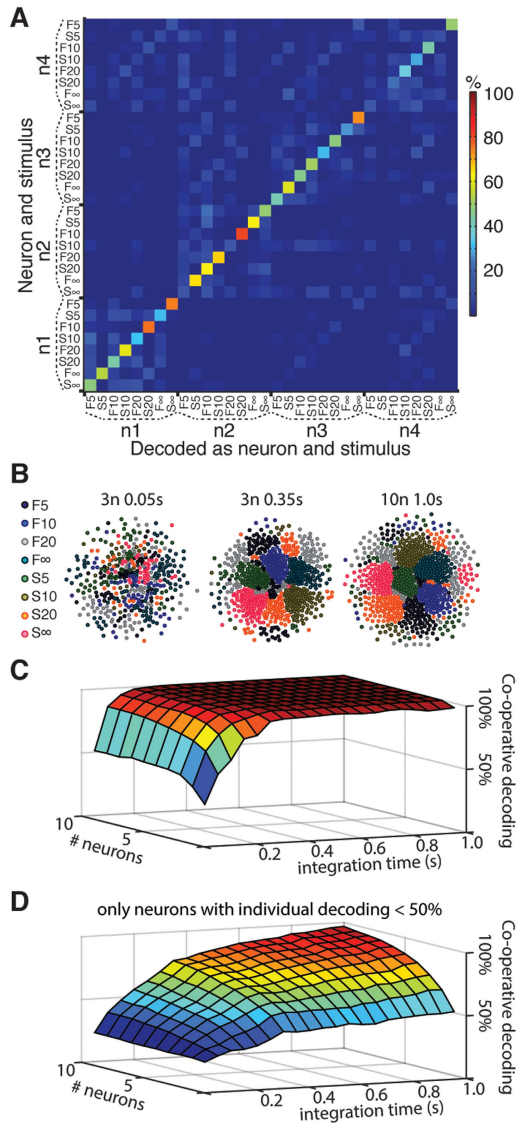
Figure 6. Potential for co-operative decoding in limited neuronal populations. (**A**) Confusion matrix for four high performing neurons, where the temporal patterns of the spike responses to the different stimulation patterns were specific to the neuron. (**B**) The cluster plots show the results of the curvilinear component analysis of the unlabelled spike responses, illustrating the segregation of individual stimulus presentations for the two optimal (with respect to co-operative decoding rate) neurons at 50 ms, the 5 optimal neurons at 350 ms, and the 10 optimal neurons at 1000 ms. The stimulation pattern is color coded as in Fig. 2B. (**C**) 3D plot to illustrate the evolution of the estimated optimal population decoding rate, as evaluated with PCA and kNN, from the repeated presentations of the stimulation patterns and an increasing number of neurons and increasing time. (**D**) The estimated optimal population decoding when the pool of neurons was limited to those with a mean decoding below 5 times chance level.
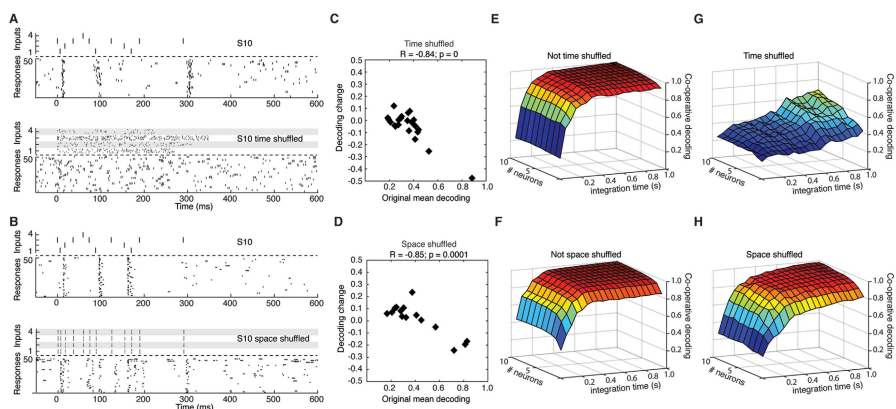
Figure 7. Effect on the decoding performance of temporal and spatial shuffling of the stimulation patterns.
(**A**) Example of the effect of temporal shuffling of the S10 stimulation pattern on the spike responses. Top, in the control, the spatiotemporal stimulation pattern was exactly the same from trial to trial. Bottom, with time shuffle, the number of stimulations per channel were held constant but their temporal distribution was shifted at random. (**B**) Similar display for the effect of spatial shuffling of the S10 stimulation pattern. (**C**) Effect of temporal shuffling on the mean decoding across the population of neurons. Note the strong relationship between the level of mean decoding in the control and the loss of decoding in the shuffled condition. (**D**) Effect of spatial shuffling on the mean decoding in another population of neurons, with a similar relationship as in (**C**). (**E,F**) Co-operative decoding before shuffling. (**G,H**) Co-operative decoding after temporal and spatial shuffling, respectively. (**E–H**), similar display as in Fig. 6C, including up to the 10 best co-operative neurons, sorted before and after shuffling.

Although such effects may not be important for the identification of the limited number of input patterns we used, they could still be essential in order to resolve a larger set of stimuli, i.e. when further qualitative details about the properties of the object, or finer shape details, need to be resolved.

Temporal resolution of the spike responses. The importance of the temporal evolution of the spike responses was further tested by evaluating the decoding obtained assuming a pure rate code (as in the study of Luczak, *et al.*[17], for example), i.e. where only the total number of spikes evoked by the stimulation pattern was taken into account (Supplementary Fig. S6, a pure rate code corresponds to using Victor Purpura spike distance, VPd, with cost $q = 0$). In this case, the decoding performance was lost and did not overcome chance level. Across the population, assuming a rate code resulted in significantly worse decoding performance ($p = 1.01e-07$, non-parametric Wilcoxon signed rank test). However, the temporal dynamics of the spike responses varied substantially between neurons. The optimal cost q was typically between $175\,s^{-1}$ and $50\,s^{-1}$, corresponding to a temporal scale of 12–40 ms (Supplementary Fig. S6).

Neuronal input segregation depends on the spatiotemporal structure of the input. We also tested directly whether the spatiotemporal structure of the stimulation patterns was a decisive factor for the decoding performance. First, we shuffled the temporal structure of the stimulation patterns (N = 21 neurons) (Fig. 7A). In neurons with high mean decoding, temporal shuffling substantially decreased the performance (Fig. 7B). In contrast, in neurons with a low mean decoding the temporal shuffling did not degrade the performance and there was a monotonically decreasing correlation between the mean decoding of the neuron and the change in performance resulting from the shuffling (Fig. 7C). We next examined the importance of the spatial structure of the stimulation patterns by maintaining the temporal patterns and the number of spikes in each stimulus channel, but by randomizing the skin site of delivery of the four channels. Although the effects of the spatial shuffling was overall weaker, which is attributable to the comparatively smaller disruptive effect on the stimulation patterns (Fig. 7C), the results were in principle similar (N = 15 neurons) (Fig. 7D). Also the population level decoding was strongly degraded by the temporal shuffling, whereas the effects were weaker but still clear for spatial shuffling (Fig. 7E–H).

Discussion

The main aim of the present study was to provide a quantitative estimate of how well neocortical neurons can identify the spatiotemporal pattern of skin tactile information, i.e. identifying the 'what' component of tactile input received[28]. The decoding accuracy or the information content was in this respect found to be very high in at least some individual neurons. A second main finding was that the same tactile afferent input could be encoded in different temporal response patterns between neurons, which suggest that the brain can channel

tactile information through multiple parallel processing networks, possibly focussing on complementary aspects of the input information. To our knowledge, this is the first time the decoding performance of neurons of the somatosensory cortex are investigated using (i) reproducible spatiotemporal patterns of skin tactile afferent activation, (ii) that are delivered in multiple, richly resolvable patterns that resemble natural tactile scenes, i.e. touch of a range of objects. The reproducibility eliminated the need to restrict the analysis to the rate codes of the neuronal responses, as in previous analyses of cortical information[17,29,30]. Instead, it became possible to focus on the details of the temporal evolution of the spike responses, which turned out to be a domain where a substantial amount of the neuronal information resided.

High neuronal decoding capacity.

Our results indicate very high individual neuronal decoding capacity (up to more than 2.8 bits per neuron, out of 3 bits of maximal information with 8 stimuli) (Fig. 2 and Supplementary Fig. S4) and reveal multiple features that give novel clues to the organization of the sensory processing in neocortical circuitry. We did not find any relationship between decoding performance and recording depth (Fig. 3), which, although a crude measure, suggests that many neuron types participated in the decoding. The high precision decoding was surprising since the internal states of the brain, as in all neurophysiological recordings, were outside our control and varied between trials and undoubtedly represented a major source of noise. During active explorative movement, the neural activity resulting from skin-object interactions can be expected to be much better in register with the brain state, under which circumstance the higher decoding capacity discovered in the intracellular recordings (Fig. 1) is likely to be better reflected also in the spike output. Furthermore, a surprising finding was that the decoding performance of many of the neurons continued to improve up to 700 ms after the termination of the tactile stimulation, which suggests that the tactile input itself affects the state of the processing circuitry with long aftereffects. In this context it might be asked how the anesthesia could affect the decoding. There would seem to be two possible scenarios that are not mutually exclusive. One is a general degradation of network function and therefore decoding. Another one could be that the oscillatory tendencies of the circuitry are facilitated which might even improve decoding, in particular at long latencies.

Heterogeneity and complementariness of neuronal responses.

The heterogeneity between neurons with respect to their selectivity for the different input patterns (Figs 2 and 5) and the complementariness of the specific temporal patterns of their responses (Fig. 6A) suggested that individual neurons may be specialized on particular aspects of the skin-object interactions, i.e. they may represent specific bits and pieces of the information that exist at the population level. These different responsive properties of the individual neurons suggest that they may be connected to partly different neuronal networks. Due to the complementariness of the neuronal responses, even single stimulus presentations were readily resolvable using a limited population of neurons (Fig. 6B–D). Our analysis further indicated that cooperativity between a limited number of neurons was sufficient for a high resolution decoding with rapid identification of stimulation patterns. Cooperativity of decoding amongst neurons have previously been proposed for salamander and macaque retina based on studies of weak pairwise spike firing correlations between pairs of neurons[31,32], but to our knowledge cooperativity based on complementary response profiles to a set of different inputs has not previously been described for cortical neurons processing tactile input. Even though we tested only eight different spatiotemporal patterns of input, in the real world the range of possible natural tactile scenes implies that a huge variety of input patterns need to be resolved from this one part of the skin alone, a situation where the capacity added by the population of neurons is likely to be crucial. Importantly, from this study we naturally cannot say how the integrated information decoding of the neocortex normally works. However, although the brain may well use other methods for segregating the information than those used here, our analysis at least indicates that the neural information is there for the brain to use–it remains to be shown if its neuronal network has the structure and functionality to take advantage of this potential.

The electrical skin interface, its relation to mechanical stimuli and its potential resolution.

Our approach of using haptic stimuli transduced into spatiotemporal patterns of tactile afferent stimulation by a set of neuromorphic artificial sensors was motivated by the aim to eliminate known limitations of mechanical skin sensor activation (see Introduction). I.e. by delivering this input electrically to the primary afferents in local skin sites we wanted to by-pass the step of potentially variable skin sensor activation that occur even with highly controlled mechanical skin stimulation[9], so that the decoding capacity of cortical neurons could be studied in relative isolation. Just like natural tactile inputs, the input we provided can be expected to be distributed and processed through the neuronal networks in the cuneate nucleus, thalamus and neocortical circuitry before it reached the neurons we recorded from. Hence, the measured decoding is bound to reflect at least in part the inherent processing mechanisms of the brain. Accordingly, in humans, electrical nerve stimulation with a much lower resolution than in the present set of experiments are known to generate sensory impressions that are in part perceived as unnatural but also to generate diversified and meaningful tactile percepts[12–16]. We expect our higher-resolution approach to have much higher potential to generate natural sensations, but how much do we know about the relationship between our spatiotemporal patterns and information generated by mechanical skin-object interactions? For each of the four skin sites used, a limited number of skin sensor afferents would be expected to be activated[21]. As the electrical activation is highly reliable[21], every single stimulation pulse can be expected to activate the local set of skin sensor afferents in synchrony. However, the fact that different sensors have different conduction velocities[33] results in that this synchrony is broken up already when the input reaches the cuneate nucleus[21]. The fact that slowly and rapidly adapting skin sensors would be expected to be activated to the same extent by the electrical stimuli may first look unnatural, as there are many reviews that tend to stress the different conditions of activation of these types of sensors. However, under the type of dynamic indentation movement we used here, available evidence indicates that there is in principle little difference in activation between slowly and rapidly adaping tactile mechanoreceptors[1] (Supplementary Fig. S2).

Fundamentally, all skin sensors transduce mechanical skin strain patterns into receptor potentials[34]–under non-static touch conditions, such receptor potentials may be relatively congruent between different types of skin sensors with the same location. The receptor potentials are then translated into patterns of spike output in the primary afferent. In central neurons, the spike generation mechanism is subjected to stochasticity[22,23] and provided that the underlying ion channel mechanisms are related this should apply to skin sensors, too. Indeed, identification of fine details of edge stimuli from recorded spike trains in human tactile afferents was found to work well when the individual spike times was convolved into Gaussian functions with kernel widths up to 8 ms, suggesting this to be a useful upper limit for the temporal precision of the spike generation. Similar findings exist for the rat whisker primary afferents[35].

The artificial fingertip allowed us to synthesize spatiotemporal patterns of skin sensor activation at quasi-natural rates that follow a natural overall temporal modulation, or 'envelope'[36], that the biological skin sensors are known to display under dynamic indentation[1] (Supplementary Fig. 2). This aspect of our approach is probably important because the circuitry of the cortex can be expected to have experienced many events with similar envelopes of tactile afferent activity and is therefore likely to have adapted its circuitry structure to effectively process variations of that kind of overall activity modulation (as in the auditory and visual cortices[17,18]). The expected congruence of the receptor potentials under a dynamic indentation would under natural circumstances tend to drive the tactile afferents spiking to follow similar overall temporal patterns. Given the presence of skin sensor spiking stochasticity, synchronized spiking activity may well occur, as detailed next. For the indentation stimuli used here, with up to 10 spikes per sensor generated during the 300 ms that the stimulus lasted and assuming that 10 local skin afferents were engaged per channel, the spike timing variability expected from the stochasticity implies that a near astronomical number of possible spatiotemporal patterns of primary afferent activation could occur even if exactly the same mechanics of the touch condition could be repeated. This can be considered the space of possible outcomes for that condition. If the same touch condition occurred, but with a slight shift of the mechanical conditions, for example a 0.1 mm change in position across the skin, the space of the possible outcomes would be further widened. With the information being distributed across a high number of tactile afferents, it is still possible for the brain to recognize the tactile experience as belonging to the same kind of object and discriminate it from other experiences. The full space of possible tactile experiences, representing any kind of physical interaction with any kind of possible object, would be very large indeed. Our electrical stimuli, with near synchronous activation of the local skin afferents, would only be required to fall within that huge space of possible outcomes in order to represent a type of input that could theoretically occur under the lifetime of a rat–depending on the actual range of spike timing variability that applies for rat skin tactile afferents, this would hardly seem unlikely.

However, a main caveat is that all the local sensors were driven to the same level of activity. It is questionable whether there exists physically possible skin-object interactions in which all local sensors can be expected to be activated within the same spiking frequency range. This probably makes our stimuli falling short of being able to produce perfectly normally perceived sensations. Rather, our synthetic spatiotemporal patterns of skin afferent activation could produce a sensory experience that would be partly perceived as natural and partly unnatural, i.e. a proper indentation sensation mixed with unnatural sensations such as tingling, where at least rough shape classification may be possible to achieve.

Naturally, whereas the resolvability of the inputs that we provided was sufficiently high to provide quantitative measures of the decoding of the individual neurons, real world mechanical stimuli would be characterized by much higher information content in the population of primary afferent activity[37,38]. The logical explanation for this is that as long as the electrical skin interface uses only four channels, and cannot control primary afferents individually, it will never be able to compare with the diversity of information that is potentially possible in the natural system.

Comparisons with previous related studies.

Previous quantitative analyses of the information decoding in somatosensory systems of the brain have focussed on the presence or absence of a vibrotactile input (i.e. 50% chance level[39]) and which body part or whisker an input arises from (i.e. the 'where' issue rather than the 'what' issue)[40,41]. The discrimination of different input patterns in S1 neurons has been explored with sinusoidal stimuli in the whisker system of the rat[42], where the highest information content was in the order of 0.3 bits over >5 bits of maximum theoretical information, which can be compared with up to 2.86 bits over 3 bits of maximum theoretical information in our study (Supplementary Fig. S4). A likely reason for the rather large discrepancy is that our 'frozen' spatiotemporal patterns of primary afferent activation represented more reproducible, and therefore more discriminable, input than mechanical peripheral stimulation, as described in the Introduction.

Electrical primary sensory afferent stimulation has previously also been used to study the responses in the brain induced by cochlear and retinal implants. However, so far, such studies have been limited to analyses of field potentials and cortical topography[43,44], neuronal response latency times[45] and firing rate[46], whereas the decoding capacity of individual cortical neurons provided with input from epiretinal implants or other audio/visual implants has not been tested.

Future developments and applications of the approach.

Our findings also have implications for the translational application of biomimetic artificial touch technology in neuroprosthetics and bionic limbs, where the aim is to impart natural sensations to the users[47,48]. In a device designed for humans, our approach would equal a very high resolution intraneural interface[13] accessing multiple terminal nerve fiber branches, innervating adjacent small patches of skin, for individual electrical activation. The activation across the sensors/nerve branches should ideally be delivered in spatiotemporal patterns that respect the realm of possible combinations of sensor activation that would occur in the biological system, i.e. at least capturing the envelope of expected spatiotemporal activation of skin sensors as we aimed for here. This approach may provide the prosthesis with

sufficiently rich and reality-like sensory information to make it tunable to the normal brain circuitry processing mode, which combined with brain network plasticity could potentially allow the prosthesis to become a natural member of the mind-body relationship.

In addition to revealing novel features of neocortical neuronal decoding of tactile input, and an approach to analyze neuroprosthetic functionality, our experimental design also offers a potential tool for the analysis of the progression of neurodegenerative disease in animal models of those diseases. The information content of single neurons is likely to be a sensitive indicator of the state of the network of neurons that innervates them–any deterioration in that network can be expected to result in degraded decoding performance. Hence, models of neurological disease, and the effect of drug candidates or training, could be benchmarked with this approach of highly reproducible inputs.

Methods

Surgical procedures. For neuronal recordings, adult male Wistar rats (N = 26, weight 300–450 g) were prepared and maintained under anesthesia with a ketamine and xylazine mixture (20:1). This type of anesthesia has no disruptive effect on the order of neuronal recruitment of neocortical neurons in spontaneous brain activity fluctuations (up states, recordings obtained using multielectrode arrays in the rat) as compared to the awake condition, which suggest that the neocortical network may work close to normal[49], even though the global brain state regulation does not. Anesthesia was induced via an i.p. injection (40 mg/kg of ketamine) and maintenance was administered through an intravenous catheter inserted into the right femoral vein (appx. 5 mg/kg per hour with a continuous infusion). The induction of the ketamine-xylazine anesthesia was preceded isofluorane sedation (2% for 30–60 s). For recording sessions, the level of anesthesia was monitored with an ECoG electrode placed in the vicinity of the recoding area. The ECoG was characterized by the irregular occurrence of sleep spindles, a sign of deep sleep[50]. The level of anesthesia was additionally characterized by an absence of withdrawal reflexes to noxious pinch to the hindpaw. The decision to run the neuronal recording experiments under anesthesia was motivated by that we needed to make sure that the mechanical stability of the brain was consistently high throughout the experiments in order to be able to run the long-term *in vivo* patch clamp recordings necessary to expose the neurons to a sufficient number of stimulus presentations (up to 2000 presentations delivered at 0.5 Hz). All animal experiment procedures in the present study were in accordance with institutional guidelines and were approved in advance by the Local Animal Ethics Committee of Lund, Sweden (permit ID M118–13).

Recordings. All recordings were made *in vivo*, in the region of the primary somatosensory cortex of the forepaw (Fig. 1C), as estimated by the focus of the local field potentials (between layers III and V) evoked by electrical stimulation of the forepaw and digit 2. The coordinates of this region were 0.0–1.0 mm rostral to bregma and 3.5 and 4.5 mm lateral to –1.0 caudal to bregma and 3.0 and 4.0 mm lateral as defined by a stereotaxic system. Individual neurons were recorded with patch clamp pipettes either in the intracellular, whole cell mode or extracellularly in the loose patch recording mode. Patch clamp pipettes were pulled from borosilicate glass capillaries to 6–15 MOhm using a Sutter Instruments (Novato, CA) P-97 horizontal puller. The composition of the electrolyte solution in the patch pipettes was (in mM) potassium-gluconate (135), KCl (6.0), HEPES (10), Mg-ATP (2), EGTA (10). The solution was titrated to 7.35–7.40 using 1 M KOH. In some cases, the solution also included 1.0% neurobiotin, used for the morphological identification of the neurons. In order to find neurons, recorded signals were continuously monitored on a display and via loudspeakers. During slow advancement of the recording electrode (approximately 0.3 μm per second), all the skin stimulation sites were activated with one pulse per second, and any neuron thus encountered were typically recorded from. In some experiments we used two pipette electrodes to obtain dual recordings, and in some cases dual recordings were obtained from a single electrode. All data was digitized at 100 kHz using CED 1401 mk2 hardware and Spike2 software (Cambridge Electronics Devices, CED, Cambridge, UK). The recording depth from the surface of the brain was annotated. For identification of neuron identity, made in a subset of our recordings, in addition to depth we used direct morphological identification, using post-mortem histological identification in a confocal microscope (Nikon A1R+), as a pyramidal cell or a non-pyramid cell combined with approximate layer identity using anatomically verified recording depth (using measurements of the distance from the pial surface) (N = 15) (Fig. 1D), and the nature of the firing during spontaneous activity (i.e. if the neuron was fast-spiking, bursting and what duration and intensity of bursts the neuron displayed). After the recording session, the animals were sacrificed and perfused with 4% paraformaldehyde. In the post-mortem histological processing, Alexa488 fluourofor conjugated with streptavidin (Molecular Probes Inc.) was used to stain the recorded neurons.

Stimulation. Four pairs of intracutaneous needle electrodes (channels 1–4) were inserted percutaneously into predetermined sites in the skin on the volar side of the second digit of the forepaw and constituted the electrical interface used for stimulus delivery (Fig. 1B). The interneedle distance in each pair of bipolar electrodes was 2–3 mm. With this type of approach, the threshold for activating individual primary sensory afferents is in the order of 0.2 mA[21,51]. Here, for each skin site, the elementary stimulation pulse was set to an intensity of 0.50 mA and stimulation pulse duration of 0.14 ms (DS3 Isolated Stimulator, Digitimer, UK), which should be well below the 4 times the threshold intensity where A-delta fibers start to become recruited (peak activation requires 6–10 times threshold intensity)[20].

Neocortical neuron recording with spatiotemporal patterns of skin activation. The experimental data was neocortical neuronal responses to eight predefined spatiotemporal patterns of skin site activation, patterns that were composed of multiple electrical stimulation pulses to the four skin sites used (see '*Generation of spatiotemporal spike stimulation patterns*' below). The eight spatiotemporal stimulation patterns were delivered in a pre-defined random (pseudo-random) order, where the stimulation patterns lasted for less than 340 ms and

the consecutive deliveries of the stimulation patterns was separated by 1.8 s in order to allow a relaxation of the cortical activity induced by the stimulation. Only neurons that could be recorded for at least 120 trials of stimulation pattern presentations were included in the analysis. However, most neurons could be recorded for at least 350–800 trials, i.e. up to 100 presentations of each of the eight predefined stimulation patterns.

Generation of spatiotemporal spike stimulation patterns. In order to achieve as realistic spatiotemporal patterns of electrical skin stimulation as possible, while preserving the aim of high reproducibility of the patterns, we used an artificial fingertip equipped with a set of four neuromorphic sensors to generate the spatiotemporal patterns of skin activation to be used in the electrical interface with the rat skin. The four electrode pairs of the interface were 1-to-1 connected to the four neuromorphic sensors of the artificial fingertip, and the neuromorphic sensors generated spiking output that was used as a trigger for the elementary electrical stimulation pulses of the interface with the animal. To induce sensor activation patterns that could occur in active touch, a scotch-yoke mechanism (Fig. 1A) was used to mechanically indent the sensorized fingertip against probes of four different shapes (Supplementary Fig. S1A–C). The core element of the sensorized fingertip was a Micro Electro Mechanical System (MEMS) sensor with 4 transducing piezoresistors implanted at the base of a cross-shaped structure[52] (Supplementary Fig. S1). The MEMS was packaged with polymeric compliant material (Dragon Skin, Smooth-On, USA). MEMS data were sampled at 380 Hz per sensor output by a 24-bit Analog to Digital Converter (ADS1258, Texas Instruments, USA) integrated in the fingertip, and acquired via SPI by a Field Programmable Gate Array (Cyclone II FPGA, Altera, USA). The FPGA streamed the acquired information via Ethernet to a PC for implementation of an artificial mechanoreceptor model.

Per each stimulation channel x (with x spanning from channel 1 to channel 4, Fig.1E and Supplementary Fig. S1), in our neuromorphic artificial touch system[53] we used customized implementations of the Izhikevich spiking neuron model[54] to emulate 2 artificial mechanoreceptor types, mimicking to some extent slowly (labelled S model) and fast (labelled F model) adapting receptors (see Supplementary Fig. S2 for comparison with electrophysiological literature under similar experimental conditions). The difference between the implementations of the two artificial mechanoreceptor types relied in the input to the model. In the S model, opponent sensor channel pairs $Sx+$ and $Sx-$ (see Supplementary Fig. S1A for labelling) were subtracted to generate a signal (S_x, see Eq. 1) that was normalized and half-rectified to produce (Eq. 2; for values of parameters, see Supplementary Table S1) the external input I_x (Eq. 3). The S model was a multi-channel implementation of a previous artificial receptor that had been used to elicit tactile percept in human subjects with single-channel intrafascicular neural stimulation[12]. In addition to the S model, we introduced the F model in which the external input was given by the time derivative of I_x (Supplementary Fig. S1A and Eq. 4) to achieve a faster sensitivity to stimulus dynamic changes. Note that the F model does not fire under a sustained indentation, however this was not appreciable in the present experimental data since the protocol did not include static post-indentation phases due to the continuous motion of the scotch-yoke mechanism (Supplementary Fig. S1C). In both models the adaptation variable u_x evolution followed Eq. 5 and if the membrane potential v_x reached the threshold value of 30 mV one spike was released and both the membrane potential and the adaptation variable were reset according to Eq. 6. In dimensioning the parameters for the Izhikevich spiking neuron model[54], we used the set of coefficients inducing regular spiking with weak adaptation[53]. Whenever the membrane potential v_x reached the threshold level (Eq. 6), a spike was triggered, v_x was set to a reset value c and u was increased of a fixed value d.

$$S_x(t) = S_{x+}(t) - S_{x-}(t), x \in \{CH1, CH2, CH3, CH4\} \tag{1}$$

$$I_x(t) = \begin{cases} \dfrac{K}{R}S_x(t), & S_x(t) \geq S_{th} \\ 0, & S_x(t) < S_{th} \end{cases} \tag{2}$$

$$\frac{dv_x(t)}{dt} = Av_x(t)^2 + Bv_x(t) + C - u_x(t) + \frac{1}{C_m}I_x(t) \tag{3}$$

$$\frac{dv_x(t)}{dt} = Av_x(t)^2 + Bv_x(t) + C - u_x(t) + \frac{\tau}{C_m}\frac{dI_x(t)}{dt} \tag{4}$$

$$\frac{dv_x(t)}{dt} = a(bv_x(t) - u_x(t)) \tag{5}$$

$$if\ (v(t^*) \geq v_{th}),\ then\ a\ spike\ occurs\ at\ t^*\ and\ \begin{cases} v(t^* + \Delta t) \leftarrow c \\ u(t^* + \Delta t) \leftarrow u(t^*) + d \end{cases} \tag{6}$$

Per each channel x (CH1 to CH4), the computed binary response constituted the output of the neuromorphic artificial touch system. Such spike sequences were broadcasted by TCP communication to successive services and graphical user interface (Labview, NI, USA), that was responsible to generate the trigger per each channel, via a BNC connection to a current stimulator (Digitimer unit, see above) allocated for each electrical channel interfaced to the skin (Supplementary Fig. S1A and Fig. 1B).

Decoding based on sensors outputs and selection of spatiotemporal stimulation patterns. In order to evaluate whether the degree of segregation of the spatiotemporal patterns of sensor output was sufficient to deliver resolvable information to the somatosensory system, we first implemented a repeated (N = 100 per stimulation pattern) delivery of the mechanical stimulation to the biomimetic fingertip. Such stimulation was carried out via the 4 different probes and with the 2 different artificial mechanoreceptor models, yielding a total set of 8 stimulation patterns (Supplementary Fig. S1).

Neurophysiological considerations[55] suggest that the nervous system appreciates the fine temporal differences between the spike trains arriving from different channels. These differences can be quantified with the Victor Purpura (VP) metrics[56]. VP metrics defines the distance between two spike trains as the minimum cost of transforming one into the other by following two operations (see Supplementary Fig. S3): adding/removing a spike (cost:1) and shifting a spike by an interval Δt (cost = q*Δt). Note that the shift cost parameter q identifies the relevant timescale for the comparison[56]. In order to introduce a distance between multi-channel spike trains, we computed the sum over the four channels of the VP distances measured on a channel by channel basis between spike train pairs (i.e., defining a 4-dimensional l^1 norm based on VP-distance, which can also be termed a 4-dimensional Manhattan VP-distance). We measured this distance across all presentations and all stimuli (Supplementary Fig. S1F). To test whether it was possible to segregate the 8 spatiotemporal stimulation patterns according to these distances we applied a k nearest neighbors (kNN) clustering decoding procedure[57], since spike trains with small distances, i.e. neighboring responses, are likely to be elicited by the same stimulation whereas spike trains with large distances are likely to be elicited by different stimulations. Specifically the kNN was implemented with k = 20 (out of 100 stimulus presentations) and using half of the trials picked at random as training set. We evaluated decoding performance computing the mutual information between presented and predicted stimulus at each trial[58], as depicted by the confusion matrix that represents (column-wise) the computed decoding (correct responses in the diagonal) per each presented stimulus (labelled row by row) (Supplementary Fig. S1G). Information was computed with the Information Breakdown Toolbox in MATLAB (MathWorks). We evaluated information bias combining quadratic estimation and bootstrap subtraction[59].

After the evaluation of the degree to which the sensor output patterns obtained from the repeated (N = 100) mechanical stimulation of the biomimetic fingertip could be segregated, we selected (Supplementary Fig. S1D) a representative spatiotemporal pattern of sensor spike output for each probe/receptor model condition to be systematically delivered in the neurophysiological experiments. Per each stimulus condition, among the spatiotemporal patterns that were below the threshold level (VPd < 1.5, Supplementary Fig. S1E), the sensor output pattern to be used as the representation of that stimulus condition was selected at random.

Decoding based on single neuron spike responses and principal component analysis (PCA). The spiking responses of single cortical neurons to the different spatiotemporal input stimuli were analysed using PCA. This analysis answered the question by which precision the spiking response could be used to distinguish one stimulation pattern from the others. We decoded the stimuli from the spiking patterns of single cortical neurons using an improved and simplified version of a method[60] based on the decomposition of the temporal profiles of the evoked spike responses into Principal Components (PCs):

 (i) We computed the mean firing rate over time in the response to each stimulus presentation.
 (ii) We converted the spike trains evoked by each stimulus presentation into continuous functions by convolving them with an exponential kernel with a characteristic time of 5 ms.
 (iii) We computed the average of the resulting functions for each stimulation pattern to obtain a template of the average temporal evolution of the response to each stimulus.
 (iv) To highlight the differences in the temporal profile we z-scored the average responses.
 (v) We extracted the principal components (PCs) of the z-scored average responses evoked by the different stimulation patterns and we computed for each individual response the score relative to each PC, that is, the scalar product between the response temporal vector and the PC temporal vector.
 (vi) The decoding was performed using the mean firing rate and the scores on each of the first 7 PCs for each individual response. The average intensity and the temporal profile of the individual response hence determined the location of that response in this 8-dimensional space;
 (vii) In order to decode the stimuli from the response patterns we used the kNN classification procedure as previously described[60]. As stated in the previous point, the response to each stimulus presentation was represented as a point in a space with 8 dimensions. Half of these points were selected as random as training set. For each trial belonging to the test set we identified the closest 9 trials in the training set with an Euclidean distance in the 8-dimensions space. The trial was then classified as elicited by the same stimulus that elicited the relative majority of the 9 neighbors. We performed 40 iterations of the decoding, each with a different training set, and we averaged the fraction of correctly decoded trials in each iteration to get the decoding average of the neuron. We also computed and averaged over all iterations the confusion matrix information (see previous subset).

The analysis of the spike responses using PCA always included the first 600 ms of the evoked responses unless otherwise indicated.

Relationship between neuron depth and decoding. The relationship between the depth of the recorded neurons and the decoding performance was tested using Pearson linear correlation analysis and Kruskal Wallis test on 200 micrometer "layers" of the recording depths.

Analysis of intracellular responses–general. In order to analyse the synaptic inputs to the cortical neurons, intracellular data from whole cell recordings was obtained (Fig. 1E–I). Using a mild hyperpolarizing current injection, the neurons were prevented from spiking and the intracellular membrane potential driven by the synaptic inputs could be analysed in isolation. The eight different stimulation patterns were presented repeatedly, in random order, to obtain multiple membrane potential responses for each stimulation pattern. As the intracellular recordings did not always last for the entire duration of the 50 times 8 stimulus presentations, the number of repetitions varied between the recordings and was 38 ± 10 repetitions per stimulation pattern and neuron.

Analysis of intracellular responses–PCA. The PCA of the intracellular responses was made in the same way as the PCA of the spike responses described above, except steps (i) & (ii) as the raw intracellular traces already corresponded to the continuous functions. First, to remove high-frequency fluctuations the traces were low-pass filtered (with a 2 ms wide moving average) and re-sampled to 1000 Hz. Secondly, to remove slow shifts in DC offset, raw traces were high-pass filtered (with a cut-off frequency of 0.5 Hz using a first order Butterworth high-pass filter in MATLAB). Then the PCA was performed as described above.

Analysis of intracellular responses–pairwise comparisons. The raw intracellular traces were low-pass filtered as described above and divided into 1 ms time bins representing averages over 100 samples (as we used a sampling frequency of 100 kHz) each ('bin averages'). The membrane potential responses obtained on repeated presentation of each stimulation pattern provided a distribution of the bin averages for each time bin. 10% of the values from this distribution were excluded as outliers in order to minimize the influence from major spontaneous changes in membrane potential. The resulting distributions without outliers were subsequently used to compare the responses of different stimulation patterns in order to see if there were any discernible differences. The Welch student's t-test was used to evaluate the individual bin averages using the test statistics as a dissimilarity measure between the distributions. The dissimilarity measures were in turn divided into two distributions, one containing the measures of a 300 ms pre-stimulus interval and one 300 ms interval with the measures from the response evoked by the stimulus. These two distributions were used to evaluate whether the difference during the stimulation was larger than that during spontaneous activity. As the p-value in this case is dependent on the number of observations included, this number was kept constant. If the one-sided two-sample Kolmogorov-Smirnov test could reject the null hypothesis that the p-values of the evoked activity were similar or larger than those from the spontaneous activity, we considered a difference to exist between the responses of the two stimulation patterns. Since there were eight stimulation patterns, for each neuron there were 28 comparisons that could be made.

Estimation of optimal population decoding. In order to analyse the additional decoding capacity that could be provided by a population of neurons, we extended the principal component analysis above. The aim of this analysis was to find the best possible decoding that could be achieved by taking the combined responses of multiple neurons into account. To illustrate how this decoding depended on the duration of the time window and the number of neurons taken into account, this analysis aimed at finding the best possible combination of neurons for each time window and each neuron added to the decoding. Due to the very high number of permutations that would have to be investigated in order to find the combination of neurons with the optimal population decoding performance, the selection process had to be approximated. For each time window, in order to find the combination of N neurons with approximately the best decoding performance, the optimal combination of N-1 neurons was extended with the neuron that had the largest positive influence upon the decoding performance when added to the N-1 neurons. This procedure was repeated for each time window (from 50 ms up to 600 ms in 50 ms steps) increasing the number of neurons from N = 1 to 10.

Cluster analysis using curvilinear component analysis. The convolved traces (see point (i) under '*Decoding based on single neuron spike responses and principal component analysis*') were also used to investigate whether the responses could be segregated using unlabeled methods that had only access to the responses but not the stimulation pattern that evoked the response. Unlike the kNN classification approach above, where the average response evoked by a specific stimulation pattern was used to compute the PCs, in the unlabeled setting the PCs were computed from the individual traces without knowledge of the ID of the stimulation patterns. For illustration purposes, the PC projections data were embedded into a 2D plane using curvilinear component analysis[61,62] where each individual response was represented by a dot (Fig. 2B).

Time and space shuffling operation and analysis. In order to explore whether the spatiotemporal patterns of the inputs was necessary for the neuronal input segregation, we also investigated for a subset of the neurons the neural responses to spatial and temporal shuffling, respectively, of the stimulation patterns. For the temporal shuffle, the number of stimuli for each channel was the same as in the normal pattern but the temporal pattern of the delivery was varied at random from trial to trial. For the spatial shuffle, the temporal pattern of each channel was preserved but the output of each channel was delivered to a random skin site.

References
1. Jenmalm, P., Birznieks, I., Goodwin, A. W. & Johansson, R. S. Influence of object shape on responses of human tactile afferents under conditions characteristic of manipulation. *Eur J Neurosci* **18,** 164–176 (2003).
2. Khalsa, P. S., Friedman, R. M., Srinivasan, M. A. & Lamotte, R. H. Encoding of shape and orientation of objects indented into the monkey fingerpad by populations of slowly and rapidly adapting mechanoreceptors. *J Neurophysiol* **79,** 3238–3251 (1998).
3. Iwamura, Y., Tanaka, M., Hikosaka, O. & Sakamoto, M. Postcentral neurons of alert monkeys activated by the contact of the hand with objects other than the monkey's own body. *Neurosci Lett* **186,** 127–130 (1995).
4. Yau, J. M., Connor, C. E. & Hsiao, S. S. Representation of tactile curvature in macaque somatosensory area 2. *J Neurophysiol* **109,** 2999–3012, doi: 10.1152/jn.00804.2012 (2013).

5. Bensmaia, S. J., Denchev, P. V., Dammann, J. F. 3rd, Craig, J. C. & Hsiao, S. S. The representation of stimulus orientation in the early stages of somatosensory processing. *J Neurosci* **28**, 776–786, doi: 10.1523/JNEUROSCI.4162-07.2008 (2008).
6. Hayward, V. *et al.* Spatio-temporal skin strain distributions evoke low variability spike responses in cuneate neurons. *J R Soc Interface* **11**, 20131015, doi: 10.1098/rsif.2013.1015 (2014).
7. Lumpkin, E. A. & Caterina, M. J. Mechanisms of sensory transduction in the skin. *Nature* **445**, 858–865, doi: 10.1038/nature05662 (2007).
8. LaMotte, R. H. & Srinivasan, M. A. Responses of cutaneous mechanoreceptors to the shape of objects applied to the primate fingerpad. *Acta psychologica* **84**, 41–51 (1993).
9. Kim, S. S. *et al.* Conveying tactile feedback in sensorized hand neuroprostheses using a biofidelic model of mechanotransduction. *Biomedical Circuits and Systems, IEEE Transactions on* **3**, 398–404 (2009).
10. Ochoa, J. & Torebjork, E. Sensations evoked by intraneural microstimulation of single mechanoreceptor units innervating the human hand. *J Physiol* **342**, 633–654 (1983).
11. Vallbo, A. B., Olsson, K. A., Westberg, K. G. & Clark, F. J. Microstimulation of single tactile afferents from the human hand. Sensory attributes related to unit type and properties of receptive fields. *Brain* **107** (Pt 3), 727–749 (1984).
12. Oddo, C. M. *et al.* Intraneural stimulation elicits discrimination of textural features by artificial fingertip in intact and amputee humans. *Elife* **5**, e09148, doi: 10.7554/eLife.09148 (2016).
13. Raspopovic, S. *et al.* Restoring natural sensory feedback in real-time bidirectional hand prostheses. *Sci Transl Med* **6**, 222ra219, doi: 10.1126/scitranslmed.3006820 (2014).
14. Tan, D. W. *et al.* A neural interface provides long-term stable natural touch perception. *Sci Transl Med* **6**, 257ra138, doi: 10.1126/scitranslmed.3008669 (2014).
15. Ortiz-Catalan, M., Hakansson, B. & Branemark, R. An osseointegrated human-machine gateway for long-term sensory feedback and motor control of artificial limbs. *Sci Transl Med* **6**, 257re256, doi: 10.1126/scitranslmed.3008933 (2014).
16. Dhillon, G. S. & Horch, K. W. Direct neural sensory feedback and control of a prosthetic arm. *IEEE Trans Neural Syst Rehabil Eng* **13**, 468–472, doi: 10.1109/TNSRE.2005.856072 (2005).
17. Luczak, A., Bartho, P. & Harris, K. D. Spontaneous events outline the realm of possible sensory responses in neocortical populations. *Neuron* **62**, 413–425, doi: 10.1016/j.neuron.2009.03.014 (2009).
18. Berkes, P., Orban, G., Lengyel, M. & Fiser, J. Spontaneous cortical activity reveals hallmarks of an optimal internal model of the environment. *Science* **331**, 83–87, doi: 10.1126/science.1195870 (2011).
19. Wallach, A., Bagdasarian, K. & Ahissar, E. On-going computation of whisking phase by mechanoreceptors. *Nat Neurosci*, doi: 10.1038/nn.4221 (2016).
20. Ekerot, C. F., Gustavsson, P., Oscarsson, O. & Schouenborg, J. Climbing fibres projecting to cat cerebellar anterior lobe activated by cutaneous A and C fibres. *J Physiol* **386**, 529–538 (1987).
21. Bengtsson, F., Brasselet, R., Johansson, R. S., Arleo, A. & Jorntell, H. Integration of sensory quanta in cuneate nucleus neurons *in vivo. PLoS One* **8**, e56630, doi: 10.1371/journal.pone.0056630 (2013).
22. Spanne, A., Geborek, P., Bengtsson, F. & Jorntell, H. Spike generation estimated from stationary spike trains in a variety of neurons *in vivo. Front Cell Neurosci* **8**, 199, doi: 10.3389/fncel.2014.00199 (2014).
23. Naundorf, B., Wolf, F. & Volgushev, M. Unique features of action potential initiation in cortical neurons. *Nature* **440**, 1060–1063, doi: 10.1038/nature04610 (2006).
24. Buzsaki, G. & Mizuseki, K. The log-dynamic brain: how skewed distributions affect network operations. *Nat Rev Neurosci* **15**, 264–278, doi: 10.1038/nrn3687 (2014).
25. Bengtsson, F., Geborek, P. & Jörntell, H. Cross-correlations between pairs of neurons in cerebellar cortex *in vivo*. *Neural Networks* **47**, 88–94 (2013).
26. Gawne, T. J. & Richmond, B. J. How independent are the messages carried by adjacent inferior temporal cortical neurons? *J Neurosci* **13**, 2758–2771 (1993).
27. Reich, D. S., Mechler, F. & Victor, J. D. Independent and redundant information in nearby cortical neurons. *Science* **294**, 2566–2568, doi: 10.1126/science.1065839 (2001).
28. Diamond, M. E., von Heimendahl, M., Knutsen, P. M., Kleinfeld, D. & Ahissar, E. 'Where' and 'what' in the whisker sensorimotor system. *Nat Rev Neurosci* **9**, 601–612, doi: 10.1038/nrn2411 (2008).
29. Gutnisky, D. A. & Dragoi, V. Adaptive coding of visual information in neural populations. *Nature* **452**, 220–224, doi: 10.1038/nature06563 (2008).
30. Rigotti, M. *et al.* The importance of mixed selectivity in complex cognitive tasks. *Nature* **497**, 585–590, doi: 10.1038/nature12160 (2013).
31. Schneidman, E., Berry, M. J. 2nd, Segev, R. & Bialek, W. Weak pairwise correlations imply strongly correlated network states in a neural population. *Nature* **440**, 1007–1012, doi: 10.1038/nature04701 (2006).
32. Pillow, J. W. *et al.* Spatio-temporal correlations and visual signalling in a complete neuronal population. *Nature* **454**, 995–999, doi: 10.1038/nature07140 (2008).
33. Abraira, V. E. & Ginty, D. D. The sensory neurons of touch. *Neuron* **79**, 618–639, doi: 10.1016/j.neuron.2013.07.051 (2013).
34. Woo, S. H., Lumpkin, E. A. & Patapoutian, A. Merkel cells and neurons keep in touch. *Trends Cell Biol* **25**, 74–81, doi: 10.1016/j.tcb.2014.10.003 (2015).
35. Jones, L. M., Depireux, D. A., Simons, D. J. & Keller, A. Robust temporal coding in the trigeminal system. *Science* **304**, 1986–1989, doi: 10.1126/science.1097779 (2004).
36. Middleton, J. W., Longtin, A., Benda, J. & Maler, L. The cellular basis for parallel neural transmission of a high-frequency stimulus and its low-frequency envelope. *Proc Natl Acad Sci U S A* **103**, 14596–14601, doi: 10.1073/pnas.0604103103 (2006).
37. Chagas, A. M. *et al.* Functional analysis of ultra high information rates conveyed by rat vibrissal primary afferents. *Front Neural Circuits* **7**, 190, doi: 10.3389/fncir.2013.00190 (2013).
38. Theis, L., Chagas, A. M., Arnstein, D., Schwarz, C. & Bethge, M. Beyond GLMs: a generative mixture modeling approach to neural system identification. *PLoS Comput Biol* **9**, e1003356, doi: 10.1371/journal.pcbi.1003356 (2013).
39. de Lafuente, V. & Romo, R. Neural correlate of subjective sensory experience gradually builds up across cortical areas. *Proc Natl Acad Sci U S A* **103**, 14266–14271, doi: 10.1073/pnas.0605826103 (2006).
40. Petersen, R. S., Panzeri, S. & Diamond, M. E. Population coding of stimulus location in rat somatosensory cortex. *Neuron* **32**, 503–514 (2001).
41. Foffani, G., Tutunculer, B. & Moxon, K. A. Role of spike timing in the forelimb somatosensory cortex of the rat. *J Neurosci* **24**, 7266–7271, doi: 10.1523/JNEUROSCI.2523-04.2004 (2004).
42. Arabzadeh, E., Panzeri, S. & Diamond, M. E. Deciphering the spike train of a sensory neuron: counts and temporal patterns in the rat whisker pathway. *J Neurosci* **26**, 9216–9226, doi: 10.1523/JNEUROSCI.1491-06.2006 (2006).
43. Mandel, Y. *et al.* Cortical responses elicited by photovoltaic subretinal prostheses exhibit similarities to visually evoked potentials. *Nat Commun* **4**, 1980, doi: 10.1038/ncomms2980 (2013).
44. Kral, A. & Sharma, A. Developmental neuroplasticity after cochlear implantation. *Trends Neurosci* **35**, 111–122, doi: 10.1016/j.tins.2011.09.004 (2012).
45. Raggio, M. W. & Schreiner, C. E. Neuronal responses in cat primary auditory cortex to electrical cochlear stimulation. I. Intensity dependence of firing rate and response latency. *J Neurophysiol* **72**, 2334–2359 (1994).

46. Schreiner, C. E. & Raggio, M. W. Neuronal responses in cat primary auditory cortex to electrical cochlear stimulation. II. Repetition rate coding. *J Neurophysiol* **75**, 1283–1300 (1996).
47. Kwok, R. Neuroprosthetics: once more, with feeling. *Nature* **497**, 176–178, doi: 10.1038/497176a (2013).
48. Tee, B. C. *et al.* A skin-inspired organic digital mechanoreceptor. *Science* **350**, 313–316, doi: 10.1126/science.aaa9306 (2015).
49. Luczak, A. & Bartho, P. Consistent sequential activity across diverse forms of UP states under ketamine anesthesia. *Eur J Neurosci* **36**, 2830–2838, doi: 10.1111/j.1460-9568.2012.08201.x (2012).
50. Niedermayer, E & Lopes da Silva, F. *Electroencephalography: Basic Principles, Clinical Applications, and Related Fields* (Williams and Wilkins, 1993).
51. Rasmusson, D. D. & Northgrave, S. A. Reorganization of the raccoon cuneate nucleus after peripheral denervation. *J Neurophysiol* **78**, 2924–2936 (1997).
52. Beccai, L. *et al.* Design and fabrication of a hybrid silicon three-axial force sensor for biomechanical applications. *Sensors and Actuators A: Physical* **120**, 370–382 (2005).
53. Spigler, G., Oddo, C. M. & Carrozza, M. C. Soft-neuromorphic artificial touch for applications in neuro-robotics. *4th IEEE RAS & EMBS International Conference on Biomedical Robotics and Biomechatronics (BioRob)* (2012).
54. Izhikevich, E. M. Simple model of spiking neurons. *Neural Networks, IEEE Transactions on* **14**, 1569–1572, doi: 10.1109/tnn.2003.820440 (2003).
55. Johansson, R. S. & Flanagan, J. R. Coding and use of tactile signals from the fingertips in object manipulation tasks. *Nat Rev Neurosci* **10**, 345–359, doi: 10.1038/nrn2621 (2009).
56. Victor, J. D. & Purpura, K. P. Nature and precision of temporal coding in visual cortex: a metric-space analysis. *J Neurophysiol* **76**, 1310–1326 (1996).
57. Quian Quiroga, R., Snyder, L. H., Batista, A. P., Cui, H. & Andersen, R. A. Movement intention is better predicted than attention in the posterior parietal cortex. *J Neurosci* **26**, 3615–3620, doi: 10.1523/JNEUROSCI.3468-05.2006 (2006).
58. Quian Quiroga, R. & Panzeri, S. Extracting information from neuronal populations: information theory and decoding approaches. *Nat Rev Neurosci* **10**, 173–185, doi: 10.1038/nrn2578 (2009).
59. Magri, C., Whittingstall, K., Singh, V., Logothetis, N. K. & Panzeri, S. A toolbox for the fast information analysis of multiple-site LFP, EEG and spike train recordings. *BMC neuroscience* **10**, 81 (2009).
60. Zuo, Y. *et al.* Complementary contributions of spike timing and spike rate to perceptual decisions in rat S1 and S2 cortex. *Curr Biol* **25**, 357–363, doi: 10.1016/j.cub.2014.11.065 (2015).
61. Demartines, P. & Hérault, J. Curvilinear component analysis: A self-organizing neural network for nonlinear mapping of data sets. *Neural Networks, IEEE Transactions on* **8**, 148–154 (1997).
62. Jorntell, H. *et al.* Segregation of tactile input features in neurons of the cuneate nucleus. *Neuron* **83**, 1444–1452, doi: 10.1016/j.neuron.2014.07.038 (2014).

Acknowledgements

Author Contributions

C.O. and H.J. share first and senior authorship based on equal contribution, including the design of the experiments and analysis, the conduction of parts of the experiments and parts of the analysis. A.S. and A.M. share second authorship based on equal contribution in particular the main part of the analysis. J.M.D.E., H.M. and F.B. performed the patch clamp recording experiments. D.C. contributed to the integration of the experimental setup. S.M. contributed to the design of the study and to the discussion of the results.

Additional Information

Supplementary Information

Artificial spatiotemporal touch inputs reveal complementary decoding in neocortical neurons

Authors: Calogero M. Oddo, Alberto Mazzoni, Anton Spanne, Jonas M.D. Enander, Hannes Mogensen, Fredrik Bengtsson, Domenico Camboni, Silvestro Micera, Henrik Jörntell

| K	A	B	C	Cm	R	A	b	c	d	v$_{th}$
15,000	$\dfrac{0.04}{sV}$	$\dfrac{5}{s}$	$\dfrac{140V}{s}$	$1F$	1Ω	$\dfrac{0.02}{s}$	$\dfrac{0.2}{s}$	$-65mV$	$8mV$	$30mV$

Supplementary Table S1. Parameters of Equations 2-6.
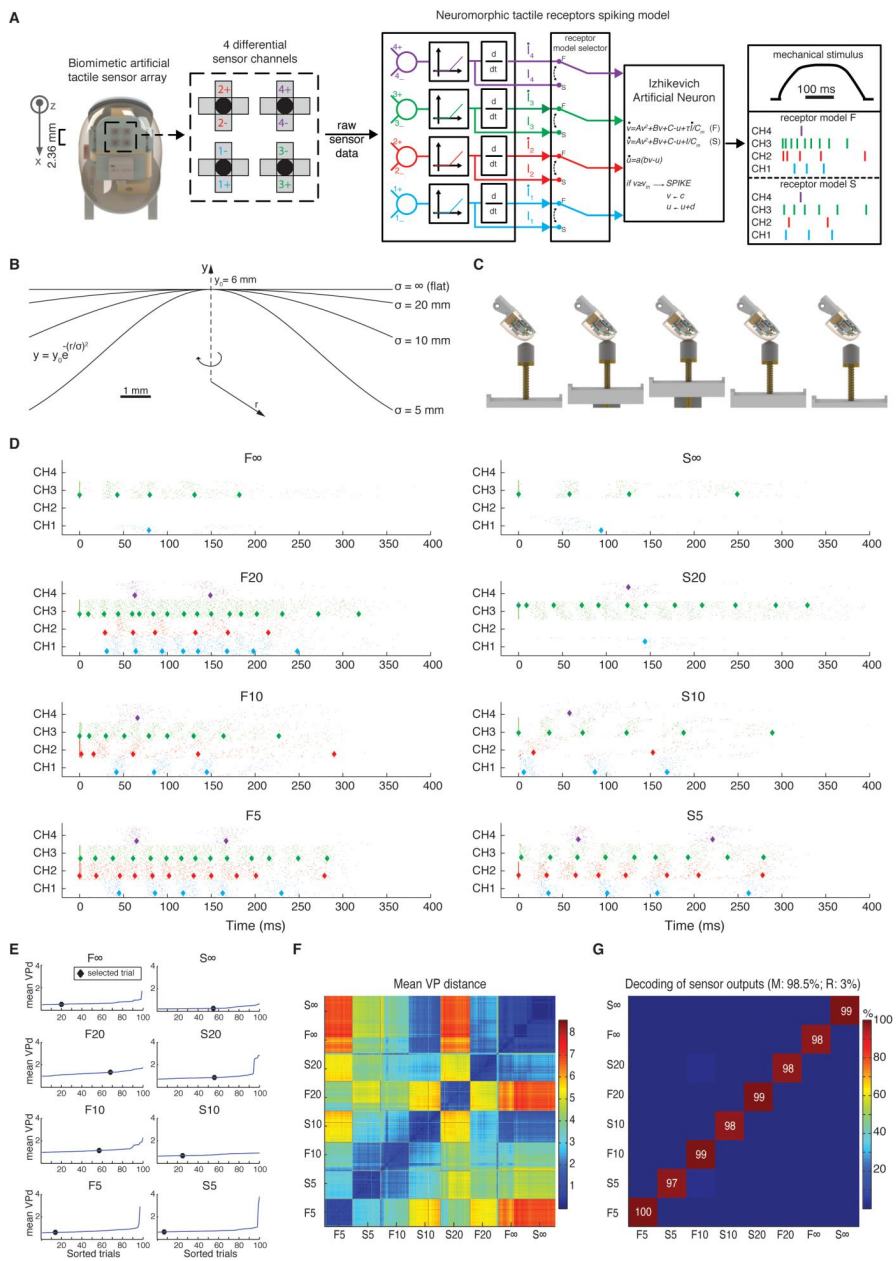
**Supplementary Figure S1. The artificial fingertip and the stimulation patterns. (A)**

Structure of artificial fingertip and properties of its sensors with spike encoding resulting from

implementation of Izhikevich artificial neuron model to four differential output pairs [1]. Two receptor models were implemented by feeding the artificial neuron with their sensor outputs directly or with their time derivative. (**B**) Diagram illustrating the parameters of the four different shapes used for mechanical stimulation. (**C**) Sequence of fingertip movement activating the mechanotransduction of the artificial tactile sensors. (**D**) Raster plots of the artificial sensor output (in the two different skin receptor models) to 100 repetitions of the mechanical stimulus delivery of each of the four shape stimuli. The selected patterns of sensor activation, which were later delivered electrically to the skin of the second digit of the rat, are indicated in stronger color/linethickness. (**E**) Degree of centrality of the selected stimulation patterns with respect to all the 100 repetitions of the mechanical stimulus delivery. (**F**) 4-dimensional Manhattan Victor Purpura distances across all presentations and all stimulation patterns (see Materials and Methods). (**G**) Segregation of the stimuli under the eight different conditions (four probes and two receptor models) illustrated in a confusion matrix of the sensor output decoding over all sessions. 'M' indicates the mean decoding, and 'R' the range of decoding (max-min). All values are obtained as the average over 50 decoding procedures with different training sets.
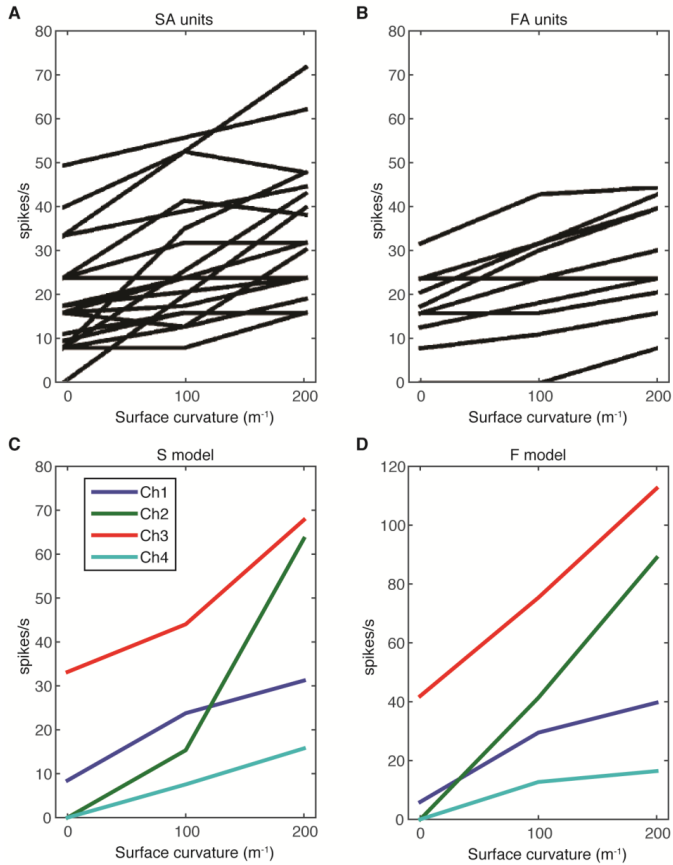
Supplementary Figure S2. The sensors of the artificial fingertip have similar activation properties as human tactile afferents. (**A,B**) Firing frequencies of rapidly adapting (A) and slowly adapting (B) human tactile afferents to indentation of the fingertip with a set of probes with different curvatures. Each line represents the firing frequencies of a single afferent across the curvatures. The data displays are modified from Figs 4A,C of Jenmalm, et al. [2] and represent the spike data from the dynamic phase of the indentation, lasting 125 ms, for the afferents with a positive correlation between their spike responses and curvature, which was the most common correlation. (**C,D**) For the neuromorphic sensors, the corresponding

relationships between the sensor spike outputs and probe curvature for the first 125 ms of indentation, i.e. similar stimulus conditions as in A and B. Each line represents the output for each sensor channel of the artificial fingertip. The data are from the specific sensor spiking output patterns selected (Supplementary Fig. S1D,E) to be delivered by electrical stimulation to the four skin sites of the second digit of the rat (Fig. 1E). Because of the overall similarities in tuning between individual biological and neuromorphic sensors with respect to the different kinds of probes used, we conclude that the synthetic patterns we generated by active touch with the artificial fingertip are likely to have at least overall similarities with patterns of skin sensor activation that could be evoked under the natural condition of active touch.
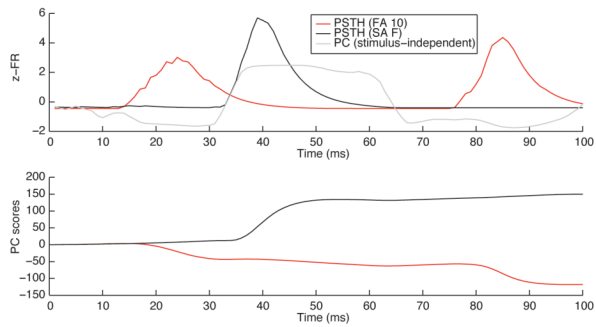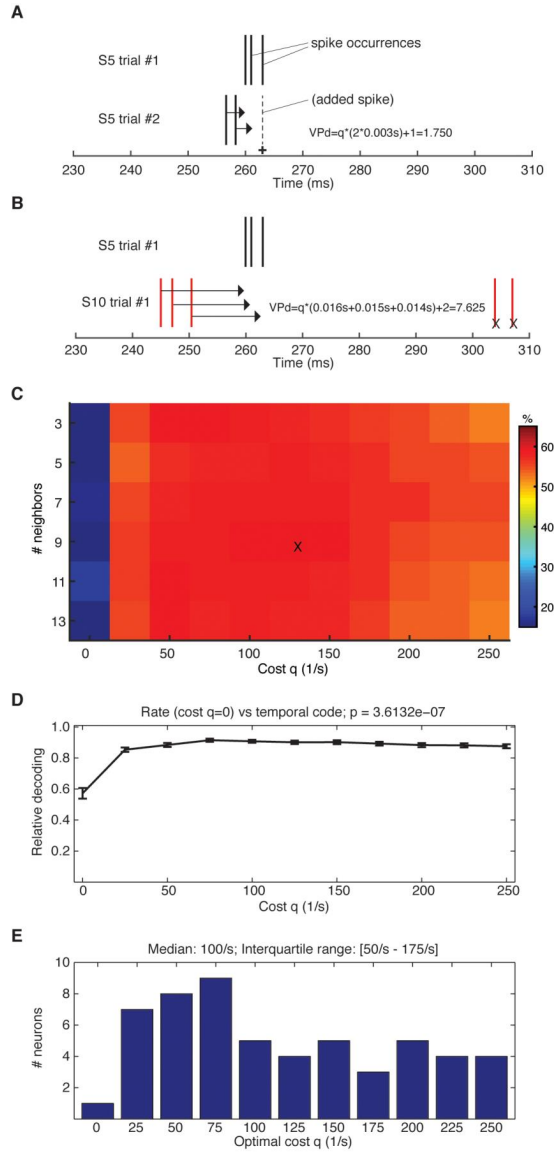
Supplementary Figure S3. Method of PCA illustrated. Smoothed curves (top) are convoluted exponential kernels of the spike responses to a stimulus presentation (here represented by the average of all stimulus presentations for clarity) illustrated for two different stimulation patterns. The binary curve in grey indicates the principal component against which the obtained curves are compared. As the black convolved trace is captured by the corresponding positive deflections of the principal component, this pattern is given a positive scalar value (bottom diagram) for this principal component. In contrast, the red convolved trace is negatively correlated with the negative deflection in the principal component and is hence given a negative scalar value for this principal component (bottom diagram). Same neuron as in Fig. 2A-C.
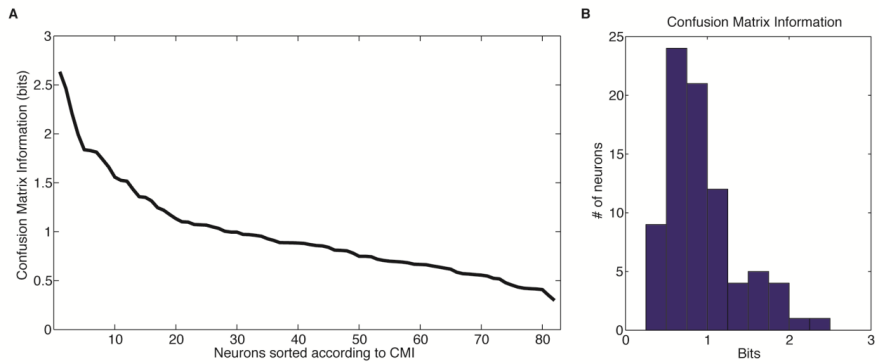
Supplementary Figure S4. Confusion matrix information for neuronal spike response decoding. (A) Similar display as in Fig. 2F but here reporting confusion matrix information rather than decoding performance. **(B)** Histogram of the distribution of the confusion matrix information across the population of neurons (similar display as in Fig. 2G, top).
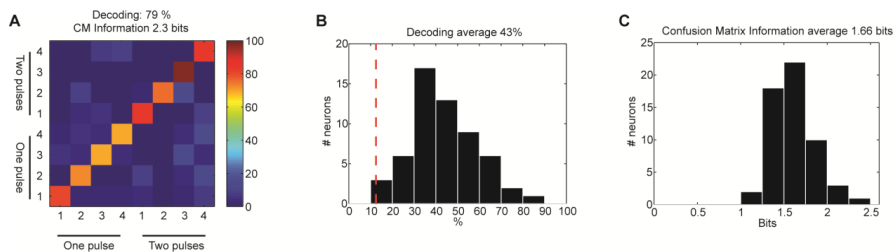
Supplementary Figure S5. Sensitivity to single and double pulse stimulation delivered to individual skin input channels. (**A**) Confusion matrix of a highly performing neuron. Numbers indicate the specific skin input channel (Fig. 1B). Single or double pulse stimulation is also indicated. (**B**) Distribution of decoding performance across 57 neurons. (**C**) Distribution of confusion matrix information across the same set of neurons.

Supplementary Figure S6. Victor Purpura distance calculations for neuronal spike responses. (**A,B**) Illustration of the method, shown by example for a portion of two sample spike trains obtained from the same stimulation pattern (**A**) and for two spike trains obtained

using different stimulation patterns (**B**). Victor Purpura distance is defined as the optimal sequence of operations minimizing the cost of moving spikes (with q cost per unit of time) and deleting or adding spikes (with 1 cost per addition or deletion) with the purpose of making two spike trains identical [3]. (**C**) Left, VPd plot from a sample neuron illustrating the decoding obtained as a function of the cost q and the number of neighboring spikes considered. The optimal decoding was obtained at the point indicated by 'X'. Cost q=0 equals analysing the spike trains as rate codes. Same neuron as in Fig. 2A-C. (**D**) Decoding performance across the population plotted as a function of VPd cost for 55 neurons, which passed the threshold of 15% of mean decoding for the VPd. For each neuron, performance is expressed as the fraction of the performance obtained at the optimal timescale for the neuron. Error bars represent standard error of the mean. The difference between the performance of the rate code (q=0) and the temporal code (q=25/s, the worst performance of temporal codes) is significant with p=1.01e-07 according to the non-parametric Wilcoxon Signed Rank Test. (**E**) Distribution of optimal cost across the same population of neurons. The median value is q=100/s (corresponding to a relevant timescale of 2/q=20 ms) and interquartile range goes from q=50/s to q=175/s (from 40 to 12 ms).

REFERENCES

1   Rongala, U. B., Mazzoni, A. & Oddo, C. M. Neuromorphic Artificial Touch for Categorization of Naturalistic Textures. *IEEE Transactions on Neural Networks and Learning Systems* (2015).
2   Jenmalm, P., Birznieks, I., Goodwin, A. W. & Johansson, R. S. Influence of object shape on responses of human tactile afferents under conditions characteristic of manipulation. *Eur J Neurosci* **18**, 164-176 (2003).
3   Victor, J. D. & Purpura, K. P. Nature and precision of temporal coding in visual cortex: a metric-space analysis. *J Neurophysiol* **76**, 1310-1326 (1996).